

Reduced Basis method for closed-form affine dependent second order systems

Ettore Lappano

Supervisors:
Prof. dr. ir. W. Desmet
Prof. Dott. Mundo
(University of Calabria)

Dissertation presented in partial
fulfillment of the requirements for the
degree of Doctor of Engineering
Science (PhD): Mechanical
Engineering

August 2018

Reduced Basis method for closed-form affine dependent second order systems

Ettore LAPPANO

Examination committee:

Prof. dr. ir. P. Van Houtte, chair
Prof. dr. ir. W. Desmet, supervisor
Prof. Dott. Mundo, supervisor
(University of Calabria)
Dr. ir. B. Pluymers
Prof. dr. ir. K. Meerbergen

M. Sc. Eng. Nijman
(Virtual Vehicle - Graz)
Prof. Dott. DI M. Schanz
(TU Graz)
Prof. Dott. M. Alfano
(University of Calabria)
Prof. Dott. L. Soria
(Politecnico di Bari)

Dissertation presented in partial fulfillment of the requirements for the degree of Doctor of Engineering Science (PhD): Mechanical Engineering

August 2018

© 2018 KU Leuven – Faculty of Engineering Science
Uitgegeven in eigen beheer, Ettore Lappano, Celestijnenlaan 300, B-3001 Leuven (Belgium)

Alle rechten voorbehouden. Niets uit deze uitgave mag worden vermenigvuldigd en/of openbaar gemaakt worden door middel van druk, fotokopie, microfilm, elektronisch of op welke andere wijze ook zonder voorafgaande schriftelijke toestemming van de uitgever.

All rights reserved. No part of the publication may be reproduced in any form by print, photoprint, microfilm, electronic or any other means without written permission from the publisher.

Preface

This thesis is the result of 4 and a half years of work spent in 3 different institutions of 3 different countries: the department of Mechanical Engineering of University of Calabria in Italy, the PMA department of KU Leuven University in Belgium and the department of NVH & Friction of the Virtual Vehicle International Research Center in Austria.

The research has been funded by the European Commission within the ITN Marie Curie Action project eLiQuiD under the 7th Framework Programme (EC grant agreement no. 316422). Additionally, the work has been partially funded by the COMET K2 – Competence Centers for Excellent Technologies Programme of the Federal Ministry for Transport, Innovation and Technology (bmvit), the Federal Ministry for Digital, Business and Enterprise (bmdw), the Austrian Research Promotion Agency (FFG), the Province of Styria and the Styrian Business Promotion Agency (SFG).

Being a researcher is a mission and requires passion and hard work. This you cannot learn by reading this sentence. I learnt this by interacting with a long list of people that have been an inspiration through the journey of this PhD work. It has been an immense privilege to interact with them and I would like to mention a few.

To begin I would like to thank my supervisor, professor and friend Domenico Mundo. He brought me on board of this difficult project showing trust in my capabilities and for this I am very grateful to him. In this journey he has been always by my side, in all situations, warning and helping me to be always resilient and not to fade under the, sometimes overwhelming, weight of scientific research. Grazie davvero!

Eugene Nijman, who supervised my work in Virtual Vehicle, influenced my approach to new problems the most: to say it with a metaphor, he has brought me to think out of the box keeping the eyes on the box (the box is the available

knowledge). Thanks!

Wim Desmet, as a supervisor, has always been the toughest on the research and I learnt a lot from this attitude: be the first to question your own results to understand where the weak points are and improve them. This allows fast development of the research and prevents stopping the flow of ideas or being “stuck ” not knowing what do. Dank u wel!

I want to thank all my former colleagues and mention some of them. Markus Polanz. I thank him for great scientific interaction during the most important phases of the PhD. I also want to thank all the other colleagues in the office at Virtual Vehicle and Jan and Toni. All of them have contributed to the positive atmosphere necessary for a successful conclusion of such an important project. From KU Leuven, I want to mention Frank who introduced me to the world of *Model OrderReduction* and Martijn.

I want to also acknowledge the effort made by my family and friends who have been always supportive in these years. Thanks for compensating with more love and consideration to my reduced time availability. Grazie cari! L'unica distanza possibile è quella geografica che riusciremo sempre a compensare in qualche modo.

Ettore Lappano

Abstract

This thesis proposes the use of *Reduced Basis* (RB) methods to improve the computational efficiency of simulations in the field of elastodynamics and acoustics including poroelastic materials. RB methods are *Model Order Reduction* techniques used to generate parametric Reduced Order Models (ROM).

There are many reasons for current researchers to focus on MOR for computational improvements. The technological development of computers and hardware has led to using brute force for calculations of large matrices projected onto simple shape-functions rather than, as it was normally done in the 60s and 70s, trying to shrink the size of the matrices using special shape-functions (i.e., specific for the different systems) [1]. The purpose of MOR techniques is to use these enormously detailed but slow (to compute and even to read) data to generate those smart shape functions. Hence, the resulting ROM contain the level of detail of those huge models, referred to as high fidelity models or full order models (FOM), offering high computational performances. These characteristics of ROM can strongly enlarge the horizons of optimization techniques enabling repeated simulation at high rate or, in some cases, allow real-time simulations paving the way for e.g. virtual sensing, haptic technology, computer graphics.

A common strategy to do MOR is to use projection-based techniques that apply to semi-discretised models (e.g. finite element models). A projection transforms the basis that describes the multidimensional space of the model to be much smaller. Thus, a projection of the model into a subspace that contains all and only the dimensions necessary to describe the model will minimize the computation effort.

The field of MOR includes dozens of methodologies and this thesis does not pretend to cover all of them. The focus of the work is to develop methods

based on projection that are able to generate ROM with explicit parametric dependency typically indicated under the category *Parametric Model Order Reduction* (PMOR). Changes of the parameters configuration affect the shape of the multidimensional space. Therefore, to obtain a reduced parametric solution, a manifold of all the basis corresponding to the different parameter configurations is needed. Among the possible approaches available to do PMOR, the RB methods achieve efficient results separating the parametric dependent and parametric independent quantities in the FOM. This enable an efficient reduction and originates ROM whose operations are independent from the size of the former FOM.

The research brought to a parametric approach in the frequency domain that can take into account the nonlinear frequency dependent characteristics of poroelastic materials (PEM). Also this methodology is verified using few numerical examples. In addition, a parametric approach to study elastodynamic problems of linear structures made of beams is presented and applied. The results of the study are discussed and validated with direct comparison to direct FE simulations.

In addition to the original contribution, the research reported in this thesis raises some new questions that could set the start of new research projects in the field of PMOR and are discussed in the conclusion to this work.

Sommario

Questo lavoro di tesi propone tecniche di *Model Order Reduction* (MOR) per migliorare l'efficienza computazionale di simulazioni elastodinamiche, poroelastiche e acustiche.

Le ragioni che portano l'attenzione verso questi studi sulle tecniche MOR sono molteplici. Wil Schilders, nella sua introduzione di un libro sull'argomento [1], richiama alcune controindicazioni legate al rapido sviluppo tecnologico in campo informatico hardware e software che spingono, anche chi si avvale di simulazioni in campo scientifico, a utilizzare il massimo delle risorse computazionali senza badare all'efficienza di tali calcoli (come era normale negli anni 1960 e 1970). Schilders suggerisce come i risultati di queste enormi simulazioni possano essere utilizzati in tecniche di MOR per costruire modelli ridotti ed efficienti a vantaggio dei tempi di computazione e dei requisiti di memoria. Quindi, i modelli ridotti (*Reduced Order Models* (ROM)) hanno lo stesso livello di dettaglio dei grandi modelli da cui sono originati e allo stesso tempo offrono elevate prestazioni computazionali. Queste caratteristiche estendono le possibilità di studi di ottimizzazione e possono permettere analisi in tempo reale.

I metodi MOR più comuni sono basati sulla costruzione di spazi vettoriali che possano descrivere, col minimo numero di vettori e con la massima accuratezza, le soluzioni di modelli discretizzati più complessi (ad esempio modelli agli elementi finiti). In un'analisi agli elementi finiti, le soluzioni del modello sono rappresentate come combinazioni lineari di moltissime funzioni di forma elementari. La proiezione sugli spazi vettoriali ridotti permette di risolvere il problema in un sottospazio vettoriale più compatto contenente vettori di funzioni di forma dettagliate e costruite sulla base dei grandi modelli (i.e., specifiche per ogni modello). Ad oggi, esistono decine di metodi per costruire questi sottospazi vettoriali (comunemente indicate in inglese come *Reduced Order Basis* (ROB)) e questa tesi non intende soffermarsi su ognuna

di esse. Lo scopo del lavoro è sviluppare metodi di parametrici di riduzione indicati in inglese come *Parametric Model Order Reduction (PMOR)*. Questi metodi si soffermano sul fatto che modifiche delle condizioni iniziali dei sistemi modellizzati generano modifiche dello spazio vettoriale. Le modifiche parametriche dello spazio vettoriale possono essere descritte da un punto di vista matematico come una *varietà* (in inglese *manifold*).

Gli sviluppi applicativi del presente lavoro di tesi sono divisi in due parti che affrontano aspetti diversi della PMOR e che utilizzano diverse esempi per verificarne la bontà. La prima parte della tesi è rivolta allo sviluppo di tecniche di riduzione per modelli contenenti materiali poroelastici. Per ottenere la riduzione ci si avvale di un approccio parametrico che tiene conto della dipendenza non lineare del modello dalla frequenza. L'approccio proposto è poi esteso su problemi con più parametri contemporaneamente

Nella prima parte si propone un metodo di PMOR basato sulla sintesi modale e sul metodo di greedy. Le trasformazioni modali, molto usate in problemi elastodinamici, non costituiscono *per se* un approccio parametrico. Quindi, in questo studio se ne vuole studiare un'estensione parametrica. Il greedy, introdotto di recente nel campo delle tecniche MOR, permette di costruire iterativamente il sottospazio vettoriale e risulta perciò un approccio particolarmente potente per compensare alla *maledizione della dimensionalità* (in inglese *curse of dimensionality*).

Il lavoro di tesi si conclude con una discussione sulle domande scaturire dei nuovi contributi che potrebbero condurre a nuove ricerche nel campo della riduzione dei modelli.

Beknopte samenvatting

Dit onderzoeksproject focust op de ontwikkeling en applicatie van parametrische model orde reductie (pMOR) technieken voor de dynamische simulatie van industriële structuren. Over het algemeen beschrijven Model Orde Reductie (MOR) technieken eender welke numerieke strategie waarbij het aantal vrijheidsgraden van een numeriek model (bijv. een eindige elementen model) gereduceerd wordt. Een veelgebruikte strategie voor het reduceren van het aantal vrijheidsgraden van numerieke modellen is het gebruik van projectie-gebaseerde methodes: de vrijheidsgraden kunnen voorgesteld worden als een multi-dimensionele ruimte. En dus, een projectie van het model op een deelruimte die alle en enkel de benodigde vrijheidsgraden bevat, leidt tot een reductie van de rekenkost. De 2 voornaamste nadelen van een gereduceerd model zijn:

- De bekomen resultaten zijn niet-fysisch en moeten opnieuw terug geprojecteerd worden naar het fysieke domein voor de interpretatie.
- De deelruimte is afhankelijk van de initiële parameters van het model. Daarom is een nieuw model nodig telkens wanneer de initiële parameters geüpdatet worden.

De combinatie van deze 2 maken sommige van de beschikbare MOR technieken onaantrekkelijk voor optimalisatie studies of wanneer een parametrisch model nodig is. De ontwikkeling van pMOR technieken heeft als doel de twee eerder genoemde nadelen op te heffen of ten minste te verminderen om zo de MOR technieken parametrisch te maken. Dit is mogelijk door middel van een gedetailleerde beschrijving van de manifold die geassocieerd wordt met het parametrisch probleem in kwestie. Het eerste deel van het werk focust op de ontwikkeling van een parametrische approach voor de studie van lineaire structuren opgebouwd uit balken. De studie leidt tot een originele pMOR

aanpak die gebruikt kan worden wanneer structuren opgebouwd uit uniforme balken gesimuleerd worden. Het tweede deel richt zich op de ontwikkeling van MOR technieken die bruikbaar zijn voor poroelastische materialen. Het onderzoek brengt een parametrische benadering in het frequentiedomein die rekening kan houden met de frequentieafhankelijke karakteristieken van dit soort materialen.

List of abbreviations

1D	one-dimensional
3D	three-dimensional
BSP	block structure preserving
BT	Balanced Truncation
DGM	discontinuous Galerkin method
PUFEM	partition of unite finite element method
DOF	degree of freedom
FE	Finite Element
FEM	Finite Element Method
FOM	Full Order Model
FRF	frequency response function
GCM	generalized complex modes
GW-L	glasswool layer
H-L	heavy layer
ID	identifier
LS	least square
MIMO	multiple input multiple output
MOR	Model Order Reduction
NVH	Noise Vibration and Harshness
PDE	Partial Differential Equation
PEM	poroelastic material
PEM-L	poroelastic layer
PMOR	parametric model order reduction
POD	Proper Orthogonal Decomposition
RB	reduced basis (method)
ROB	reduced order basis
ROM	reduced order model
SVD	singular value decomposition
SEA	statistical energy analysis
TF	transfer function
$u - U$	displacement-displacement
$u - p$	displacement-pressure
WBM	wave based method

List of Symbols

\mathcal{A}	system matrix
C	damping matrix
c_0	sound speed
E	Young modulus
G	shear modulus
$[\tilde{\mathbf{H}}]$	kinetic energy matrix PEM fluid phase
J	warping shape factor
J_x	rotational inertia
K	stiffness matrix
k	form factor for shear
K_b	bulk modulus of skeleton
K_f	bulk modulus of the fluid
K_s	bulk modulus of the solid material
$[\mathbf{K}]$	stiffness matrix PEM solid phase
$[\tilde{\mathbf{M}}]$	mass matrix PEM solid phase
N	second Lamé coefficient
N_h	number of DOF in high fidelity model
n_s	nuber of snapshots
P	elastic Biot coefficient
Q	elastic Biot coefficient
$[\tilde{\mathbf{Q}}]$	compression energy matrix PEM fluid phase
R	elastic Biot coefficient
\mathbb{S}	snapshot matrix
s_i	snapshot vector
\mathbb{U}	left singular matrix
V	orthonormal vectorial space
x	state vector
Z	right singular matrix

Greek symbols

$\tilde{\alpha}$	tortuosity
∇	nabla operator
δ_{ij}	Kronecker delta
ε_{POD}	threshold truncation POD
θ^f	dilatation of the fluid
θ^s	dilatation of the frame
λ_j	eigenvalue
Φ	left projection space - orthogonal space
Λ	characteristic viscous length
Λ'	characteristic thermal length
η	structural loss factor
μ	system parameters
$\rho_{\#}$	mass density
Σ	matrix of singular values
σ	flow resistivity ¹
σ_{ij}^f	stress tensor of the fluid
σ_{ij}^s	stress tensor of the solid
$\underline{\underline{\sigma}}$	stress tensor
Υ	vector of POD DOF
v	left singular vectors
ϕ	porosity
Ψ	orthonormal space - right projection space - reduced order basis
ω	frequency

Contents

Abstract	iii
Sommario	v
Contents	xiii
List of Figures	xvii
List of Tables	xxiii
1 Introduction	1
1.1 Context and motivation	2
1.2 Research objectives	7
1.3 Research approach	8
1.3.1 Model order reduction	9
1.3.2 Projection	10
1.3.3 Reduced Order Basis generation	11
1.4 Contributions	11
1.5 Structure of the thesis	12
2 State of the art on MOR techniques for linear second order systems	15

- 2.1 Structural dynamics and acoustics models 15
 - 2.1.1 systems representation 17
 - 2.1.2 Efficient Parametric Model Order Reduction 19
 - 2.1.3 Model Order Reduction techniques
in structural dynamics 24
- 2.2 Poroelastic Materials modelling and simulation 32
 - 2.2.1 Poroelastic materials modelling 32
 - 2.2.2 Poroelastic Finite Element model 36
 - 2.2.3 Other approaches 37
 - 2.2.4 Model Order Reduction techniques for Poroelastic
materials 38
- 2.3 Conclusions 43
- 3 Efficient Parametric Model Order Reduction 45**
 - 3.1 Derivation of affine models 45
 - 3.1.1 Intrusive approach 46
 - 3.1.2 Non-intrusive approach 47
 - 3.2 Derivation of global Reduced Order Basis 48
 - 3.2.1 POD-SVD approach 49
 - 3.2.2 Modal-SVD approach 51
 - 3.2.3 Modal-greedy approach 52
- 4 Model Order Reduction of Poroelastic Materials components 57**
 - 4.1 The proposed technique 58
 - 4.1.1 Projection of the system 59
 - 4.1.2 Affine representation of the Biot equations 60
 - 4.1.3 Reduced order basis generation 62
 - 4.2 Simulations 63

4.2.1	Surface impedance of a single PEM layer	63
4.3	Conclusions	67
5	Applications to systems with poro-elasto-acoustic coupling	69
5.1	Modelling of poro-elasto-acoustic problems	69
5.2	Reduction scheme	71
5.3	Results	72
5.3.1	Multilayer system containing PEM	72
5.3.2	Air cavity with surface absorption by means of an insulation liner	81
5.4	Conclusions	86
6	Multi-parameter study on vibroacoustic systems containing poroe- lastic materials	89
6.1	Preliminary study on a single layer of PEM layer	90
6.2	Flow resistivity variations in the PEM layer of a trim component connected to an acoustic cavity	92
6.2.1	ROB generation for a 2-dimensional parametric space	92
6.3	Results	95
6.4	conclusions	102
7	Model Order Reduction of Lattice Girder	104
7.1	Introduction	105
7.2	Affine representation for beams	105
7.3	Case study	111
7.3.1	Preprocessing and detailed parametric model generation	114
7.3.2	PMOR using the Modal-SVD approach	116
7.3.3	PMOR using the greedy algorithm	119
7.4	Conclusions	122

8 Conclusion	125
8.1 Discussion	125
8.2 Future research	128
Bibliography	131
Curriculum Vitae	141
List of publications	143

List of Figures

1.1	Computational science, together with theory and experiments, is now recognized as fundamental discipline for scientific development.	2
1.2	The McKinsey Digital Compass maps Industry 4.0 levers to the 8 main value drivers [3]. The figure shows how Industry 4.0 . . .	3
1.3	Examples of beam networks.	7
1.4	Use of poroelastic materials in automotive. Highlight of the carpet of a passenger vehicle.	8
4.1	PEM layer used for the surface impedance problem [49].	64
4.2	Trend of the singular value for the snapshot matrix of the problem depicted in figure 4.1. The horizontal dashed line shows the truncation threshold.	65
4.3	Surface Impedance of a semi-infinite layer of PEM calculated with a ROM and with the direct solution of the FE simulation.	66
5.1	Elements at the interface between the elastic heavy layer and the PEM layer.	70
5.2	Continuity condition imposed using the partitioning method. The procedure results in a condensation of the linearly dependent DOF at the interface.	71
5.3	Multilayer system: a heavy layer and a foam layer clamped on a rigid wall	73

5.4 Patch pressure transfer functions for a pressure excitation of first patch. The graph on top shows the transfer functions, the graph at the bottom shows the difference in dB between the ROM and the FE used as reference. ■■ refers to patch 1; ■■ refers to patch 2; ■■ refers to patch 3; ■■ refers to patch 5; ■■ refers to patch 6. The light grey continuous lines in the graph on top are the transfer functions calculated with the FE model. 74

5.5 Patch velocity transfer functions for a pressure excitation of first patch. The graph on top shows the transfer functions, the graph at the bottom shows the difference in dB between the ROM and the FE used as reference. ■■ refers to patch 1; ■■ refers to patch 2; ■■ refers to patch 3; ■■ refers to patch 5; ■■ refers to patch 6. The light grey continuous lines in the graph on top are the transfer functions calculated with the FE model. 75

5.6 Patch velocity transfer functions for a velocity excitation of first patch at the bottom of the foam layer. The graph on top shows the transfer functions, the graph at the bottom shows the difference in dB between the ROM and the FE used as reference. ■■ refers to patch 1; ■■ refers to patch 2; ■■ refers to patch 3; ■■ refers to patch 5; ■■ refers to patch 6. The light grey continuous lines in the graph on top are the transfer functions calculated with the FE model. 76

5.7 Patch pressure transfer functions for a velocity excitation of first patch at the bottom of the foam layer. The graph on top shows the transfer functions, the graph at the bottom shows the difference in dB between the ROM and the FE used as reference. ■■ refers to patch 1; ■■ refers to patch 2; ■■ refers to patch 3; ■■ refers to patch 5; ■■ refers to patch 6. The light grey continuous lines in the graph on top are the transfer functions calculated with the FE model. 77

5.8 Computational gain obtain with the MOR approach (dashed line) presented against the FE simulation (solid line). The total computaional costs of the ROM for 1000 frequency lines of the reconstruction of the transfer functions are 12× cheaper than the costs of the FOM. 79

5.9 Multilayer system: a heavy layer and a foam layer clamped on a rigid wall. 81

- 5.10 Reducibility assessment. Decay of the singular values for increasing number of snapshots. Increasing the number of snapshots brings to a change in the decaying rate of the singular values indicating a satisfactory amount of information. The horizontal dashed line shows the truncation threshold. ■ 80 snapshots; ■ 120 snapshots; ■ 140 snapshots; ■ 150 snapshots. 82
- 5.11 Simulation results of the system in figure 5.9. Mean squared pressure $\langle \bar{P} \rangle$ in the air cavity and pressure at receiver location p_r . The solid grey lines in the top graph refer to the direct simulation of the FE model. The dashed black lines refer to the ROM. The graph at the bottom represents the difference in decibel between direct FE results and ROM results. 83
- 5.12 Simulation results of the system in figure 5.9. Mean squared velocities of the heavy layer $\langle \bar{V}_{HL} \rangle$ and of the aluminium plate $\langle \bar{V}_P \rangle$. The solid grey lines in the top graph refer to the direct simulation of the FE model. The dashed black lines refer to the ROM. The graph at the bottom represents the difference in decibel between the FE results and the ROM results. 84
- 5.13 Nodal normal velocities of a cut-through of PEM at $4.67mm$ from the interface with the plate. This motion pattern corresponds to the system resonance at 200 Hz (figure 5.11). 85
- 6.1 Surface impedance for variations of the flow resistivity in range $[2e4 \ 5e4] Pa \ m^{-1}s$ and in the frequency range $[300 \ 1300] Hz$. The red lines refer to $\sigma = 5e4 Pa \ m^{-1}s$; the blue lines to $\sigma = 4e4 Pa \ m^{-1}s$; the green lines to $\sigma = 3e4 Pa \ m^{-1}s$; the violet lines to $\sigma = 5e4 Pa \ m^{-1}s$; dashed lines refer to imaginary part, solid lines to real part. In grey scale are the solution obtained with the ROM that appear to lose some accuracy only in the higher frequency range. 91
- 6.2 Decay of the singular values for different numbers of snapshots to generate a POD basis to include variations of the flow resistivity in the range $[5e4 \ 1.2e5] Pa \ m^{-1}s$ with random sampling and in the low frequency range up to 1000 Hz with the stratified sampling. ■■ 800 snapshots; ■■ 720 snapshots; ■■ 640 snapshots; ■■ 560 snapshots; ■■ 480 snapshots. 93

- 6.3 Decay of the singular values for different number of snapshots to generate a POD basis to include variations of the flow resistivity in range [$5e4$ $1.2e5$] $Pa\ m^{-1}s$ with 4 master values and in the low frequency range up to $1000\ Hz$ with stratified sampling. ■■ 720 snapshots; ■■ 640 snapshots; ■■ 560 snapshots; ■■ 480 snapshots; ■■ 320 snapshots. 95
- 6.4 Simulation results of the system in figure 5.9 for flow resistivity of the PEM layer $\sigma = 5e4\ Pa\ m^{-1}s$ using the ROB of section 6.2.1. Mean squared pressure $\langle \bar{P} \rangle$ in the air cavity and pressure at receiver location p_r . The solid grey lines in the top graph refer to the direct simulation of the FE model. The dashed black lines refer to the ROM. The graph at the bottom represents the difference in decibel between direct FE results and ROM results. 96
- 6.5 Simulation results of the system in figure 5.9 for flow resistivity of the PEM layer $\sigma = 9e4\ Pa\ m^{-1}s$ using the ROB of section 6.2.1. Mean squared pressure $\langle \bar{P} \rangle$ in the air cavity and pressure at receiver location p_r . The solid grey lines in the top graph refer to the direct simulation of the FE model. The dashed black lines refer to the ROM. The graph at the bottom represents the difference in decibel between direct FE results and ROM results. 97
- 6.6 Simulation results of the system in figure 5.9 for flow resistivity of the PEM layer $\sigma = 12e4\ Pa\ m^{-1}s$ using the ROB of section 6.2.1. Mean squared pressure $\langle \bar{P} \rangle$ in the air cavity and pressure at receiver location p_r . The solid grey lines in the top graph refer to the direct simulation of the FE model. The dashed black lines refer to the ROM. The graph at the bottom represents the difference in decibel between direct FE results and ROM results. 98
- 6.7 Simulation results of the system in figure 5.9 for flow resistivity of the PEM layer $\sigma = 12e4\ Pa\ m^{-1}s$ using the ROB of section 6.2.1. Mean squared pressure $\langle \bar{P} \rangle$ in the air cavity and pressure at receiver location p_r . The solid grey lines in the top graph refer to the direct simulation of the FE model. The dashed black lines refer to the ROM. The graph at the bottom represents the difference in decibel between direct FE results and ROM results. 99

- 6.8 Simulation results of the system in figure 5.9 for flow resistivity of the PEM layer $\sigma = 9e4 Pa m^{-1}s$ using the ROB of section 6.2.1. Mean squared pressure $\langle \bar{P} \rangle$ in the air cavity and pressure at receiver location p_r . The solid grey lines in the top graph refer to the direct simulation of the FE model. The dashed black lines refer to the ROM. The graph at the bottom represents the difference in decibel between direct FE results and ROM results. 100
- 6.9 Simulation results of the system in figure 5.9 for flow resistivity of the PEM layer $\sigma = 11e4 Pa m^{-1}s$ using the ROB of section 6.2.1. Mean squared pressure $\langle \bar{P} \rangle$ in the air cavity and pressure at receiver location p_r . The solid grey lines in the top graph refer to the direct simulation of the FE model. The dashed black lines refer to the ROM. The graph at the bottom represents the difference in decibel between direct FE results and ROM results. 101
- 7.1 Cross-sectional surface partitioning [91]. The portions indicated as flange are those where most bending energy is absorbed. The shear is dominant in the web. The notation comes from the *I*-shaped cross-section and it is used analogously for the hollowed rectangular cross-section [96]. 109
- 7.2 Gantry bridge of the laser-cutting machine [91]. 112
- 7.3 Gantry bridge of the laser-cutting machine [91]. 113
- 7.4 Cross-sections used in the model. Cross-section a) is rectangular of dimensions h and w , b) and c) are squared of edge h and w respectively. The wall-thickness t is the same for all the three cross-sections. 113
- 7.5 Configuration of the motor. Collocated FRF. The representation is split in two. Above the Transfer Function (TF) obtained with the matrices of Nastran is plotted with the TF obtained with the unreduced parametric mode [91]. 115

7.6 Comparison on the frequency response function located at the laser head. The parametric FE model is used as reference. The FRF are calculated on two configuration points where ROB used for the PMOR are retrieved and the comparison is given at an intermediate point where the local ROB is not available. [91]. 117

7.7 Relative error plots for different parameter combinations in the region of interest. The lowest 3 frequencies are evaluated as they are dominated by the bending behaviour who is the most important for the application of this example. In each row of the table, the parameter h is held constant. The parameters t and w are used as variable in each graph. The surface shows the evolution of the relative error. [91]. 118

7.8 The prism represents the parameter domain that is gridded and used to construct the global ROB through the greedy algorithm presented in section 3.2.3. The enumerated points represent the parameter configuration selected by the greedy algorithm at each iteration [82]. 119

7.9 Normalised value of the actual error and of the residual at each iteration [82]. 120

7.10 Collocated frequency response functions of the gantry bridge at the centre point where the load is imposed. Each response function line is generated using the ROM and corresponds to a different parameter configuration in the range of interest [82]. . 121

7.11 Error distribution for the FRF plotted in figure 7.10. $e(\omega) = \left| \frac{y_{ROM}(\omega) - y_{FOM}(\omega)}{y_{FOM}(\omega)} \right|$ [82]. 121

List of Tables

4.1	Material Parameters of glasswool layer	64
5.1	Parameters of the materials in the trim component; glasswool layer (GW-L), aluminium plate, poroelastic layer (PEM-L), heavy layer (H-L), rigid air cavity.	80
5.2	Calculation time for the HFM and for the ROM. The simulation ran on Python 3.5 and on an Intel(R) Core(TM) i5-4310U CPU 2.00GHz 2.60GHz	86
7.1	Example of affine functions derived for a beam with hollow rectangular cross-section [91].	111
7.2	List of functions retrieved according to table 7.1 and derived unique monomials [91].	114
7.3	List of functions retrieved according to table 7.1 and derived unique monomials [91].	116
7.4	Calculation time for the HFM and from the ROM based on the Modal-SVD ROB. The simulation run using Matlab R2015b on an Intel(R) Core(TM) i5-4310U CPU 2.00GHz 2.60GHz	117

Chapter 1

Introduction

Technological development is driven more often by optimisation processes than by groundbreaking inventions and products. This kind of innovation requires profound knowledge of the systems and of the effects of any perturbation to its initial status in order to be able to generate improvements. This knowledge can be provided by *theory, experiments and simulations*. Measurements and experiments can offer an accurate representation of the real physical problem but usually at high costs. Simulations, on the other hand, can describe idealized problems that can be adapted to any level of detail: a high degree of flexibility at a low cost with respect to experiments. In the last decades, performing simulations has become so important that is now considered one of the pillars of scientific development, on the same level of theory and experiments [1, 2] (figure 1.1). Their use is also beneficial for reducing the costs for industry by significant amounts increasing the operational margins for success in the market. It is appreciable how the *time to market* of new products has reduced over the years especially thanks to simulations that, without extra costs, reproduce the performance of dozens of different configurations allowing more robust optimisation of the products. The last frontier of simulation is in the industry 4.0, where sensors, actuators and models are integrated to communicate and interact. This can provide further enhancing of performance and personalization of services and products (see figure 1.2).

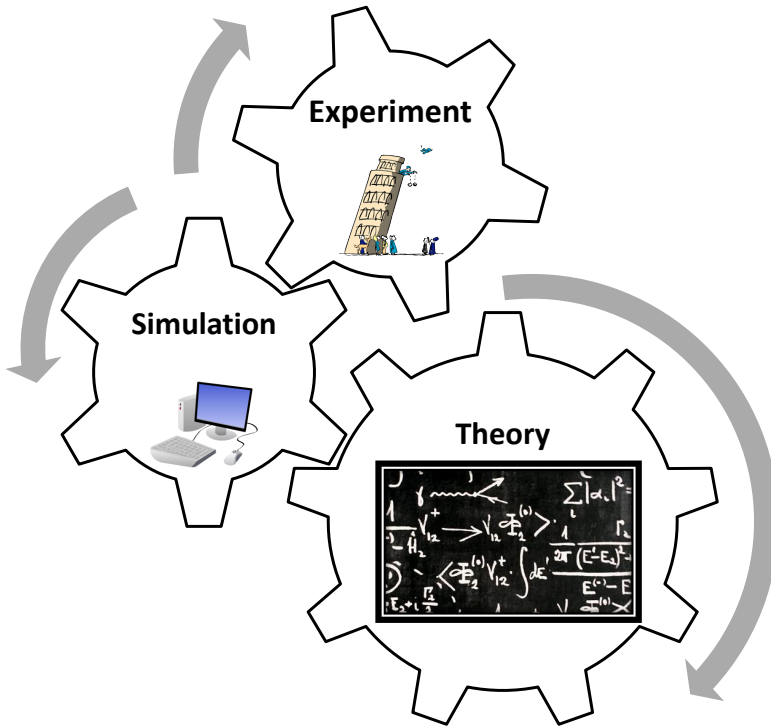
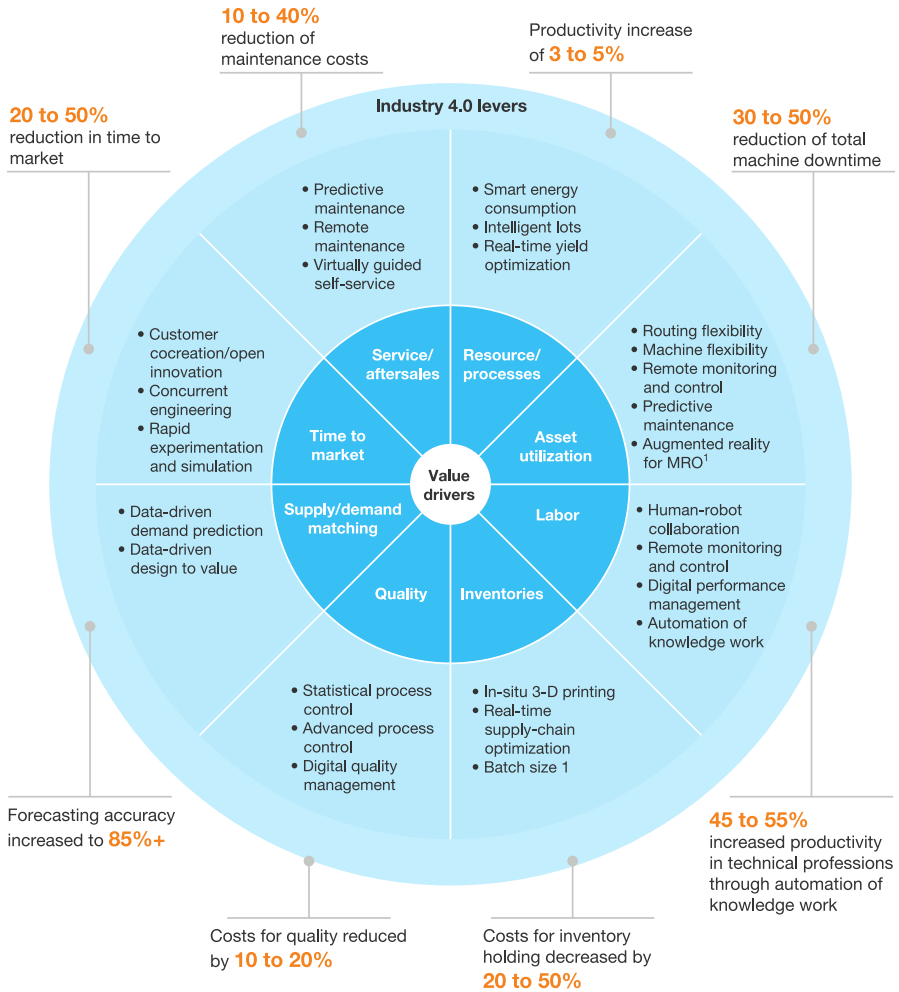


Figure 1.1: Computational science, together with theory and experiments, is now recognized as fundamental discipline for scientific development.

1.1 Context and motivation

Virtual models allow cheap analysis of different designs before production or to virtually measure quantities otherwise not accessible in real measurement set-ups. This ability of simulations opens new important possibilities for the engineers.

However, simulation requirements appear to grow with the same trend of computational capabilities and they reached a point where large global and multi-domain systems have to be analysed. As a matter of fact, integrated multi-domain design is becoming relevant in industry. For example, in optimisation strategies, industry is experiencing the steps from component-level



¹Maintenance, repair, and operations.

Source: "Industry 4.0: How to navigate digitization of the manufacturing sector," McKinsey Digital, 2015
McKinsey&Company

Figure 1.2: The McKinsey Digital Compass maps Industry 4.0 levers to the 8 main value drivers [3]. The figure shows how Industry 4.0

to system-level optimisation. Nevertheless, to be able to perform multi-query problems such as optimisation procedures, the computational costs of the simulations of these large models should be kept low.

In this context, *Model Order Reduction* (MOR) techniques have been developed. MOR techniques enable the compression of large models to generate new *Reduced Order Models* (ROM) that are fast to provide solutions with accuracy comparable to that of high fidelity models.

The capabilities of MOR are not only of great use in system-level modelling, but they can be of great use for what is known as *virtual sensing* and design optimisation problems. In virtual sensing, simulations and measurements run in parallel to provide new information that go far beyond the possibilities of both conventional measurements and simulations. Measurements can feed complex models that can be used to control the system and to make it adaptable to the current situation. This can extend enormously the possibilities of the products in the digital era. In this framework, MOR finds its place in boosting the computational performances of simulations allowing for the access in short time to a high number of quantities with a high degree of accuracy. Optimization studies, that require the exploration of large parameter spaces (e.g., Montecarlo simulations [4]), can be improved by MOR techniques even when they involve multiple sub-systems combined together (e.g. mechanical and its control system [5, 6, 7]).

Model Order Reduction is now a general term and accounts for techniques that can be very different from one another. For this reason, MOR techniques are classified according to their characteristics: whether they work in frequency or time domain; whether they are for linear or nonlinear problems; whether they work *a priori* or *a posteriori* [8].

One first distinction is done between techniques labelled as *a-priori* and those labelled as *a-posteriori*. The a-priori are those that create a reduced model without recurring to previous knowledge from existing models (e.g. the Proper Generalized Decomposition (PGD) [9]). A-priori techniques are not considered in this research and will not be discussed further. A-posteriori techniques are those techniques that require knowledge from existing models or from measured data.

A-posteriori MOR techniques typically apply to existing discretised models that contain a lot of details and are, therefore, very slow to solve. Discretised models are expressed as matrices and have become a typical approach to simulation since the first appearance of digital computers. Hence, *big model* also reads as *large matrix* and matrices can be reduced in dimension using

projection methods that are at the basis of the most popular MOR techniques.

The aim of a projection-based MOR technique is to find a sub-space of low dimensionality that still contains the solutions of the original large model. To the development of these techniques contributed mathematicians, engineers, physicists and computer scientists. Therefore, it is quite common to find the same technique under different names [10, 11] and different classifications exist according to the different communities. MOR techniques developed for structural dynamics and acoustics, that is the field of the applications of this thesis, are typically divided in frequency and time domain approaches. However, these categorizations do not always make sense for MOR techniques as, for example, methods that are typically used for the time domain can be proposed in the frequency domain (if they show to provide better performances).

This thesis will tackle frequency domain problems and will focus on *a posteriori* approaches (not necessarily confined to frequency domain methods) based on projection of a discretized model. Of the many discretization techniques available (e.g. finite element method, finite difference, boundary elements method, Trefftz methods), this article will employ only models based on the Finite Element Method (FEM). The FEM requires to construct a mesh of nodes over the domain and to find approximated solutions in between these nodes using shape functions that fulfil the requirements of boundary and initial conditions and minimize the residual in the differential equations to be solved. This allows a high level of flexibility and applicability on a large number of industrial problems. The bottleneck is very often the lack of computational power for large simulations. Also in the field of *Noise Vibration & Harshness* (NVH), FE simulations are an important tool in all sorts of acoustic and vibrational prediction. These FE models appear often to be large and slow; in fact, as the phenomena to be simulated evolve in time (or frequency), solutions are computed at each frequency-step (or time-step) and MOR techniques would be beneficial.

Among the MOR techniques available, projection-based approaches are the special interest of this work. A projection-based MOR works in two steps: given a discretized high fidelity model (for example a FE model), step one consists in the construction of a projection basis, called *reduced order basis* (ROB); step two in the projection of the full order model on the ROB. The solution is then obtained solving the resulting reduced order model (ROM).

Albeit a projection procedure can assure a reduction of the order (in this case order refers to the number of DOF or, equivalently, to the size of the system

matrix) it does not guarantee a reduction of the total computational time. Thinking of the aforementioned optimisation problems, when many simulations of the same model are required for different configurations, the MOR methods discussed up to this point require operations with computational complexity dependent on the size of the original FOM model (e.g. when a parameter is changed, the matrices of the *Full Order Model* (FOM) and of the ROB have to be updated and, as a result, the projection has to be repeated). To cope with this fact, the so called *parametric model order reduction* (PMOR) methods are developed. These methods generate reduced matrices that are independent from the size of the matrices of the original FOM. Among the techniques available to obtain PMOR, the work on this thesis is based on the *Reduced Basis* method that is based on two main pillars: (i) affine representation of the system and (ii) generation of a global ROB. Affine (or separable) means that the the projection of the FOM can be offline and have parametric simulations of the ROM that are independent of the size of the FOM. This hypothesis constitutes the basis for the Reduced Basis (RB) method. When the affine assumption does not hold in continuum, other methods are involved to reproduce this property. For non-affine problems, an approximate affine representation can be obtained by the *empirical interpolation method* (EIM) or the discrete alternative referred to as *discrete empirical interpolation method* (DEIM) [12]. This thesis does not cover cases where EIM and DEIM are necessary and focuses the efforts on determining affine function based on theoretical considerations.

In principle, the RB method can be applied to any discretised model but not always it can guarantee computational advantages. Therefore in this thesis, the focus will be tailoring the RB method to some classes of problems that can benefit from its application. These are models containing poroelastic materials and models of interconnected beams.

Many authors worked on MOR applications to models of PEM that showed to be a difficult task. The big challenge for these methods was to account for the nonlinearities of the parameters that characterize them and led to not fully satisfactory trade-off between accuracy and efficiency of the simulation.

The applications of RB method to simulate models of interconnected beams could provide useful support in early phase design of lattice structures especially in view of combined optimisation of structures and control units as in the work of [5, 6, 7].

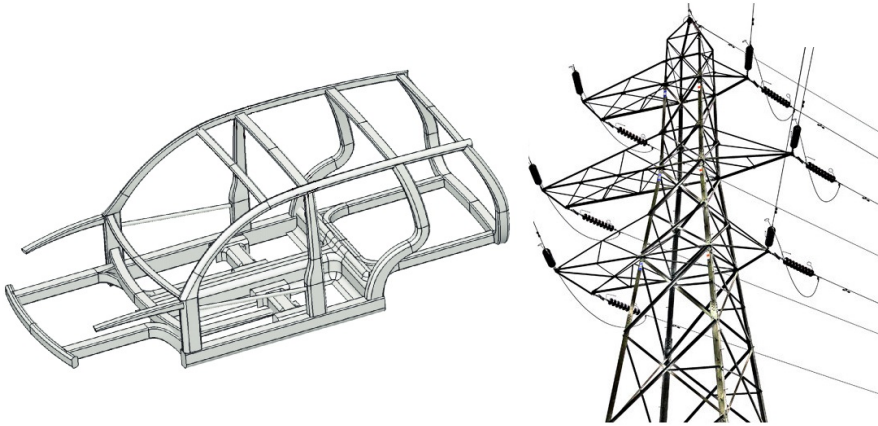


Figure 1.3: Examples of beam networks.

1.2 Research objectives

There are many fields of application that can benefit from further development of RB methods [10, 13, 14]. In this thesis, the chosen fields of application are linear vibroacoustics with higher focus on systems with nonlinear dependencies on the parameters and/or on the frequency. Many industries could benefit from the implications of these findings; hence, representative models that will be familiar to many have been chosen. The main two systems analysed in the thesis are lattice girders and poroelastic materials. The lattice girder and, more in general, beam-based structures can be identified as a constitutive structure of many machines like cars, cranes, transmission towers ecc. (figure 1.3). Poroelastic materials are used in all field of industry mainly as noise- and thermo-absorbers (figure 1.4). In fact, they respond to dynamic excitations with strong interactions between their two phases (solid and fluid) that produces a strong dissipation of the propagating waves [15].

The main objective of the thesis is to develop computationally efficient and accurate models for this group of problems developing and employing *parametric model order reduction* (PMOR) techniques. The tools developed should be designed in view of being used for optimisation procedures, virtual sensing, co-simulation or real-time simulations.

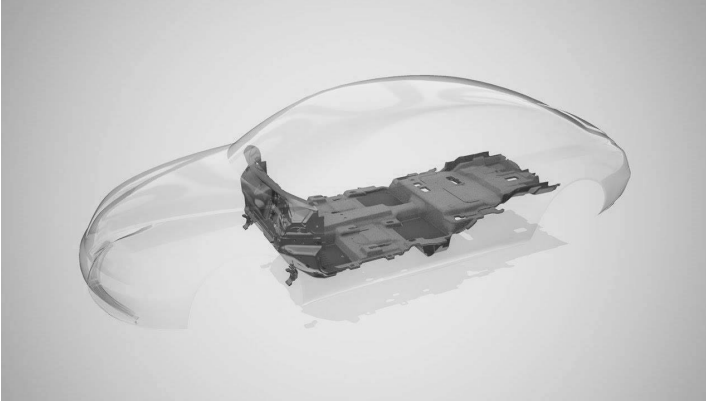


Figure 1.4: Use of poroelastic materials in automotive. Highlight of the carpet of a passenger vehicle.^a

^athe owner of the picture is Autoneum, <https://www.facebook.com/autoneumgroup/photos/pcb.2035574226673621/2035573880006989/?type=3&theater>

1.3 Research approach

In the text, the development of PMOR is indicated as the overall goal. This is obtained applying the RB method and looking at the MOR techniques available for reduction of the classes of problems chosen for the analysis. In this case and in the rest of the thesis, MOR refers only to the techniques to generate a ROB for a non-parametric system, e.g., to a model with frequency-dependent (or time-independent) characteristics simulated in the frequency (or in time) domain for a given configuration of the parameters. PMOR differs from a standard MOR for the ability to take account of parameter variations in the simulation process without recurring to operations with computational complexity that depends on the original size of the problem. The two challenges to address are: the construction of suitable ROB to describe the model in all its configurations; the representation of the system using the *affine parametric dependence* assumption.

In this thesis, ROB of classical MOR are labelled as *local* while those of PMOR as *global* having as objective of the work the development of suitable global ROB in the most efficient way and for different classes of problems.

As discussed in the introduction, the RB approach is based on the hypothesis of affine parameter dependence [13] that brings the other objective of this work: finding analytical and closed form affine representations of the systems thus

avoiding approximations (e.g., polynomial expansions). This representation enables the implementation of ROM whose range of validity depends only on the quality of the ROB used for the projection of the FOM.

The class of *high fidelity models* chosen to cope with the goals of the thesis are a modular network of beams and vibroacoustic simulations of systems containing poroelastic materials. The network of beams is considered to be in the linear-elastic revealing a good example for systems where the RB method can apply based on the affine assumption. The beam-elements are characterized by geometrical and material parameters whose dedicated theory (from Bernoulli to Timoshenko) put together in closed form to define stiffness and mass distribution. Once the affine representation of the system is determined, the research focuses entirely on approach to generate appropriate ROB to improve the accuracy and performance of ROM.

Similarly to the beam case, poroelastic materials are supported by robust theories that can allow for affine representation. Moreover, the literature on MOR applied to these systems, appears to have some gaps that are intended to be filled by the implementation of the RB method.

In both cases, the FEM will be employed for the construction of the high-fidelity models (HFM).

1.3.1 Model order reduction

The part of Model Order Reduction of interest for this thesis is that based on projection. This introductory section is to describe the main aspects of projection-based MOR.

MOR procedures consist of a few operations that are:

- (i) generation of a Full Order Model (FOM);
- (ii) generation of the global ROB;
- (iii) projection of the FOM on the subspace spanned by the ROB to generate a ROM;
- (iv) resolution of the ROM.

These operations can be executed offline (executed only once in the preprocessing) or online (executed during the simulation). In classical MOR, all these operations are executed for each different configuration of the system

i.e. all the operations are executed online. The effort of a PMOR approach is to execute most of the computational effort off-line with the ideal implementation when operations (i-iii) are all made offline and only operation (iv) is performed online.

In the following sections, these operations are examined to build the basis for understanding and developing PMOR techniques.

1.3.2 Projection

Projection methods are used to convert vectors from one coordinate system to another. They are therefore important tools in the field of MOR where they are used to extract approximations for solutions of large linear systems [16]: large part of the MOR methods project the system equations onto subspaces of compact dimensions therefore reducing the computation time of the solution (i.e. the matrix operations required have computational complexity proportional to the size of the new sub-space and not to the former larger space).

The use of projection techniques to transform a system requires two subspaces: the *projection subspace* (or right subspace), used to approximate the solution, and the *subspace of constraints* (or left subspace), that is chosen to be orthogonal to the residual introduced by this approximation.

Given an elasto-dynamic system in matrix form

$$Kx + C\dot{x} + M\ddot{x} = Bf_b, \quad (1.1)$$

the vector of motion x can be projected on a new sub-space represented by a matrix $\Psi \in \mathbb{R}^{n \times q}$. The vector of motion is thus represented as a linear combination of the vectors of this subspace

$$\hat{x} = \Psi x_r. \quad (1.2)$$

Vector $x_r \in \mathbb{R}^{q \times 1}$ is the new state vector and contains the coefficients of the linear combination (its components are referred to as modal participation factors when a modal reduction is applied).

If the column span identified by Ψ in equation (1.2) is not complete (and most of the times it is not in order to produce the reduction), this operation

introduces an approximation. As a result, using \hat{x} in equation (1.1) produces a residual term $r = K\hat{x} + C\dot{\hat{x}} + M\ddot{\hat{x}} - Bf_b$. A subspace of constraints spanned by Φ is then needed such that $r \perp \Phi$ (i.e. the projection of the residual on Φ is 0).

$$\Phi^T K \Psi x_r + \Phi^T C \Psi \dot{x}_r + \Phi^T M \Psi \ddot{x}_r = \Phi^T B f_b \quad (1.3)$$

This two-sided approach is called *Petrov-Galerkin* projection and is an oblique projection. When $\Phi = \Psi$ the Petrov-Galerkin condition is called Galerkin condition and is said to be an orthogonal projection [16].

For the work presented in this book, Galerkin projections are used.

It should be noted that any parameter change in the equation (1.3) requires operations with computational complexity proportional to the size of the FOM i.e. if the system matrices K, M, C and B are affected by the parameter changes, they should be updated and projected again at each new simulation.

1.3.3 Reduced Order Basis generation

MOR techniques based on projection require a short note on what are the possibilities to generate Reduced Order Bases (ROB). Many techniques exist and they are often sorted in different categories [8, 17]. These categories may help the user in the choice of the method to adopt but, considering that their characteristics can overlap to a certain extent, knowledge of the available techniques is necessary for the selection of the most suitable one for a given problem.

1.4 Contributions

This work contributes to the development of reduced basis method applied to two classes of problems: acoustics simulation of systems containing poroelastic materials and structural dynamic problems of beam networks.

In chapter 3, the contributions are gathered and presented without a link to a specific problem. In fact, all of these approaches are expected to be adaptable to different sort of dynamic problems.

In chapter 4 and 5, the contributions are related to applicative acoustic problems that include sound absorbing material and in particular PEM. The equations that describe the behaviour of these materials are nonlinearly dependent on the frequency; thus, this work proposes a new approach for reduction based on the reduced basis method that accounts for these nonlinearities at low computational cost. The method is applied not only on simplified models of single PEM blocks but also to larger multilayer systems with and without an air cavity connected. These examples show the flexibility and applicability of the method that could be of support for optimisation techniques and even larger simulations.

In chapter 7, the contributions are linked to the development of parametric model order reduction for network of beams. In this case, the affine representation involves the geometrical parameters of the cross-sections of the beam elements that compose the structures. Euler-Bernoulli and Timoshenko beam theory are rearranged in the FOM to get the required affine representation for the system matrices. Moreover, the global ROB is obtained combining MOR based on modal bases to the adaptiveness of the greedy algorithms.

1.5 Structure of the thesis

State of the art

In this chapter, the equations modelling the problems investigated in the thesis are recalled. These are structural dynamics and acoustic equations and the equations that describe the vibroacoustic behaviour of poroelastic materials. Moreover, the chapter lists some of the most relevant *model order reduction* techniques for the specific problems of interest.

Efficient Parametric Model Order Reduction

Chapter 3 resumes the scientific contributions of this work. It shows how to implement Reduced Basis methods for different classes of problems and using affine parametric functions based on the theory of the physical phenomena they represent.

The chapter is divided in two parts. The first part deals with approaches for the derivation and use of affine functions for parametric problems. The second part illustrates some techniques to retrieve global ROB.

Model Order Reduction of Poroelastic materials components

Chapter 4 shows the development of a PMOR strategy for acoustic problems involving Poroelastic Materials (PEM). The modelling of PEM has to take account for the complex interactions occurring between their fluid and solid phase that, when approached with discretization techniques, can lead to large and computationally expensive simulations.

The proposed technique applies to FE models of PEM based on the mixed u - p formulation, unlike most of the previous MOR methodologies that are based on the u - U formulation. Moreover, the proposed technique can account for the frequency nonlinearities of the Biot equations. Together with the high level of accuracy, the method shows high computational performances with respect to other techniques.

PMOR applied to vibroacoustic models of multilayer systems containing poroelastic materials

Chapter 5 contains some vibroacoustic simulations of systems containing trim materials and PEM. The work done in this chapter shows that the approach developed for the simple case of chapter 4, where only small models were used, can be applied to larger models where the PEM is coupled to different layers of other materials and to an air cavity. This complexity is added in order to reproduce a realistic scenario.

Multi-parameter investigations in vibro-acoustic systems containing poroelastic materials

Chapter 6 exploits the implementation of 5 to originate a parametric ROM that accounts for variations of the flow-resistivity. The study shows what are the limitations of the method and underlines the choices that can determine its success or failure.

Model Order Reduction of Lattice Girder

Chapter 7 focuses on the development of PMOR techniques for elastodynamics problems showing applications on a lattice girder.

The chapter employs the adaptive technique presented in chapter 3 that combines a greedy algorithm to MOR based on modal bases. The greedy algorithm exploits the residuals of the eigenvalue equation associated to the elastodynamic problem to estimate the error and refine the ROB.

Chapter 2

State of the art on MOR techniques for linear second order systems

This chapter puts the contribution of this work into its scientific frame. A general introduction to the equations that model the behaviour of the systems targeted in this thesis is given as well as the descriptions of some of the most common methods for the generation of ROB. The chapter then gives an overview on problem-specific modelling methodologies most relevant for this work: on the one hand linear structural dynamics simulations (represented by the network of beams in the numerical examples), on the other hand proelastic materials and acoustic simulations.

2.1 Structural dynamics and acoustics models

The research presented in this thesis aims at the development of MOR techniques and requires to set up and perform simulations. In this section, the modelling of two kinds of problems are investigated: structural-dynamics problems and acoustics problems. Some of the typical representations used for these models are introduced and in the last subsection, the MOR methods most commonly used in this field are shortly described.

Structural-dynamics modelling

Linear structural problems can be modelled by writing together the law of momentum conservation, the material constitutive law and proper boundary conditions. These are

$$\underline{\nabla} \cdot \underline{\sigma} + F_b = \rho_s \frac{\partial^2 u}{\partial t^2} \quad \text{in } \Omega, \quad (2.1)$$

$$\underline{\sigma} = \mathbf{C} \varepsilon, \quad (2.2)$$

$$\underline{\sigma} \underline{n} = \underline{F} \quad \text{in } \partial\Omega_1 \quad (2.3)$$

$$\underline{u} = \underline{u}_b \quad \text{in } \partial\Omega_2 \quad (2.4)$$

In these equations, $\underline{\sigma}$ being the stress tensor, ρ_s the density of the body, F_b the body force vector, u the displacement of the body, \mathbf{C} is the fourth order elastic tensor representing Hooke's law and \underline{F} the prescribed load on the boundary. Ω represents the domain of validity for the equation (2.1), while $\partial\Omega_1$ and $\partial\Omega_2$ represent respectively the portions of boundary where the Neumann condition of equation (2.3) is valid and where the Dirichlet condition of equation (2.4) is valid. $\underline{\nabla}$ indicates the *nabla operator* [18].

The first term in equation (2.1) indicates the divergence of the stress tensor that is in equilibrium with the summation of the external forces and the inertial forces (on the right hand side of the equation).

Acoustics modelling

In acoustic problems, acoustic wave propagations are of interest. Therefore, in addition to Newton second law, the gas law and the law of conservation of mass are required to generate the model. These yield the following model

$$\nabla^2 p(\underline{x}, t) - \frac{1}{c_0^2} \ddot{p}(\underline{x}, t) = -Q(\underline{x}, t), \quad (2.5)$$

where $p(\underline{x}, t)$ represents the acoustic pressure distribution in a fluid media characterized by density ρ_0 and speed of sound c_0 for the excitation distribution $Q(\underline{x}, t)$.

To model structural-acoustic phenomena, the interaction between structure and fluid has to be taken into account. Therefore some coupling conditions are set at the boundaries of interaction. The system has to guarantee normal displacement continuity and stress continuity at the interface that are expressed by equations (2.6) and (2.7)

$$\frac{1}{\rho_0 \omega^2} \frac{\partial p}{\partial n} = \underline{u} \cdot \underline{n} \quad (2.6)$$

$$\underline{\sigma} \underline{n} + p \underline{n} = 0. \quad (2.7)$$

Theoretical consideration allowed to generate models as in equations (2.1-2.5) and many others can be set up (e.g., the models for poroelastic materials discussed in chapter 2.2). The simulation of these models implies the discretisation of the domain to solve the model equations for smaller elements of regular shape. This discretization process can involve the time (or frequency) and/or the space (in which case we talk about mesh). As previously mentioned, this work makes use of the FEM that requires a discretisation of the full spatial domain occupied by the system under investigation.

Applying FE to the problem of equations (2.1)-(2.4) and considering viscous material properties, the following system of equations can be written

$$Kx + C\dot{x} + M\ddot{x} = Bf_b. \quad (2.8)$$

In this equation $K, C, M \in \mathbb{R}^{n \times n}$ are respectively the semi-discretised stiffness, damping and mass matrices. $x \in \mathbb{R}^n$ is the vector of nodal displacements (state vector) and $B \in \mathbb{R}^{n \times m}$ is the force application matrix for the m input forces f_b .

2.1.1 systems representation

In many cases, mathematical models are expressed such that inputs and outputs are clearly designated. For example, given a general *multiple inputs*

multiple output (MIMO) system, this can be expressed as

$$\begin{cases} \mathcal{F}(\underline{x}, \underline{u}, t) = 0 \\ \underline{y} = \mathcal{G}(\underline{x}, \underline{u}, t), \end{cases} \quad (2.9)$$

or equivalently in state space form

$$\begin{cases} \dot{\underline{x}} = \hat{\mathcal{F}}(\underline{x}, \underline{u}, t) \\ \underline{y} = \mathcal{G}(\underline{x}, \underline{u}, t). \end{cases} \quad (2.10)$$

where \underline{u} represents the input vector, \underline{x} the state vector, \underline{y} the output vector and t the time variable.

The representations of equations (2.9) and (2.10) help for a straightforward implementation of coupling between subsystems and can be also used to include information from discrete 3D simulations into 1D environments (see for example [19]).

For a *linear time invariant* (LTI) system, the state space representation in the Laplace domain can be written as

$$\begin{cases} s\mathbf{E}\underline{x} = \mathbf{A}\underline{x} + \mathbf{B}\underline{u} \\ \underline{y} = \mathbf{C}^T\underline{x} + \mathbf{D}\underline{u} \end{cases} \quad (2.11)$$

where matrix \mathbf{A} is referred to as system matrix, \mathbf{B} is the input matrix, \mathbf{C} is the output matrix, \mathbf{D} is the feedthrough matrix (that is 0 for most of the systems and all those analysed in this work) and \mathbf{E} is a descriptor matrix that in most cases is equal to the identity matrix.

The input-output relations of the second order system of equation (2.8) can be therefore expressed as

$$\begin{cases} (K + sC + s^2M)\underline{x} = B\underline{u} \\ \underline{y} = C^T\underline{x} \end{cases} \quad (2.12)$$

or equivalently

$$\left\{ \begin{array}{l} \mathbf{E} \begin{Bmatrix} \ddot{\underline{x}} \\ \dot{\underline{x}} \end{Bmatrix} = \begin{bmatrix} -M^{-1}C & -M^{-1}K \\ I & 0 \end{bmatrix} \begin{Bmatrix} \dot{\underline{x}} \\ \underline{x} \end{Bmatrix} + \begin{bmatrix} 0 \\ B \end{bmatrix} \underline{u} \\ \underline{y} = \mathbf{C}^T \begin{Bmatrix} \dot{\underline{x}} \\ \underline{x} \end{Bmatrix}. \end{array} \right. \quad (2.13)$$

2.1.2 Efficient Parametric Model Order Reduction

This chapter contains all the scientific contributions of the thesis. After an introduction of the relevant literature on the topic, the chapter proposes some new methods and techniques and goes through their features.

In recent years, parameterized MOR approaches have been developed with the aim to bring enhanced computational performances especially in the field of optimisation in a multi-dimensional parameter space [20, 21]. The scope of this section is to create a link between the MOR techniques discussed in 1.3.2 and the applications to parametric problems.

The challenges of performing an efficient reduction can be introduced considering the model of a n-DOF system expressed in matrix form in the frequency domain with light damping

$$(K + i\omega C - \omega^2 M)\underline{X} = Bf_b, \quad (2.14)$$

where $K, C, M \in \mathbb{R}^{n \times n}$ are respectively the stiffness, damping and mass matrices. $X \in \mathbb{R}^n$ is the vector of nodal displacements (state vector) and $B \in \mathbb{R}^{n \times m}$ is the force application matrix for the m input forces f_b . Looking at the frequency as the only parameter of the model, it can be seen as a parametric model and all the methods presented in section 1.3.2 would be included for a moment in the category of parametric model order reduction. In fact, those ROB would enable the calculation of solutions for any configuration of the parameter ω and without computational operations of complexity depend on the size of the matrix of the original FOM.

A more difficult scenario would be if the system matrices are also frequency dependent

$$K(\omega) - \omega^2 M(\omega) = B(\omega)f_b. \quad (2.15)$$

Applying the classical MOR approaches discussed in section 1.3.2 to such problems would require operations that depend on the original size of the FOM matrix at every frequency step. An example of this category of problem is given by the poroelastic materials (PEM) that are the topic of chapter 4. The complex nature of PEM can be described using FE models based on the Biot theory (see appendix 2.2) that are characterized by having nonlinearly frequency dependent matrices. Many scientists have tried to extend classical MOR to cope with this problem introducing substantial approximations [22, 23].

Frequency is not the only parameter that can vary in the model and more general consideration may be needed. The most general case is when the system is dependent not only on frequency but on a full set of parameters μ

$$K(\mu, \omega) - \omega^2 M(\mu, \omega) = B(\mu, \omega) f_b, \quad (2.16)$$

or also, it could be dependent only on the set of parameters μ and not on frequency

$$K(\mu) - \omega^2 M(\mu) = B(\mu) f_b. \quad (2.17)$$

Applying classical MOR techniques to the parametric problem of equation (2.16) or 2.17 could result in a cumbersome approach and PMOR represents an important step up in the simulation capabilities enabling optimisation studies, real-time simulations or virtual sensing at lower costs.

It should be noted that parameter perturbations affect at the same time the matrices of the FOM and the ROB where it is projected.

The effects of the modifications of the FOM can be dealt with differently according to the parameter dependence if it is affine (i.e. separable) or not. In the first case, approaches based on the Reduced Basis method (see section 2.1.2) appear to be a very efficient approach for PMOR. When the affine representation is not possible, other methodologies are necessary based on matrix interpolation [24, 25, 26]. An approach that has gained popularity in dealing with non affine models is the Empirical Interpolation method (EIM) and in particular its discrete version: the discrete empirical interpolation method (DEIM) [12].

The different ROB obtained at different parameter configurations cannot be interpolated in a classical sense because they are elements of a manifold.

Depending on the characteristics of this manifold different approaches can be used. An important property of the manifold is its Kolmogorov n-width. This parameter indicates how well the manifold can be approximated using an n-dimensional subspace. In particular, if the Kolmogorov n-width is small the elements of the manifold have small variations and they can all be spanned by the current global ROB. At local level (for the specific parameter configuration), the global ROB does not necessarily offer the maximum reduction but should provide the same required accuracy for all the parameter configurations of interest.

When the Kolmogorov n-width is large, the number of vectors required in the global ROB is large thus the resulting reduction will not be sufficient for the performance required and typically other approaches have to be employed. Interpolation methods for manifold are an interesting field of research as there is an open challenge in trying to keep consistency of the reduced coordinates from one ROB to another [26]. Recently [25], new PMOR techniques based on partitioning of the parameter space have been developed showing interesting potential for complex nonlinear problems. In these techniques, a good balance between the accuracy of the local ROB calculated offline and the speed of the ROB selection for the online simulation is essential. The PEBL-ROM [25] generates a partitioning of the parameter space with a bisection tree structure that gives performance advantages also in the online simulation.

In this thesis, the focus is on parametric models described by equations (2.15 - 2.17) assuming the condition of a small Kolmogorov n-width and using the RB method with a global ROB.

The construction of the ROB for a PMOR is based on the MOR techniques discussed in section 1.3.3. Particularly suitable are the proper orthogonal decomposition (POD) and the greedy algorithm. The POD fits well the RB scheme because its construction is based on solution vectors that can be obtained for any parameter configuration. When the number of parameters involved in the problem is large, the POD finds its limitations and alternatives to it have been proposed [27]. Assuming that the manifold associated with the parametric problem is of small Kolmogorov n-width, there would be a big mismatch between the number of snapshots required for the POD method (that grows exponentially with the number of parameters) and the final number of vectors in the ROB (that will not follow this growth and will remain of small size because the manifold is assumed to be small). In these cases, the ROB can be generated using sampling techniques based on greedy algorithms [27]. *Greedy algorithms* (see section 3.2.3) are iterative optimisation procedures that allow finding local minima at relatively low computational cost. They

are based on an estimation of the error distribution over the parameter space to choose the location of a new vector at each iteration.

The remainder of the chapter is organised as follows: in section 2.1.2 the reduced basis method is described: this is the base for the methods developed and discussed in the thesis. The rest of the chapter goes more in detail through the methodologies proposed; in section 3.1, the approach adopted to generate and use the closed form affine functions is presented. In section 3.2 a number of approaches for the derivation of global ROB in the frequency domain are presented.

Reduced Basis method

Reduced Basis (RB) methods focus on the generation of parametric ROM and apply to parametric partial differential equations. Detailed literature upon these methods is condensed in the book of Quarteroni et al. [13] that the interested reader should refer to.

RB methods require the model to be affine with respect to the parameters of interest and consist of an offline-online combination of operations to retrieve parametric solutions of the system. The reduced order basis (ROB) should enable reconstructing solutions over the entire parameter space.

Typical approaches to retrieve a ROB for RB methods are the POD (section 3.2.1) and greedy algorithms ((section 3.2.3)).

A system is affine with the parameters μ when the effect of these parameters on the system can be expressed by equations where parameter dependent quantities and parameter invariants can be separated. For example, given the discrete model

$$\mathcal{A}(\mu)u(\mu) = f(\mu), \quad (2.18)$$

where $\mathcal{A} \in \mathbb{R}^{n \times n}$ represents the system matrix, u represents the state vector and f a load vector, it would be possible to rewrite it as

$$\sum_{j=0}^{nf} \mathcal{A}_j f_j(\mu) u(\mu) = f(\mu) \quad (2.19)$$

where the \mathcal{A}_j are parameter independent matrices and $f_j(\mu)$ are the *affine functions*.

Given a general parametric n-DOF system in matrix form without damping

$$K(\mu)x + M(\mu)\ddot{x} = Bf_b \quad (2.20)$$

where $K(\mu), M(\mu) \in \mathbb{R}^{n \times n}$, are respectively the parametric stiffness and mass matrices, $x \in \mathbb{R}^n$ is the vector of nodal displacements and $B \in \mathbb{R}^{n \times m}$ is the force application matrix for the m input forces f_b . Using the affine representation of equation (2.19), the system matrices can then be represented as

$$\sum_{i=0}^{nf} K_i f_i^K(\mu)x + \sum_{i=0}^{nf} M_i f_i^M(\mu)\ddot{x} = Bf_b. \quad (2.21)$$

Equation (2.21), can be reduced through a Galerkin projection on the subspace spanned by the ROB indicated as $\Phi \in \mathbb{R}^{n \times q}$ with q generalized coordinates

$$\Phi^T \sum_{i=0}^{nf} K_i f_i^K(\mu)\Phi x_r + \Phi^T \sum_{i=0}^{nf} M_i f_i^M(\mu)\Phi \ddot{x}_r = \Phi^T Bf_b. \quad (2.22)$$

Thanks to the affine representation, the projection of the constant matrices can be done offline with enhancements of the computational performance. In fact, if the f_i^K and f_i^M are scalar functions, the projection will affect only the parameter independent matrices K_i and M_i . The resulting ROM is

$$\sum_{i=0}^{nf} \Phi^T K_i \Phi f_i^K(\mu)x_r + \sum_{i=0}^{nf} \Phi^T M_i \Phi f_i^M(\mu)\ddot{x}_r = \Phi^T Bf_b. \quad (2.23)$$

Equation (2.22) represents already a ROM but this implies that the projection of the full system matrices is performed in the offline phase prior to simulation. With equation (2.23), the affine representation of the system is exploited and the constant matrices K_i and M_i of equation (2.22) can be reduced offline to generate the reduced constant matrices $K_{i,r}$ and $M_{i,r}$.

Some authors have used similar implementations to the RB method using approximated affine functions. For example, in Hong et al. [28], the variation of the stiffness of a plate with respect to one geometrical parameter is described

without the need of interpolation using a Taylor polynomial. A general polynomial expansion of d variables of order η would lead to η^d monomials and in a multivariate problem, as the one herein presented, this approach results unfeasible and a different approach has to be found. In this thesis, the goal is to obtain affine functions that are in closed form and, therefore, extend the validity ranges of the ROM much further than that imposed by the use of a global ROB and, in some cases, to be the same of the FOM from which they originate (see sections 3.1.1 and 3.1.2). This is achievable by making some theoretical considerations on the parameter effect on the model. In the following sections the development for some specific sub-classes of problems will be presented to explain the approach.

2.1.3 Model Order Reduction techniques in structural dynamics

Linear problems of structural dynamics described by equation 2.8 are very common in industry and their computation has stimulated the development of numerous MOR approaches. In this section, the the most famous and commonly used methods are shortly described.

This section does not pretend to give an exhaustive description of all the methods and techniques available to perform projection-based MOR in this field, but aims at illustrating the choices in the rest of the thesis.

Mode superposition methods

This category refers to those techniques that make use of truncated sets of undamped *eigenmodes* of the system to generate the reduced order basis (ROB). The reduction of the system is obtained by a general *Petrov-Galerkin* projection (e.g. equation (1.2)). This can be considered the most popular among the families of MOR techniques [17, 29].

Given the second order problem described by equation (2.8) and (2.14), the associated *eigenvalue* problem writes as the free vibration of the system in the Laplace domain neglecting damping

$$(K - \omega^2 M)X(\omega) = 0. \quad (2.24)$$

All the eigenmodes (or normal modes) ϕ_n of equation (2.24) correspond to the shapes that the system can assume without external forces at their corresponding natural frequencies ω_n .

Modal-based MOR approaches express the states of the system as a linear combinations of the eigenmodes. Therefore, in structural dynamics, the motion of the system will be described by the superposition of these normal modes.

There is not a clear rule for the selection of the eigenvectors to be used in a ROM. To obtain a reduction, the number of eigenvectors selected as basis should be smaller than the number of DOF of the original system. On the other hand, the methods have to guarantee that the accuracy requirements are met. In most cases, the truncation is done according to the rule of thumb based on the frequency range of interest: all the vectors corresponding to the eigenfrequencies below a certain threshold (e.g. two times the highest frequency of interest in the problem under investigation) are kept. As this is a crucial point of the methodology, in section 3.2.3 a new approach for eigenvector selection based on the greedy algorithm is presented.

The projection onto a mass-orthonormalized modal basis of the system of equation (2.24), in the hypothesis that stiffness and mass matrix are symmetric, produces the following reduced matrices

$$M_r = \Phi^T M \Phi = I_r, \quad (2.25)$$

and

$$K_r = \Phi^T K \Phi = \Lambda_r, \quad (2.26)$$

where I_r and $\Lambda_r \in \mathbb{R}^{r \times r}$ are respectively the identity matrix and the diagonal matrix containing all the kept eigenvalues of the problem (2.24) sorted from small to big. The value r corresponds to the number of eigenpairs included with the truncation and $\Phi \in \mathbb{R}^{N \times r}$ is the matrix containing the eigenvectors kept by the truncation.

Truncation introduces approximations. Therefore, scientists have been studying measures to mitigate the inaccuracies introduced by the truncation. *Static correction* is an example: this can be realized either adding a constant correction factor $x = \Psi x_r + x_{cor}$ (i.e. the derivatives remain $\dot{x} = \Psi \dot{x}_r$ and $\ddot{x} = \Psi \ddot{x}_r$) with the x_{cor} proportional to the static contribution of the neglected vectors. Alternatively the x_{cor} could be used to generate *augmented modal*

spaces, in which case the added vector becomes an extra generalized DOF (i.e. the final ROB is $\Psi_f = [\Psi, x_{cor}]$). Other improvements can be obtained making a partition of the DOF. This can improve computational efficiency or accuracy especially when the system to be reduced is made up of subsystems weakly coupled as it allows to obtain *block structure preserving* (BSP) projections [10, 11, 30, 31, 32]. Also in techniques like *component mode synthesis*, that can be assigned to the family of *model superposition methods*, partition is a key element.

Another aspect that is taken into account to improve accuracy is considering that the information contained in the eigenvector calculated with (2.24) neglects all the input/output relations of the system. Hence, the augmentation can also be used to provide enhancements of the accuracy for given input/output configurations. On the one hand, this makes the approach less general, i.e., the same ROB cannot be used for all different input/output configurations; on the other hand, this improves accuracy for the given configurations [33].

Balanced Truncation

This method is recognised to be the most popular MOR technique in the field of systems and control [17]. The goal of the method is to select the most significant modes according to criteria of *observability* and *controllability*.

Detailed discussion on the definition of *controllability* and *observability* is given in [34] and for the purpose of this manuscript, only some aspects are reported.

In simple words, a dynamic system is controllable through its inputs and is observable through its outputs. Therefore, the normal modes of the system required to describe the motion can be limited to those that can be controlled and observed.

Observability and controllability are assessed by their corresponding observability and controllability functions. The definitions of these functions can be expressed in a quadratic form that employs the *gramians*. The controllability gramian, indicated with \mathbf{P} , and the observability gramian, indicated with \mathbf{Q} , can be estimated solving the two *Lyapunov equations* [17, 34]

$$\mathbf{AP} + \mathbf{PA}^\dagger + \mathbf{BB}^\dagger = 0, \quad (2.27)$$

and

$$\mathbf{A}^\dagger \mathbf{Q} + \mathbf{Q} \mathbf{A} + \mathbf{C}^\dagger \mathbf{C} = 0 \quad (2.28)$$

where \mathbf{A} , \mathbf{B} and \mathbf{C} are the matrices of the state space representation of a MIMO system in the laplace domain of (2.11).

To generate the reduction, the most observable and most controllable modes have to be chosen univocally. This is done through a *balanced realization*: an algebraic transformation of the model matrices by means of a common orthonormal basis Φ built such that the transformed observability and controllability gramians result to be the same diagonal matrix. This is an important requirement to automatically identify the priority between controllable and observable vectors that, for optimality, should not be done separately. The procedure to obtain this particular diagonalisation matrix Φ is the following. It can be verified easily that a Galerkin projection of the state space system of equation (2.11) on this basis Φ produces the following transformed gramians

$$\bar{\mathbf{P}} = \Phi \mathbf{P} \Phi^\dagger, \quad (2.29)$$

$$\bar{\mathbf{Q}} = \Phi^{-\dagger} \mathbf{Q} \Phi^{-1}. \quad (2.30)$$

From these, it follows that the product of the 2 transformed gramians

$$\bar{\mathbf{P}} \bar{\mathbf{Q}} = \Phi \mathbf{P} \mathbf{Q} \Phi^{-1} = \Sigma^2 \quad (2.31)$$

has its set of eigenvalues independent of the choice of Φ .

The definition of the matrix Φ can be obtained from the decomposition of the two gramians. A Cholesky decomposition of the controllability gramian \mathbf{P} can be performed as it is a Hermitian, positive-definite matrix

$$\mathbf{P} = \mathbf{L} \mathbf{L}^\dagger. \quad (2.32)$$

It is recognized that the eigenvalue decomposition of the product

$$L^\dagger \mathbf{P} L = \Upsilon \Sigma \Upsilon^\dagger \quad (2.33)$$

has the same eigenvalue matrix as in equation (2.31), from which it follows that the matrix is calculated as

$$\Phi = \Sigma^{1/2} \Upsilon^\dagger L^{-1}. \quad (2.34)$$

The vectors of this matrix Φ correspond to a set of modes that are sorted according to their observability and controllability and that at this point can be truncated to obtain the reduction.

The method offers an a-priori expression for an error-bound based on the residual energy of the neglected modes in the basis Φ . On the other hand, the computational complexity of this approach is proportional to the cube of the matrix characteristic dimensions that limits its application to rather small systems.

The computationally expensive part of the method consists in solving equations (2.27) and (2.28) and approximate balance truncations methods. Unfortunately, unlike the original version, these approximated methods do not offer error bounds [33, 35, 36]. In these cases, the greedy algorithm could also be used to generate an adaptive mesh and get knowledge on the accuracy of the reduced model [37].

Krylov subspaces

These methods are MOR techniques used to approximate *frequency response functions* of dynamic systems.

Starting from the model representation of equation (2.12), the input/output relation through the system is given by

$$\underline{y} = C^T (K + sC + s^2M)^{-1} B \underline{u} \quad (2.35)$$

where the transfer function (TF) is

$$TF(s) = C^T (K + sC + s^2M)^{-1}B \quad (2.36)$$

which can be approximated by a power series centred in an expansion point s_k ,

$$TF(s) \approx \hat{TF}(s) = \phi_0 + \sum_{i=1}^q \phi_i (s - s_k)^i. \quad (2.37)$$

The vectors ϕ_i of the power series are obtained, in a similar fashion than a *Taylor expansions*: as successive derivatives of the quantity in equation (2.36) for the nominal value of the variable s_k .

$$\phi_0 = (K + sC + s^2M)^{-1}B\underline{u} \quad (2.38)$$

and for $i \geq 1$

$$\phi_i = (K + sC + s^2M)^{-1}\phi_{i-1}. \quad (2.39)$$

In practice, the vectors of the ROB are obtained employing power algorithms (e.g., *Arnoldi algorithms*).

The method of Krylov subspaces, sometimes referred to as *moment matching*, requires predefined input/output configurations similarly to the balanced truncation. More detailed discussion upon the method and available algorithms can be found in [17, 34, 38, 39].

It should be noted that Krylov bases can be enriched in two ways: increasing the order of the approximation or, alternatively, by choosing multiple expansion points. In the second case, vectors corresponding to different expansion points are not necessarily orthogonal. This requires application of orthonormalisation procedures in the process of assembling the different vectors.

Proper Orthogonal Decomposition

There are some categories of nonlinear problems (e.g. in fluid dynamics) where modal superposition is not applicable or cannot provide benefits in the simulation performance. As a matter of fact, the dynamic behaviour of a system in transition would require modes from different configurations of the system with the eventuality to generate a ROB that is too large and not suitable for MOR. The *Proper Orthogonal Decomposition* (POD) is an approach that results to be better suited for this kind of nonlinear problems that are typically analysed in time domain [40].

POD utilizes solution vectors s_i of the full order model (FOM), also known as *snapshots*, for different configurations of the system to generate the ROB. The set of vectors is orthonormalised and truncated through an eigenvalue decomposition (or a *singular value decomposition*).

Looking at this approach in the frequency domain, the solution vectors s_i would be direct solution of the problem of equation (2.12). This leads to an approach that is equivalent to applying Krylov subspace of the first order with multiple expansion point.

The POD is discussed in more details in section 2.2 of this thesis. The method is then applied in chapters 4, 5 and 6 dedicated to MOR for models of poroelastic materials.

Greedy Algorithms

Greedy algorithms were introduced in the seventies as optimisation techniques [41]. They increased their popularity in many field because, despite the fact they do not necessarily find a global optimal solution, they succeed in finding local optima in a relatively short time [27].

In the field of MOR, greedy algorithms are used to construct subspaces adding iteratively new vectors to the basis. The objective function is the accuracy of the solution coming from the ROM. Therefore, the method will seek where, in the parameter range of interest, the solution at iteration $q - 1$ is worst for the existent ROB V_{q-1} and adds new information using the FOM.

The evaluation of the accuracy is based on an error estimator. This serves as an indicator of the real error committed with the ROM with respect to the FOM. Error estimators are used in many MOR schemes to generate adaptively the ROB.

The general workflow of a greedy algorithm is the following:

- (i) selection of the parameter domain and sampling;
- (ii) initialization of the procedure with a nominal basis vector;
- (iii) employing an a posteriori error estimator to localize the combination that yields the worst result;
- (iv) updating of the available set of basis vectors.

The method will iterate between (iii) and (iv) until the tolerance threshold set for the error estimator is matched. The procedure has several crucial characteristics: if N is the number of samples chosen for the ROB generation, the error estimator will be called N times per iteration. Therefore, the error estimator has to be cheap to compute and not be dependent on the complexity of the FOM.

An error estimator is an indicator of the error committed with the ROM with respect to the FOM. Error estimators are used in many MOR schemes to generate adaptively the ROB. As discussed above, the error estimator should be fast to compute as it is called many times in the ROM creation algorithm and should be asymptotically correct with respect to the actual error [13].

Given a continuous and coercive parametric variational problem, a relation between error and residual can be expressed in matrix form as

$$r(v, \mu) = \mathcal{A}e(v, \mu) \tag{2.40}$$

where \mathcal{A} is the system matrix. If \mathcal{A} is *non-singular* both sides can be pre-multiplied by \mathcal{A}^{-1} . Calculating the norm on both sides and exploiting the triangle inequality yields

$$\|e\| = \|\mathcal{A}^{-1}\| \|r\| \leq c\|r\|. \tag{2.41}$$

This important result allows finding local parameter combinations that minimize the residual and can give some indications also for the actual error committed by the approximation. It is important to underline that these error estimations do not always provide useful results [42] and their applicability should be verified from cases to cases.

In section 3.2.3, a specific error estimator to be used in the construction of ROB is presented and, in chapter 7, this is tested in a numerical example.

2.2 Poroelastic Materials modelling and simulation

Poroelasticity is an attribute used to refer to those materials composed by a thick lattice of elastic material permeated by an interstitial fluid. The dynamic behaviour of poroelastic materials (PEM) is strongly influenced by their biphasic nature that needs a large number of parameters to thoroughly describe their characteristics. These parameters can be tuned to have strong coupling effects in the audio frequencies, hence, providing noise attenuation. They are extensively used in vehicles (automobiles, airplanes, trains) to improve the comfort of passengers but, as any other component in a vehicle, their mass and distribution must be optimised to ensure premium performances. For these reasons, in the last decades, big efforts have been made to model PEM using different approaches and levels of accuracy. Their biphasic nature can be handled in different ways depending on the grade of interaction of the two phases; sometimes this interaction can be neglected allowing for mono-phasic models (equivalent fluid models or structural models) but most of the times, it is necessary to describe this coupling accurately requiring higher detail in the models. A complete overview on the possibilities available for the modelling of PEM for acoustic analysis is available in the book of Allard and Atalla [15]. In this thesis, the Biot-Allard model is adopted to model the interaction between the elastic solid and the interstitial fluid. The description of this model is given in section 2.2.1.

The remainder of the chapter exposes some of the techniques adopted for the solution of the Biot-Allard equation with a high focus on FE Method and MOR techniques specifically developed for models of these materials.

2.2.1 Poroelastic materials modelling

Biot [43, 44] has developed a model for the analysis of PEM that is arguably the best trade-off between detail of the analysis and computational feasibility. The model relies on the hypothesis that the shortest wavelength of interest in the analysis is much larger than the characteristic length of the material (i.e. the nominal dimension of the pores). As this is acceptable in most of the industrial problems, the Biot model obtains large popularity to become the basis also for commercial software specifically developed for the analysis of PEM. The model assumes two geometrical discretizations; one for the solid phase and one for the fluid phase, and assumes that these two phases occupy

the same space at the same time. This translates into a set of equations and coupling terms that are briefly recalled in this section.

The first formulation of the model proposed by Biot has seen several improvements. Particularly important are the contributions of Johnson et al. [45] and Champoux and Allard [46] to account for the viscous and thermal effects.

Biot theory

Assuming solid phase and fluid phase to move at the same time, Biot has derived the following system of equations to model the dynamic behaviour of PEM.

$$\begin{cases} -\omega^2(\tilde{\rho}_{11}\mathbf{u}^s + \tilde{\rho}_{12}\mathbf{u}^f) = (P - N)\nabla\nabla \cdot \mathbf{u}^s + N\nabla^2\mathbf{u}^s + Q\nabla\nabla \cdot \mathbf{u}^f \\ -\omega^2(\tilde{\rho}_{22}\mathbf{u}^f + \tilde{\rho}_{12}\mathbf{u}^s) = R\nabla\nabla \cdot \mathbf{u}^f + Q\nabla\nabla \cdot \mathbf{u}^s. \end{cases} \quad (2.42)$$

This system of equations puts in relation the displacements of solid and fluid phase (respectively \mathbf{u}^s and \mathbf{u}^f) combining the equation of motions (2.43 - 2.44) and the constitutive laws of the solid and fluid material of equation (2.45 - 2.46).

Ingredients of Biot theory

This recalls all the equations and expressions required for the model in (2.42).

Equations of motion:

$$\nabla \cdot \boldsymbol{\sigma}^s + \omega^2(\tilde{\rho}_{11}\mathbf{u}^s + \tilde{\rho}_{12}\mathbf{u}^f) = 0, \quad (2.43)$$

$$\nabla \cdot \boldsymbol{\sigma}^f + \omega^2(\tilde{\rho}_{22}\mathbf{u}^f + \tilde{\rho}_{12}\mathbf{u}^s) = 0. \quad (2.44)$$

Constitutive equations:

$$\sigma_{ij}^s = [(P - 2N)\theta^s + Q\theta^f]\delta_{ij} + 2Ne_{ij}^s, \quad (2.45)$$

$$\sigma_{ij}^f = (Q\theta^s + R\theta^f)\delta_{ij}. \quad (2.46)$$

Elastic material parameters:

$$P = \frac{4}{3}N + K_b + \frac{(1-\phi)^2}{\phi}K_f(\omega), \quad (2.47)$$

$$Q = (1-\phi)K_f(\omega), \quad (2.48)$$

$$R = \phi K_f(\omega), \quad (2.49)$$

Complex frequency dependent Biot densities:

$$\tilde{\rho}_{11} = \rho_1 + \rho_a - j\sigma\phi^2\frac{G(\omega)}{\omega}, \quad (2.50)$$

$$\tilde{\rho}_{22} = \phi\rho_0 + \rho_a - j\sigma\phi^2\frac{G(\omega)}{\omega}, \quad (2.51)$$

$$\tilde{\rho}_{12} = -\rho_a + j\sigma\phi^2\frac{G(\omega)}{j\omega}. \quad (2.52)$$

The parameter N is the second Lamé coefficient of the bulk material of the frame. The material parameters P , Q , N and R can be obtained starting from the ‘*gedanken experiments*’ as referred to by Biot [47]. These experiments provide a measure of N and of the *bulk moduli* K_b of the skeleton at constant pressure in air, K_s of the material of the solid and K_f of the fluid which takes account of the thermal effects according to the model of Johnson-Champeaux-Allard developed for equivalent fluid models [45, 46]. The poroelastic materials typically used for acoustic applications are characterised by $K_s \gg K_f$, therefore it is a good approximation to consider the bulk modulus of the

skeleton material as incompressible and the expressions (2.47 - 2.49) can be used. The complex and frequency dependent quantities $\tilde{\rho}_{\#}$ are dynamic densities derived by Biot as a function of the static densities and report in equations (2.50 - 2.52). ρ_1 is the density of the skeleton material, ρ_0 is the density of the interstitial fluid, ρ_a is an inertial coupling coefficient. ϕ is the porosity which indicates the portion of domain actually occupied by the fluid phase. θ^s and θ^f represent the dilatation of frame and fluid respectively. The δ_{ij} is the Kronecker delta. σ_{ij}^s and σ_{ij}^f are the stress tensors while e_{ij}^s represents the strain tensor of the frame material. The parameter $G(\omega)$ is used to correct the effective density and takes account of the viscous effect induced by the fluid phase.

The model of equations (2.42) uses the original formulation introduced by Biot, i.e. using 3 displacements per node for the solid and 3 for the fluid to predict the dynamics of the systems. This is commonly referred to as u - U formulation. Through the years, many other formulations have been proposed [48]. These mainly differ in the description of the DOF of the fluid phase. In this thesis, the mixed u - p formulation as used by Atalla et. al [49, 50] is adopted. This formulation exploits the fact that the fluid phase has isostatic stress; therefore, only one DOF per node is enough to describe the state of the fluid phase.

Using the u - p formulation, the Biot model writes

$$\begin{cases} \nabla \cdot \hat{\boldsymbol{\sigma}}^s(\mathbf{u}^s) + \tilde{\rho}\omega^2\mathbf{u}^s + \tilde{\gamma}\nabla p = 0 \\ \Delta p + \frac{\tilde{\rho}_{22}}{\tilde{R}}\omega^2 p + \frac{\tilde{\rho}_{22}}{\phi^2}\tilde{\gamma}\omega^2\nabla \cdot \mathbf{u}^s = 0. \end{cases} \quad (2.53)$$

where $\hat{\boldsymbol{\sigma}}^s(\mathbf{u}^s)$ is a partial stress tensor independent from the fluid displacement of the original formulation. The parameter $\tilde{\gamma}$ is defined as

$$\tilde{\gamma} = \phi(\tilde{\rho}_{12}/\tilde{\rho}_{22} - \tilde{Q}/\tilde{R}). \quad (2.54)$$

The representation of equation (2.53) is possible by the transformation of the fluid displacement as

$$\mathbf{u}^f = \frac{\phi}{\tilde{\rho}_{22}\omega^2}\nabla p - \frac{\tilde{\rho}_{12}}{\tilde{\rho}_{22}}\mathbf{u}^s. \quad (2.55)$$

As it will be showed in the remainder of the chapter, most of the existing MOR techniques are incapable to cope with this formulation but work only with the model formalised as in equation (2.42). That has driven the research of this thesis to a MOR technique applied to the mixed u - p formulation.

2.2.2 Poroelastic Finite Element model

This section describes the finite element model associated with the Biot equation (2.53). Hence, assuming u and p as primary variables of the model and harmonic oscillations, and assuming $\delta \mathbf{u}$ and $\delta \mathbf{p}$ being the admissible variations respectively of \mathbf{u} and \mathbf{p} , the weak integral of the Biot equation (2.53) writes

$$\int_{\Omega_p} \hat{\boldsymbol{\sigma}}^s(\mathbf{u}) : \boldsymbol{\varepsilon}^s(\delta \mathbf{u}) d\Omega - \omega^2 \int_{\Omega_p} \tilde{\rho} \mathbf{u} \cdot \delta \mathbf{u} d\Omega - \int_{\Omega_p} \tilde{\gamma} \nabla p \cdot \delta \mathbf{u} d\Omega - \int_{\partial \Omega_p} [\hat{\boldsymbol{\sigma}}^s \cdot \mathbf{n}] \cdot \delta \mathbf{u} dS = 0, \quad (2.56)$$

$$\int_{\Omega_p} \left[\frac{h^2}{\omega^2 \tilde{\rho}_{22}} \nabla p \cdot \nabla \delta p - \frac{h^2}{\tilde{R}} p \delta p \right] d\Omega - \int_{\Omega_p} \tilde{\gamma} \nabla \delta p \cdot \mathbf{u} d\Omega + \int_{\partial \Omega_p} \left[\tilde{\gamma} u_n - \frac{h^2}{\tilde{\rho}_{22} \omega^2} \frac{\partial p}{\partial n} \right] \delta p dS = 0. \quad (2.57)$$

This is for any admissible $\delta \mathbf{u}$ and $\delta \mathbf{p}$ test function.

The numerical implementation of the model of equations (2.56) and (2.57) is given in the paper of Atalla et al [49]. Given a grid discretization of the domain Ω_p , displacement and pressure fields within an element can be approximated using a linear combination of the nodal quantities as

$$u^e = [N_s] \{u_n\}^e \quad \text{and} \quad p^e = [N_f] \{p_n\}^e. \quad (2.58)$$

Substituting equation (2.58) into (2.56) and (2.57) yields

$$\begin{bmatrix} [\mathbf{K}] - \omega^2[\widetilde{\mathbf{M}}] & -[\widetilde{\mathbf{C}}] \\ -\omega^2[\widetilde{\mathbf{C}}]^T & [[\widetilde{\mathbf{H}}] - \omega^2[\widetilde{\mathbf{Q}}]] \end{bmatrix} \begin{Bmatrix} \{u_n\} \\ \{p_n\} \end{Bmatrix} = \begin{Bmatrix} \{F_s\} \\ \{F_f\} \end{Bmatrix}. \quad (2.59)$$

where $\{u_n\}$ and $\{p_n\}$ represent the nodal displacements of the skeleton and pressure values of the interstitial fluid respectively, F_s and F_f represent the excitation applied to solid and fluid respectively, \mathbf{K} and $\widetilde{\mathbf{M}}$ represent stiffness and mass matrix of the skeleton, $\widetilde{\mathbf{H}}$ and $\widetilde{\mathbf{Q}}$ are stiffness and mass matrices of the fluid phase, $\widetilde{\mathbf{C}}$ is the coupling matrix. Superscript “ \sim ” indicates an implicit complex frequency dependency. Therefore, the matrix on the left hand side of equation (2.59) is different at each frequency.

2.2.3 Other approaches

In addition to FEM, PEM can be modelled using other discretization techniques or statistical models.

Among the alternative discretization techniques, *Wave Based Method* WBM [51] can be indicated as a possible approach for the analysis of PEM [52]. WBM belongs to the family of the Trefftz methods [53]. The WBM is a discretization approach that is particularly suitable for dynamic problems described by Helmholtz equations. WBM partitions the spatial domain in a small number of elements of large size where a relatively large number of *wave functions* is used to describe the solutions. These *wave functions* are chosen to inherently satisfy the Helmholtz equation within the elements. On the other hand, they do not automatically fulfil the boundary conditions and a error minimization is required to converge towards the correct solution [52]. This is an opposite trend to most of the other element-based approach which tendency is to have a large number of small elements where polynomials of low degree are used to approximate the solution. To ensure computational advantages using WBM instead of method like FEM, the domain of the problem is required to be convex. In fact, in case on non convex problem, the method require to subdivide the domain in a smaller number of convex elements [52] jeopardizing the computational advantages. This fact is a limitation to the use of the WBM that is not considered further in the thesis.

In the higher frequency range, deterministic approaches usually fail to give useful information. This brings the engineers to adopt statistical approaches like the Statistical Energy Analysis (SEA) [54, 55]. With this method, the

systems are partitioned in sub-system of which energy levels, modal densities, coupling and damping loss factors are considered for their representation. The system excitations are instead expressed as input powers. This representation of the system in energy terms still allows the evaluation of the required dynamic quantities with good levels of accuracy. The high frequency range is not considered in the thesis and, therefore, is not discussed further.

2.2.4 Model Order Reduction techniques for Poroelastic materials

The major difficulties of applying MOR techniques to PEM are the strong coupling between solid and fluid and the low stiffness to mass ratio that results in a high modal density in the lower frequency range. In [56], the authors show that the separation of the 2 phases to generate the projection basis in a more economical way is not accurate because of the strong coupling. In [57, 58], applications of modal-based MOR approaches for $U-u$ are presented and it is shown how a high number of modes is required to maintain accuracy. Therefore, although substantial, the reductions obtained using the $U-u$ formulation turns out to be marginal when compared to the un-reduced equivalent $u-p$ formulation (e.g. [59] shows to be 3.1 to 4.4 times faster than the un-reduced $U-u$ model and only 1.25 times compared to the $u-p$ model). Moreover, many authors show that only a part of the eigenvectors used for the projection manifests in the *frequency response functions*, showing that greater reductions could be achievable [58, 59]. Another crucial point of modal-based technique is how to solve the nonlinear eigenvalue problem. Very often, these nonlinearities are neglected to generate approximated eigenvectors. Dazel et al. [22] proposed the *generalised complex modes* to obtain better approximations of these vectors at the cost of a linearisation procedure of the eigenvalue problem. The eigenvectors are calculated from a matrix d times larger than that of the reference model with d being the order of the polynomial approximation used to describe the nonlinearities of the system.

In addition to projection-based reduction, Padé approximation applied to PEM problems showed interesting results [59, 60]. In [59], it is also shown how the technique can work in combination with projection-based MOR.

The goal of the present research is to provide an *a posteriori* MOR scheme that is well suited for the mixed $u-p$ formulation and capable of accounting for strong coupling.

The PEM problem is nonlinearly dependent on frequency and, as a consequence,

modal techniques are difficult to be used and most of the times providing insufficient gains. Hence, the problem will be treated as parametric and the methods developed in this context will be adopted.

The solution of parametric problems is associated with a *manifold* [13]: i.e. for each parameter configuration, the optimal basis to represent the solution changes and all these optimal bases are elements of the manifold. Therefore, describing this manifold is of utmost importance for a successful parametric MOR (PMOR) approach.

The approach of the proposed technique is to consider the frequency as the unique parameter of interest with the intent to solve the model order reduction of PEM systems in an efficient way. *Reduced basis* (RB) methods can be readily employed to obtain an efficient reduction of this parametric PEM model.

Modal approach

In the introduction of this thesis, the popularity of the modal synthesis was already mentioned. It can be applied with accurate results to linear structures and it can provide reduced matrices that are diagonal [61].

Literature shows many examples of attempts to apply modal synthesis to PEM. The main challenge for this method is dealing with the frequency nonlinearity of the associated eigenvalue problem [15]. In fact, in each frequency range the modes would be varying. Neglecting these nonlinearities of the system would mean choosing nominal values of frequency to get the system parameters, introducing this way an approximation. This cannot be done for large frequency ranges. Bouhioui and Hodgson [62] proposed to split the frequency spectrum of interest in bands and to consider the problem to be frequency independent in each band. The main drawback of this approach is that the ROB may become very large, leading to marginal reductions.

Sgard and Atalla [56] verified the possibility to make modal synthesis of the separated solid and fluid phase. This approach neglects completely the interaction between fluid and solid phase which is unacceptable in most industrial cases. Dazel et al. [58] have recently retaken the idea of separating the basis for enhanced accuracy with interesting results. They solve some of the accuracy problem shown in the previous works providing important computational improvements.

Generalised Complex Modes

In the last decade, Dazel et al. [22, 63] proposed a method to cope with the problem of the nonlinearities of the eigenvalue problem using the generalised complex modes (GCM). The idea of the method is to approximate the frequency nonlinearities using Taylor expansions to express these as explicit polynomial functions. According to Dazel et al. [63], a Taylor polynomial of order 4 can be sufficient to describe the frequency dependent functions that govern the system behaviour.

The Taylor expansion of system (2.59) writes

$$Z(\omega)x(\omega) \approx \sum_{i=0}^d Z_i x^{(i)}. \quad (2.60)$$

where $Z(\omega)$ is the system matrix in the left hand side of equation (2.59) the Z_i are the constant coefficient matrices of the Taylor expansion and the $x(0), x^{(1)}, \dots, x^{(d-1)}$ the successive derivatives of the state vector with respect to the evolution variable. This approximated relations are used in the Generalised Complex Modes method to express the system in terms of the associated generalised state vector [64] defined as

$$X = \left\{ \begin{array}{c} x^{(d-1)} \\ \vdots \\ x^{(1)} \\ x^{(0)} \end{array} \right\}, \quad (2.61)$$

and the system to solve writes

$$\mathbf{A}X = \mathbf{B}\dot{X}. \quad (2.62)$$

Using the Taylor monomials of equation (2.60), the system writes

$$\begin{bmatrix} [Z_{d-1}] & [Z_{d-2}] & \dots & [Z_1] & [Z_0] \\ & [\Gamma_{n(d-1)}] & & & [0] \end{bmatrix} X = \begin{bmatrix} [Z_d] & [0] \\ [0] & [\Gamma_{n(d-1)}] \end{bmatrix} \dot{X} \quad (2.63)$$

where $\Gamma_{n(d-1)}$ is a $n(d-1) \times n(d-1)$ matrix that can be chosen such that the equalities between derivatives of the same order hold.

The method offers a way to extract eigenvectors with good approximation. This is obtained exploiting a Taylor expansion and a linearisation of the equation via a Duncan's transformation. This linearisation is done at the cost of expanding the size of the system equation of as many times as the order of the polynomial approximation. Moreover, the Taylor expansion introduces approximations.

In its original version [63], the technique suffers from some instability given by the artificial matrices that can result ill-conditioned. Moreover, the linearisation procedure could be improved by the use of new cheap linearisation techniques as in [65].

The results in [22, 63] show potential and limitations of the method and offer interesting ideas on how to generate the parameterization of PEM.

Padé approximation

Padé approximation is not a method based on projection. Nevertheless, given the impact of this methodology in the field of MOR for PEM models, its basic idea is here recalled.

As for the GCM, also Padé approximation deploys Taylor expansions. However, in this case, the Taylor expansion is used to reconstruct the state of the system.

Rewriting system of equation (2.59) as

$$Z(\omega)x(\omega) = f \tag{2.64}$$

the approximation of the state in an interval around an expansion point ω_0 writes

$$x(\omega) \approx \sum_{k=0}^d a_k (\omega - \omega_0)^{(k)}, \tag{2.65}$$

where d is the order of the Taylor expansion and the coefficient vectors a_k are defined as

$$a_k = \frac{x^{(k)}(\omega_0)}{k!}. \tag{2.66}$$

The reconstruction of functions containing poles and zeros (e.g., a frequency response function) is better approximated by the ratio of two power series rather than a Taylor expansion [59]

$$x(\omega) \approx \frac{\sum_{i=0}^L p_i(\omega - \omega_0)^{(i)}}{\sum_{j=0}^M q_j(\omega - \omega_0)^{(j)}}. \tag{2.67}$$

The coefficient vectors p_k and q_k are determined by combining equations (2.65) and (2.67) and setting $q_0 = 1$

$$\sum_{i=0}^L p_i(\Delta\omega)^{(i)} - \sum_{k=0}^d a_k(\Delta\omega)^{(k)} \sum_{j=0}^M q_j(\Delta\omega)^{(j)}. \tag{2.68}$$

In the case of PEM, the successive derivatives $x^{(k)}$ of equation (2.66) can be obtained from

$$Z(\omega_0)x^{(k)}(\omega_0) = f^{(k)}(\omega_0) - \sum_{j=0}^{k-1} \binom{k}{j} Z^{(k-j)}(\omega_0)x^{(j)}(\omega_0), \tag{2.69}$$

$$\forall k = 1, \dots, (L+M)$$

where the binomial coefficients are defined as

$$\binom{k}{j} = \frac{k!}{l!(k-l)!}. \tag{2.70}$$

More details on this method and applications to PEM are available in [66].

In practice, in the implementation of the Padé approximation, there are more than one expansion points to expand the frequency range of the reconstruction and maintain a good level of accuracy. These points are referred to as *master frequencies*.

To resume, there are few steps needed for the implementation: (i) choice of the master frequencies (ii) evaluation of solution vector and its derivatives with respect to the frequency at the master frequencies (iii) feed of the equations of the polynomial expansions to retrieve the necessary coefficients (iv) reconstruction of the solution within the different intervals centred in the

master frequencies as in a Taylor expansion.

An interesting fact of the Padé approximation approach is that it can be used in combination with projection-based techniques [59] offering interesting developments of final reduction achievements.

2.3 Conclusions

The literature reported in this chapter shows a wide range of methodologies available to perform the different parts of a *parametric Model Order Reduction*. The first goal of the work will be to tailor the techniques available to generate ROB to the modelling requirements of the set of problem chosen in this thesis.

The Reduced Basis method will be the core approach in the thesis. The efforts will be concentrated in finding efficient and accurate affine representations as well as to identify the most suitable methodology for the ROB generation available in the literature.

In the specific case of vibroacoustic simulation of poroelastic materials, it appears that there are still some gaps in the application of MOR. Most of the times, the common frequency-domain approaches are not capable to account for the frequency dependency of the system matrices and provide results that can be either affected by inaccuracies or with marginal computational advantages with respect to direct methods. Therefore, the goal is also to identify a better alternative than those available to perform MOR and PMOR for system made of PEM.

Chapter 3

Efficient Parametric Model Order Reduction

This chapter isolates the main ideas and contributions of the thesis putting them in general terms and without applications that are included in later chapters. This aims to give an application-independent view on the methods developed that could be extracted and applied to other problems than networks of beams and systems of poroelastic materials.

The specific application and development for the class of problems discussed in the introduction is given within the chapters 4, 5 and 7.

The rest of the chapter is organised as follows: section 3.1 treats the general approaches developed to retrieve the affine representation of the models. Section 3.2 contains the methods developed to generate the global ROB.

3.1 Derivation of affine models

Affine parametric dependence is a fundamental requirement for the application of RB methods.

In this section, two approaches to derive an affine model are given. An intrusive approach that requires to have access to the FE code (see section 3.1.1); and a non-intrusive approach that treats the FE Model as a black box and generates an affine model based on the Least Square (LS) Method (see section 3.1.2).

3.1.1 Intrusive approach

To apply this method it is required to have full access to the FE code in order to make some changes to the implementation of the original model. The entries of the FE matrices are varied according to a limited number of functions that will be assumed to be also the affine functions of the parametric problem.

Therefore, this approach is valid only for those systems whose parameters are also parameters of the FE element. Examples are: material parameters, temperature or, for specific classes of elements like beams and shells, cross-section parameters or plate thickness.

This intrusive method requires to modify the expressions of the FE implementation, i.e., rewrite the system matrices separating the constant terms as coefficient matrices and the parameter dependent terms as basis functions.

To illustrate this concept, a general elasto-dynamic FE model is considered and the method applied to a FE stiffness matrix of an elastic body obtained as in [67]

$$K = \int_V B^T D B dV, \quad (3.1)$$

where V represents the volume of the body, B is the result of the product of a differentiation operator and the element shape functions and puts in direct relation the nodal displacement with the strain of the body. In case of linear elastic behaviour of the body, the D matrix is an elastic matrix that is dependent on the material properties and type of element. Thus, if these properties are also parameters of the problem, their functions can be isolated. This is a practical approach only if the number of expression to be taken into account is limited. Hence, in those cases where the properties vary within the domain of the problem and cannot easily grouped, the method may not be appropriate.

For example, considering the Hooke's law in plane stress, the matrix D writes

$$D = \frac{E}{1 - \nu^2} \begin{bmatrix} 1 & \nu & 0 \\ \nu & 1 & 0 \\ 0 & 0 & (1 - \nu)/2 \end{bmatrix}. \quad (3.2)$$

where E represents the Young modulus and ν is the Poisson's ratio.

Assuming uniform characteristics, that in an elasto-dynamic problem are any configuration with the parameters constant over the full spatial domain, the parametric model could be expressed using affine functions of these two parameters. These are

$$\frac{E}{1 - \nu^2} \quad \frac{E\nu}{1 - \nu^2} \quad \frac{E}{1 + \nu}. \quad (3.3)$$

In the applications to poroelastic materials of chapter 4, this approach will be used to retrieve affine functions of for the Biot parameters and for the frequency.

It should be noted that the affine model obtained with this approach is equivalent to original FOM. This means, for an ideal global subspace used for the reduction, that the ROM has the same validity range of the FOM.

3.1.2 Non-intrusive approach

The big limitation of the intrusive approach of section 3.1.1 is that, most of the times, the user does not have access to the FE code and the approach results inapplicable.

In this section, a method to retrieve and use affine functions for *black-box* models is presented.

The affine functions can be retrieved following a similar approach to that of section 3.1.1. In fact, the affine functions can be derived starting from the definition of the element used in the mesh. What is very different is that the matrices of coefficient cannot be derived and isolated within the code but they can be retrieved using a least squared (LS) approach.

The coefficient matrices \mathcal{A}_i of equation (2.19) can be obtained, for each element of matrix K , with the minimisation

$$\min_{\mathcal{A}_{1:q}^{ij}} (\|K_{ij}(\mu) - F(\mu) \cdot \mathcal{A}_{1:q}^{ij}\|^2) \quad (3.4)$$

with μ a configuration of the parameters and $F(\mu)$ the matrix that contains the affine functions (as shown in equations (3.3)) evaluated for the configuration of the parameters. If the affine functions selected are 5 and the parameter combinations for the LS are 10, the $F(\mu)$ matrix is of dimension 10×5 . This

method will be further explained in chapter 7 where it is used to retrieve the affine model of the gantry system. For the entry i - j the problem reduces as

$$\mathcal{A}^{ij} = F(\mu)^\dagger \cdot [K_{ij}(\mu)] \quad (3.5)$$

where the symbol \dagger refers to the pseudo inverse operation.

The LS approach can of course be used to force the system into some approximated polynomial expansions as in [28]. However, in this thesis, it will be used in chapter 7 to exploit affine functions that refer to the specific FE element used. Above all, it is important to select the affine functions for the system to be linearly independent. Using correct basis function for the affine representation can lead to accurate models. Nevertheless, given the fact that the LS method is approximated, the validity range of the affine representation may depend on the sampling choice. Therefore, this should be designed to maximise the validity range of the new representation that can extend far beyond the parameter range of interest.

3.2 Derivation of global Reduced Order Basis

The scope of the section is to find valid ROB for parametric problems of different types; therefore, it is organised in some paragraphs.

In problems as (2.15) many authors generate ROB using modal bases. This was possible only introducing certain approximations (e.g. solving an eigenvalue problem assuming constant matrices). It was shown that, for small frequency ranges, these approaches could be acceptable. To overcome these limitations, a method typically used in time-domain problems is adopted. This is presented for applications in the frequency domain in paragraph 3.2.1. The same approach can be used for the more complex problems of equations (2.16) and (2.17). Nevertheless, for problems of equation (2.17), the methods in paragraphs 3.2.2 and 3.2.3 are adopted.

Paragraph 3.2.2 describes an approach to generate the ROB combining modal basis with a singular value decomposition and is used in the numerical examples of chapter 7.

In section 2.1.3, a paragraph was dedicated to the fundamentals of greedy algorithms for the construction of ROB; paragraph 3.2.3 instead presents the

implementation of an approach to combine the greedy algorithm to modal bases (also used in chapter 7).

3.2.1 POD-SVD approach

The *proper orthogonal decomposition* (POD) [40] results to be an efficient approach for the kind of problems of equations (2.15) and (2.16) and is used in this context to generate the ROB. The method is applied in chapter 4 for the generation of ROB for poroelastic materials models.

The POD requires a set of solution vectors s_i of the full order model (FOM) for different configurations of the system. These vectors are often referred to as *snapshots* and are generated by direct simulation of the model (i.e. solving equations (2.15) and (2.16)).

A *snapshot matrix* \mathbb{S} can be defined being a concatenation of the snapshots s_i

$$\mathbb{S} = [s_1 \dots s_i \dots s_{n_s}]. \quad (3.6)$$

Matrix \mathbb{S} contains all the rough data that needs to be orthogonalised and compressed. The POD basis is then defined as a truncated set of eigenvectors corresponding to the higher eigenvalues of the correlation matrix $\mathbb{S}^\dagger \mathbb{S}$ (with \dagger indicating complex conjugate). It can be proven that this optimal set can be obtained with higher accuracy using the *singular value decomposition* (SVD) that is therefore employed [40].

The SVD is a factorization that represents a general matrix as two orthogonal matrices and one diagonal matrix. Given $\mathbb{S} \in \mathbb{R}^{N_h \times n_s}$ the SVD writes

$$\mathbb{S} = \mathbb{U} \mathbb{\Sigma} \mathbb{Z}^T, \quad (3.7)$$

where $\mathbb{U} \in \mathbb{R}^{N_h \times N_h}$ is the orthogonal matrix of the *left singular vectors*, $\mathbb{\Sigma} \in \mathbb{R}^{N_h \times n_s}$ is the diagonal matrix of the *singular values* and $\mathbb{Z} \in \mathbb{R}^{n_s \times n_s}$ is the orthogonal matrix of the *right singular vectors*. The size of these SVD matrices depends on the rank of \mathbb{S} . In fact, given the rectangular matrix \mathbb{S} with $N_h > n_s$, the rank is $r \leq n_s$. When the snapshots are linearly independent, $\mathbb{U} \in \mathbb{R}^{N_h \times n_s}$, $\mathbb{\Sigma} = \text{diag}(\sigma_1, \dots, \sigma_{n_s})$ and $\sigma_1 \geq \sigma_2 \geq \dots \geq \sigma_{n_s} \geq 0$ and $\mathbb{Z} \in \mathbb{R}^{n_s \times n_s}$.

The POD basis W is given by a truncated selection of N *left singular vectors* (\mathbb{U}). This truncation can be done according to different methods and a choice

should be made [68, 13]. It can be proven that, for a given number of left singular vectors, the set V that minimises the error is that corresponding to the highest singular values [40]

$$\|\mathbb{S} - VV^T\mathbb{S}\|_X^2 = \min_W \|\mathbb{S} - WW^T\mathbb{S}\|_X^2. \quad (3.8)$$

A typical way to define a truncation is by the following error formula [68, 13]

$$\sum_{j=1}^{n_s} \|s_j - \sum_{k=1}^N (s_j \cdot v_k)v_k\|_X^2 = \sum_{k=N+1}^{n_s} \sigma_k^2. \quad (3.9)$$

This gives an *error bound* dependent on the the total number of snapshots. Alternatively, the truncation can be done defining a tolerance ε_{POD} ; the vectors will be kept for the singular values $\sigma_i \geq \sigma_1 \cdot \varepsilon_{POD}$.

An accurate POD can be obtained only if the snapshot matrix \mathbb{S} contains all the necessary data. Therefore, prior to truncation (equation (3.9)), a reducibility check should be carried out. A reducibility assessment can be performed by analysing the *singular value* decay. When the parametric problem to be reduced is of small Kolmogorov n-width and the number of snapshots taken is sufficient, the graph of the singular values starts decaying at a slower rate showing an “elbow” in the trend. This can be associated with the fact that new vectors add very little information with respect to what is already given by the existing ones. When there is no elbow in the decay, it indicates that more snapshots may be needed to ensure accuracy. In case the singular values would decay slowly from the beginning, it may indicate that the selected parameter space range is too large and consequently the reduction technique may underperform or fail. Examples of *singular values* graphs can be found in [13].

The snapshot generation usually represents the most expensive part of the POD procedure: it requires a direct simulation of the FOM for each snapshot. For this reason, also the sampling criteria play an important role for an accurate POD performance. There is good evidence that a *random* or *quasi-random* sampling for the selection of the snapshots performs sensibly better than a tensorial sampling [13]. In high dimensional problems, it is recommended to use *Monte Carlo sampling* or *Latin hypercube* to improve convergence. For a mono-dimensional problem, the sampling technique is less critical and a tensorial approach can be used. Nevertheless, also in this case semi-random sampling techniques can be used.

The SVD operation can also be very expensive if the matrix to be decomposed is large. In fact, given a matrix $\mathcal{A} \in \mathbb{R}^{n \times m}$ the computational cost has complexity $O(m^2n)$. This makes it a very expensive operation for $m \approx n$. However, here SVD is applied to the matrix of snapshot \mathbb{S} whose number of columns is much smaller than the number of rows ($m \ll n$) making its computational costs reasonable with respect to the inversion of the sparse system matrix of the FOM. It has to be mentioned that, for a sparse matrix, the inversion is done by iterative methods. Therefore, the “flops” required for this operation vary with the sparsity of the matrix that is assessed by some numerical examples [16].

Assuming the computational complexity for a matrix inversion to be $O(n^2.373)$, for a model of 10000 DOF, the SVD will have comparable computation time for a set of 557 vectors; going to a model with 1e5 DOF, the comparable dimension for the SVD is 2707 vectors. The case studies analysed in chapter 5, where the HFM contains 21444 DOF, allow to apply the SVD with comparable computational time for up to more than 900 snapshots.

Multidimensional extensions of the presented technique can be obtained enriching the ROB by sampling not only the frequency but also the other parameters that may be of interest for a parametric study. In fact, the affine functions derived in previous section show affinity not only with the frequency but also with all the other material parameters and in particular with the Biot parameters. For multidimensional problems with large ranges, the problem of basis generation would scale up exponentially with the number of parameters to investigate. Therefore, optimal selection of snapshots would be essential. In such a case, popular criteria for snapshots selection are based on iterative use of error estimators (e.g. the *greedy algorithm*) [13]. These techniques are not considered in this paper as the system is perturbed only by the changing frequency and the range is small enough to allow for an efficient use of the POD procedure.

3.2.2 Modal-SVD approach

A global ROB may be generated assembling the local ROB obtained from different parameter configurations. In [24], the authors implemented a Petrov-Galerkin projection using precomputed local ROB for the projection of the vector of motion and a global ROB to back project. This global space is obtained by taking some local ROB in the parameter range of interest and putting them together in a unique matrix

$$\Psi_{all} = [\Psi_1 \dots \Psi_i \dots \Psi_n]. \quad (3.10)$$

The Ψ_i represents the local ROB, hence, Ψ_{all} contains the information required to describe the motion in the selected range. However, matrix Ψ_{all} cannot be taken as the ROB because it is a large non orthogonal matrix, usually with a bad condition number, but it is used to originate a ROB by means of the SVD [69] applied to make a principal component selection.

$$\Psi_{all} = V \Sigma U^T. \quad (3.11)$$

In equation (3.11), the global projection space is represented by the columns of the matrix V associated with the largest singular values that satisfy some accuracy requirements; thus for instance being $\sigma > tol$.

A priori determination of the best parameter sampling scheme is not generally possible. Therefore, a posteriori error estimation is needed in order to establish the optimal location of the parameter space where new local information is needed. This can be achieved using greedy algorithm [27] developed to retrieve the best global ROB using an error estimator.

3.2.3 Modal-greedy approach

In this section, a greedy based approach for the construction of adaptive ROB of eigenvectors is developed. The method is based on the same concepts and has the same aims of RB method of which the standard greedy is discussed in 2.1.3.

The challenge addressed by the approach is in the error estimator that has to take information from eigenvalue problems. To ensure the generality of the method some analytical considerations are made.

Given a general elasto-dynamic problem of equations (2.1)-(2.4) modelled using FEM to obtain 2.8, its associated eigenvalue problem writes

$$KX_j - MX_j\lambda_j = 0, \quad (3.12)$$

where X_j and λ_j represent the j -th eigenvector and eigenvalue, respectively. Using a Modal synthesis to generate the ROB, a set of the X_j associated to the lower eigenvalues λ_j can be used.

Given a parameter domain of interest that is limited as $\mu_{low} \leq \mu \leq \mu_{high}$, for each parameter configuration there is a different eigenvalue problem with different eigenvectors. As the scope is to generate a ROB valid over a range of parameter configurations, we seek for a greedy algorithm that can select eigenvectors from the eigenvalue problems of any parameter configuration of interest.

The procedure starts choosing as initial ROB a truncated set of eigenvectors of a nominal configuration of the parameters indicated as V_0 . At each iteration i , the system is updated by a set of new vectors chosen according to an error estimator that has to be designed. The new ROB V_i is then obtained as the combination of the old ROB V_{i-1} and this new set of vectors selected by the estimator.

At each iteration i , the ROB V_i is used to approximate mass and stiffness matrices as in equation (1.3) to obtain approximated eigenpairs of the problem (3.12). This produced a residual that can be used as error estimator as in the scheme of section 2.1.3 (similarly to equation (2.40))

$$r = (K - M\hat{\lambda}_{ij})\hat{X}_{ij}, \quad (3.13)$$

where $\hat{\lambda}_{ij}$ and \hat{X}_{ij} come from the ROM while K and M are the FOM matrices that are considered parameter dependent. If $\hat{\lambda}$ and \hat{X} are an eigenvalue and the corresponding eigenvector for the problem of equation (2.40), the residual term will be zero. In the general case, $\hat{\lambda}$ and \hat{X} are not expected to be a solution of equation (2.40); therefore, a residual $r \neq 0$ is obtained. From equation (3.13) it is not straightforward to obtain error bounds as it is in equations (2.40-2.41). In fact, equation (3.13) has two error sources and requires finer considerations: for very accurate approximation of the eigenvectors the residual may still be very high if the paired approximated eigenvalue is far from the actual eigenvalue. Vice versa, having a precise eigenvalue, i.e. a small residual, does not necessarily guarantee a good approximation for the eigenvector.

The Proof that the residual of equation (3.13) can be used as error estimator for a greedy algorithm can be done introducing the theory on matrix perturbations [70] and the definition of eigenvectors and eigenvalues with respect to the Reyleigh quotient [71].

The accuracy of the approximated eigenvalues depends on the conditioning of the diagonalisation matrix. If this results ill-conditioned, the residual norm will not represent a thoroughly trustable error estimator. This is formalised in a theorem proved in [70] that is here recalled.

Theorem 1. Given a semisimple matrix $\mathcal{A} \in \mathbb{C}^{n \times n}$, suppose $V^{-1}\mathcal{A}V = D$, where D is a diagonal matrix and V is non-singular. Given a perturbation of the matrix $\delta\mathcal{A}$, $\hat{\lambda}$ is an eigenvalue of the matrix $\mathcal{A} + \delta\mathcal{A}$. It follows that \mathcal{A} has an eigenvalue λ such that

$$|\hat{\lambda} - \lambda| \leq \text{cond}(V) \|\delta\mathcal{A}\|_p \quad (3.14)$$

where $\text{cond}(V)$ represents the condition number of the matrix V and $\|\cdot\|_p$ represents the p-norm and $p \leq \text{inf}$. This tells that, the approximation of the eigenvalues is good if the condition number of the matrix of eigenvectors V is good and the perturbation of the system A is small. The other requirement is on the eigenvectors of the perturbed system that should be a good approximation of the exact eigenvectors. A condition number for eigenvectors can be obtained using a Schur-like decomposition of the system (see chapter 6 of [70]). A condition number estimator for the eigenvectors is just given by the quantity $\|\mathcal{A}^{-1}\|$ [70]. Moreover, the Rayleigh quotient for a matrix \mathcal{A} is a functional that has as stationary points the eigenvectors [72]. Therefore, an improved approximation of the eigenvector is expected to reduce the residual in equation (3.13).

Algorithm 1 shows the function GREEDYALGORITHM proposed. The function takes as input $\mu, V_{\mu_0}, \varepsilon_{tol}$ that are respectively the list of parameter configurations in the sampling, the ROB at the current iteration and the tolerance prescribed for accuracy. This gives as output, an enriched ROB of the next iteration. To enrich the basis, the matrices of the HFM (K_i, M_i) are extracted for each parameter configuration (μ_i) and the eigenpair of the current ROM ($X_{r,i}, \lambda_{r,i}$) is back projected in the domain of the HFM domain and used in the equation of the eigenvalue problem that generate the residual (r_i). This quantity guides the greedy procedure: the parameter configuration that generates the highest value of residual is used to enrich the V_{μ_0} .

To favour readability the error estimation is here based on only one eigenvalue pair but the essence of the algorithm does not change if the estimate is done using more pairs. The matrices K_i and M_i may be large depending on the complexity of the model. Therefore it is convenient pre-computing them as this will bring important improvements of computational costs also in the preprocessing time. Unlike other greedy approaches present in literature, where a single vector contribution per iteration is usually added, this procedure requires to add a set of vectors at each iteration. This is done to improve the convergence of the method. The added set corresponds to the parameter configuration whose largest amount of information is missing. The drawback of adding a set of vectors is that some of the information spanned by the added vectors is probably already available in the temporary global ROB and has to be filtered out. Therefore, the union operation of line 12 is done through SVD. Algorithm 1 is implemented and discussed in the numerical example of section 7.3.

Algorithm 1 Greedy approach based on the residual of one eigenvector

```

function GREEDYALGORITHM( $\mu, V_{\mu_0}, \varepsilon_{tol}$ )
   $V_g = V_{\mu_0}$ 
  while  $R_{MAX} > \varepsilon_{tol}$  do
    for  $i = 1 : N$  do
       $[K_i, M_i] = \text{getFOMmatrices}(\mu_i)$  ▷ get FOM matrices
       $K_r = V_g^T K_i V_g; \quad M_r = V_g^T M_i V_g$ 
       $[X_r, \lambda_r] = \text{eig}(K_r, M_r, n \text{ lower modes})$ 
       $r_i = K_i V_g X_r - M_i V_g X_r \lambda_r$ 
       $[R_{max}, ID] = \text{max}(r)$ 
       $V_{\mu_{ID}} = \text{eig}(K, M)_{\mu_{ID}}$  ▷ get eigenvectors
       $V_g = V_g \cup V_{\mu_{ID}}$ 
  return  $V_g$ 

```

Chapter 4

Model Order Reduction of Poroelastic Materials components

In this chapter, the RB method is applied to poroelastic materials (PEM). The Biot model (see section 2.2) appears to belong to the category of problems identified by equation (2.15).

The scheme of the PMOR approach adopted is discussed in sections 3.1 and 3.2 and exploited to retrieve the affine representation and ROB for the particular case of PEM.

That of PEM is an import class of materials for acoustical and thermal applications. They are in fact efficient passive insulators. Their modelling has some challenging aspects regarding the coupling of the fluid phase and solid phase that requires the construction of large discretised models (see for instance [73, 74, 75]). The mesh density criteria suggested for FE models of PEM (e.g. $\lambda/6$, with λ being the shortest wavelength in the system) can lead to a very large number of equations to be solved thus a high computational burden. In the specific case of discretised models of PEM, it was shown in the literature that for some cases where the shear waves have to be taken into account, the mesh size has to follow an even more stringent $\lambda/24$ criterion [76]. This requirement brings a consequent dramatic growth of the model size even for smaller systems. In this chapter, it is shown that the high

refinement required in FE meshes for PEM can be strongly compensated by the application of MOR techniques.

Biot-Allard equations have been solved using a large variety of discretization approaches, such as the *Wave Based Method* (WBM) [51], *Partition of Unity Finite Element Method* (PUFEM) [77] or *discontinuous Galerkin method* (DGM) [78]. However, also for this class of problems, FEM represents the preferred way and is also used in this and the next chapter to generate the *high fidelity models*.

Through the years, many different Biot FE formulations have been developed [49, 15, 48]; they can be classified as *displacement-displacement* ($U-u$) formulations [15, 48, 43, 44, 79] and *displacement-pressure* ($u-p$) formulation [49, 50]. In a 3D problem, the $U-u$ formulations use 6 DOF per FE-node, while the $u-p$ formulation requires only 4 DOF per FE-node combining 3 displacement DOF for the solid phase with 1 pressure DOF for the fluid [49]. The $u-p$ formulation shows the same level of accuracy as the $U-u$ providing better computational performances [49]. Nevertheless, many MOR approaches introduced in literature are based on a $U-u$ formulation [48, 57, 58, 59, 80]. While, the attempts done on the mixed formulation $u-p$ still have computational issues and result unappealing [22, 63].

This chapter is organised as follows: in section 2.2.4 some of the existing MOR approaches for PEM are briefly discussed. Section 4.1 shows how to model the problem of PEM using MOR approaches based on POD. The affine representation of the PEM matrices, the separated projection method and the ROB generation are also discussed in section 4.1. Section 4.2 contains some 3D simulations to show the quality of the approach presented in terms of both accuracy and computational efficiency.

4.1 The proposed technique ¹

The vibro-acoustic problem of a multilayer system containing poro-elastic materials needs to be improved from a computational point of view and starting from the FE discretization of the weak $u-p$ integral formulation based on the Biot-Allard theory (see section 2.2). The scope is then to develop a PMOR scheme based on the RB method to equation (2.59) reported here

¹Reproduced with permission from [81] © 2017, Acoustical Society of America.

$$\begin{bmatrix} [\mathbf{K}] - \omega^2[\widetilde{\mathbf{M}}] & -[\widetilde{\mathbf{C}}] \\ -\omega^2[\widetilde{\mathbf{C}}]^T & [[\widetilde{\mathbf{H}}] - \omega^2[\widetilde{\mathbf{Q}}]] \end{bmatrix} \begin{Bmatrix} \{u_n\} \\ \{p_n\} \end{Bmatrix} = \begin{Bmatrix} \{F_s\} \\ \{F_f\} \end{Bmatrix}. \quad (4.1)$$

The implementation of the method is described in sections 3.1.1 and in 3.2.1. Therefore, the affine functions and associated matrices are retrieved rearranging the FE matrices as in 3.1.1; the ROB is obtained by combining direct solutions at some sampled frequencies then orthonormalised exploiting the SVD (section 3.2.1). The scope of the following sections is then to assess accuracy and performances of this technique.

4.1.1 Projection of the system

Having general polynomials to generate the shape functions typically used in discretization techniques (e.g. FEM) has advantages of adaptability i.e. they can describe well any change of the system (e.g. geometry and material properties variations, different boundary and loading conditions). However, this generality is obtained at the cost of going far from computational efficiency. As discussed before, PMOR techniques aim at finding the minimum set of basic functions to describe the system retaining the parametric nature of the models.

The problem of equation (2.59) is expected to be of small Kolmogorov n-width when the frequency range of interest is limited and when it is the only parameter taken into consideration. It is in fact shown in literature how among other approaches, though often recurring to some computational compromises, MOR could be successfully performed with a single global reduction basis over the full frequency range of interest[57, 58, 59].

The Galerkin projection of equation (2.59) on the global ROB V , assuming it is orthonormal, writes

$$V^T \begin{bmatrix} [\mathbf{K}] - \omega^2[\widetilde{\mathbf{M}}] & -[\widetilde{\mathbf{C}}] \\ -\omega^2[\widetilde{\mathbf{C}}]^T & [[\widetilde{\mathbf{H}}] - \omega^2[\widetilde{\mathbf{Q}}]] \end{bmatrix} V \{\Phi\} = V^T \begin{Bmatrix} \{F_s\} \\ \{F_f\} \end{Bmatrix}, \quad (4.2)$$

$$\{\Phi\} = V^T \begin{Bmatrix} \{u_n\} \\ \{p_n\} \end{Bmatrix}. \quad (4.3)$$

4.1.2 Affine representation of the Biot equations

The expressions for the frequency dependent sub-matrices in (2.59) are given in Atalla et al. [49] and recalled in equations (4.4 - 4.6) in the hypothesis that the properties of the porous materials stay the same over the entire spacial domain

$$\{\delta u_n\}^T [\tilde{\mathbf{M}}] \{u_n\} = \tilde{\rho} \int_{\Omega_p} \underline{u} \cdot \delta \underline{u} \, d\Omega, \quad (4.4)$$

$$\{\delta p_n\}^T [\tilde{\mathbf{H}}] \{p_n\} = \frac{\phi^2}{\tilde{\rho}_{22}} \int_{\Omega_p} (\nabla p \cdot \nabla \delta p) \, d\Omega, \quad (4.5)$$

$$\{\delta p_n\}^T [\tilde{\mathbf{Q}}] \{p_n\} = \frac{\phi^2}{\tilde{R}} \int_{\Omega_p} p \cdot \delta p \, d\Omega. \quad (4.6)$$

The coupling terms of equations (4.7) and (4.8) are taken from the enhanced u - p formulation [50] and write

$$\{\delta u_n\}^T [\tilde{\mathbf{C}}_1] \{p_n\} + \langle \delta p_n \rangle [\tilde{\mathbf{C}}_1]^T \{u_n\} = \frac{\phi}{\tilde{\alpha}} \int_{\Omega_p} \nabla p \cdot \delta \underline{u} \, dS, \quad (4.7)$$

$$\{\delta u_n\}^T [\tilde{\mathbf{C}}_2] \{p_n\} + \langle \delta p_n \rangle [\tilde{\mathbf{C}}_2]^T \{u_n\} = \phi \left(1 + \frac{\tilde{Q}}{\tilde{R}} \right) \int_{\Omega_p} \nabla p \cdot \delta \underline{u} \, dS. \quad (4.8)$$

The poro-elastic domain is indicated by Ω_p , and ϕ represents the *open porosity*. The complex functions $\tilde{\rho}$ and $\tilde{\rho}_{22}$ are two of the *dynamic densities* defined by the Biot theory, \tilde{R} is an elastic coefficient and $\tilde{\gamma}$ is a complex expression dependent on the Biot densities and on the elastic coefficients, as reported in section 2.2.1 and in [15]. These complex functions describe the frequency nonlinearities of the system. The interesting aspect is that they are geometry

independent (uniform behaviour through the PEM), therefore they can be taken out from the integrals (4.4) - (4.8). This yields some affine expressions for the complex frequency dependent submatrices of equation (2.59):

$$[\widetilde{\mathbf{M}}] = [\mathbf{M}_{cte}]\widetilde{\rho}, \quad (4.9)$$

$$[\widetilde{\mathbf{H}}] = [\mathbf{H}_{cte}]\frac{\phi^2}{\widetilde{\rho}_{22}}, \quad (4.10)$$

$$[\widetilde{\mathbf{Q}}] = [\mathbf{Q}_{cte}]\frac{\phi^2}{\widetilde{R}}, \quad (4.11)$$

$$[\widetilde{\mathbf{C}}] = [\mathbf{C}_{1cte}]\frac{\phi}{\widetilde{\alpha}} + [\mathbf{C}_{2cte}]\phi \left(1 + \frac{\widetilde{Q}}{\widetilde{R}} \right). \quad (4.12)$$

The system matrix can therefore be rewritten separating the constant frequency-independent sub-matrices. These sub-matrices have only to be constructed once and are multiplied by the complex frequency-dependent functions at each frequency step. This results in the following affine representation of the global system of equation (2.59)

$$[\widetilde{\mathbf{Z}}] = \begin{bmatrix} [\mathbf{K}] - \omega^2[\widetilde{\mathbf{M}}] & -[\widetilde{\mathbf{C}}] \\ -\omega^2[\widetilde{\mathbf{C}}]^T & [[\widetilde{\mathbf{H}}] - \omega^2[\widetilde{\mathbf{Q}}]] \end{bmatrix} = \sum_{i=1}^{\Gamma} \mathbf{Z}_i f_i(\omega), \quad (4.13)$$

where the \mathbf{Z}_i are constant global matrices

$$\begin{aligned} & \begin{bmatrix} [\mathbf{K}] & 0 \\ 0 & 0 \end{bmatrix}, \begin{bmatrix} -[\mathbf{M}] & 0 \\ 0 & 0 \end{bmatrix}, \begin{bmatrix} 0 & -[\mathbf{C}_1] \\ 0 & 0 \end{bmatrix}, \begin{bmatrix} 0 & -[\mathbf{C}_2] \\ 0 & 0 \end{bmatrix}, \\ & \begin{bmatrix} 0 & 0 \\ -[\mathbf{C}_1]^T & 0 \end{bmatrix}, \begin{bmatrix} 0 & 0 \\ -[\mathbf{C}_2]^T & 0 \end{bmatrix}, \begin{bmatrix} 0 & 0 \\ 0 & [\mathbf{H}] \end{bmatrix}, \begin{bmatrix} 0 & 0 \\ 0 & -[\mathbf{Q}] \end{bmatrix}. \end{aligned} \quad (4.14)$$

The associated affine functions f_i are given respectively by

$$\begin{aligned} 1, \quad \omega^2 \tilde{\rho}, \quad \phi/\tilde{\alpha}, \quad \phi(1 + \tilde{Q}/\tilde{R}), \\ \omega^2 \phi/\tilde{\alpha}, \quad \omega^2 \phi(1 + \tilde{Q}/\tilde{R}), \quad \phi^2/\tilde{\rho}_{22}, \quad \phi^2/\tilde{R}. \end{aligned} \quad (4.15)$$

Therefore, the left hand side of equation (4.2) can be rewritten as

$$V^T [\tilde{\mathbf{Z}}] V \{\Phi\} = \sum_{i=1}^{\Gamma} V^T [\mathbf{z}_i] V f_i(\omega, \mu) \{\Phi\} \quad (4.16)$$

or equivalently as

$$\begin{aligned} \left[V_s^T [\mathbf{K}] V_s - V_s^T [\mathbf{M}_{cte}] V_s \omega^2 \tilde{\rho} - V_s^T [\mathbf{C}_1] V_f \phi/\tilde{\alpha} - V_s^T [\mathbf{C}_2] V_f \phi(1 + \tilde{Q}/\tilde{R}) \right. \\ \left. - V_f^T [\mathbf{C}_1]^T V_s \omega^2 \phi/\tilde{\alpha} - V_f^T [\mathbf{C}_2]^T V_s \omega^2 \phi(1 + \tilde{Q}/\tilde{R}) \right. \\ \left. + V_f^T [\mathbf{H}_{cte}] V_f \frac{\phi^2}{\rho_{22}} - V_f^T [\mathbf{Q}_{cte}] V_f \omega^2 \frac{\phi^2}{\tilde{R}} \right] \{\Phi\} = \{V_s^T F_s + V_f^T F_f\}. \end{aligned} \quad (4.17)$$

The matrices V_s and V_f represent the partitions of the projection space $V = \langle\langle V_s \rangle\rangle \langle\langle V_f \rangle\rangle^T$ where subscript s refers to solid DOF and f to fluid DOF. The result of equation (4.17) is a key element of this contribution. It tells that the reduction of the system can be performed offline as only the constant sub-matrices are transformed by the projection and the frequency dependency regards only the complex functions $\tilde{\rho}, \tilde{\alpha}, \tilde{\rho}_{22}, \tilde{R}, \tilde{Q}$.

For further details on the derivation of these equations and the Biot-Allard theory the reader is referred to [15]. For the sake of completeness, the appendix reports the explicit expressions of the Biot functions used in the calculation models implemented in this thesis.

4.1.3 Reduced order basis generation

There are many possibilities to find a valid ROB V for a problem in the frequency domain. For example, many authors generate ROB using eigenvectors. In this case, a selection criterion for the eigenvectors is necessary: for a vibro-acoustic problem, a selection can be made truncating the higher frequency eigenmodes. This approach works well for linear elastic structures

[82]. On the other hand, the characteristics of the PEM system of equations (2.59) (frequency dependent parameters, high damping and high coupling) make the modal approach often computationally inefficient and cumbersome or provide inaccurate solutions [57, 63, 22]. Moreover, PEM have often a high density of modes in the low frequency range with the direct consequence of large bases of eigenvectors (i.e. low computational gain achievable). It was also observed that, for PEM, most modal vectors do not manifest as clear resonances in the frequency response functions (FRF) due to the high damping [83]. Therefore, alternatives to modal approaches are proposed.

In this chapter, the POD is used following the implementation discussed in section 3.2.1.

4.2 Simulations

This section describes the simulations performed to assess the proposed PMOR technique. A summary of the properties of the materials used for the components of the systems is given in table 5.1.

4.2.1 Surface impedance of a single PEM layer ²

The simulation of the surface impedance of a single poro-elastic layer simulated in [49] is repeated using the MOR method of section 4.1 where the frequency space is sampled using the stratification method and the bases is obtained applying the SVD to the resulting set of vectors.

The experimental configuration is depicted in figure 4.1; an infinite foam layer of thickness $t = 100mm$ is attached to a rigid wall and excited by a normal incident plain wave of unit amplitude. The properties of the PEM are reported in table 4.1. The boundary conditions of the foam layer are of plain strain.

The system is modelled using a FE mesh of $1 \times 1 \times 20$ elements (20 elements along the thickness). Using the $u-p$ formulation and considering the constraints, this leads to a total of 80 DOF. Real and Imaginary part of the surface impedance are calculated with a 1 Hz sampling step between 300 Hz and 1300 Hz.

For this system, the FE model writes as equation (2.59). The reducibility analysis of 15 equally distributed snapshots through the frequency range of

²Reproduced with permission from [81] © 2017, Acoustical Society of America.

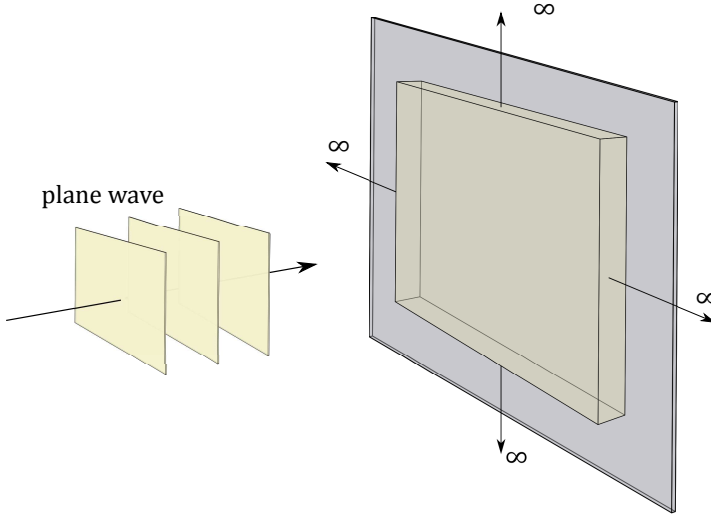


Figure 4.1: PEM layer used for the surface impedance problem [49].

Table 4.1: Material Parameters of glasswool layer

Quantity	Sym.	units	GW-L
Structural density	ρ_s	$[kg/m^3]$	130
Young's modulus	E	$[MPa]$	4.4
Poisson's ratio	ν	-	0.00
Structural loss factor	η	-	0.10
Open porosity	ϕ	-	0.94
Flow resistivity	σ	$[Ns/m^4]$	4.0E4
Tortuosity	α_∞	-	1.06
Char. visc. length	Λ	$[\mu m]$	56
Char. therm. length	Λ'	$[\mu m]$	110
Fluid density	ρ_0	$[kg/m^3]$	1.213
Kinematic viscosity	ν_0	$[m^2s^{-1}]$	1.71E-5
Adiabatic index of fluid	γ	-	1.402

interest is shown in figure 4.2. The application of the POD leads to a base of 9 vectors obtained truncating the initial set according to $\varepsilon_{POD} = 10^{-11}$.

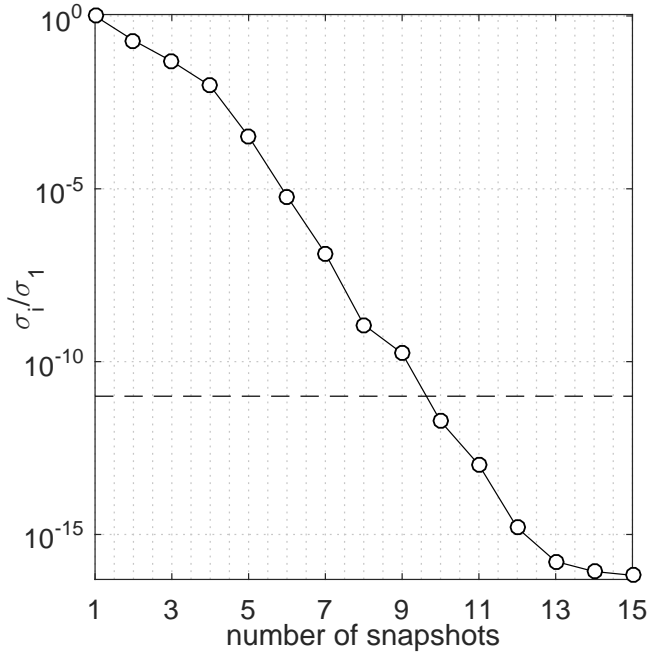
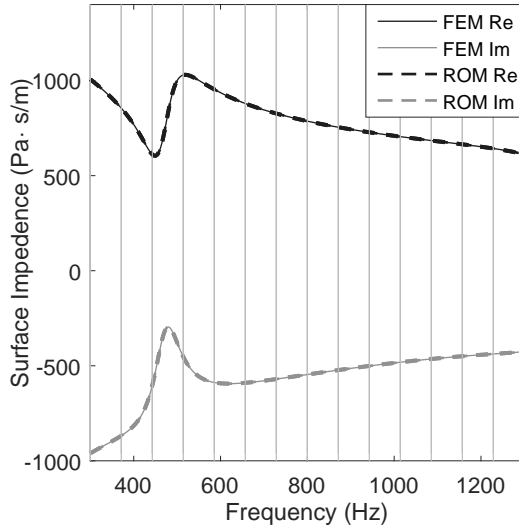


Figure 4.2: Trend of the singular value for the snapshot matrix of the problem depicted in figure 4.1. The horizontal dashed line shows the truncation threshold.

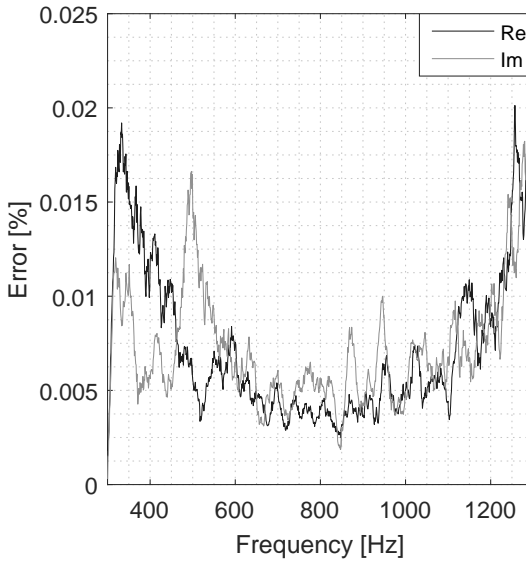
The results of the surface impedance calculated with ROM and the comparison with the FOM are shown in figure 4.3.

This example shows how, also for a small model, a dramatic reduction of the DOF is achievable. Even though the simulation with the FOM was already very fast, there is still a considerable computational gain by applying MOR. For 1000 frequency lines, the ROM results to be, on average, 4 to 5 time faster than the FOM. This includes the offline time required for the method to generate the ROB and to do the projection.

This speed-up does not compromise the accuracy of the results (figure 4.3) as the introduced error appears to be negligible in this case.



(a) Surface impedance of an infinite poro-eastic plate. Solid lines refer to the direct simulation of the FE model. Dashed lines refer to the ROM. Dark colour is used for real part and light colour for the imaginary part. The vertical lines correspond to the location of the snapshots.



(b) Percentage error on the calculation of the surface impedance ROM vs FEM. Dark line refers to the real part, light line to imaginary part.

Figure 4.3: Surface Impedance of a semi-infinite layer of PEM calculated with a ROM and with the direct solution of the FE simulation.

4.3 Conclusions

In this chapter, a strategy to perform *model order reduction* (MOR) of *Finite Element* (FE) models for *poro-elastic materials* (PEM) was presented.

The nonlinear frequency-dependency and the strong coupling of the PEM were shown to be accurately described using the proposed *parametric model order reduction* (PMOR) technique. The method uses the *proper orthogonal decomposition* (POD) to generate the *reduced order basis* (ROB), and *affine modelling* of the *Biot-Allard* equations that lead to a *reduced basis* (RB) scheme for PEM systems.

The POD approach allows to account accurately for the strong coupling and the nonlinearities introduced in the vibro-acoustic problem by the PEM. The affine functions allow to generate a *reduced order model* (ROM) whose simulation is independent from the original size of the parental model used as reference and to generate the snapshots.

In the second part, the method is applied to simulate perturbations of some of the Biot parameters and it appears to perform good results for the given model. In order to extend the conclusions on the performances of a multi-parameter study, more models should be simulated.

In conclusion, the results obtained with the method are satisfactory in terms of accuracy and speed-up. Nevertheless, the method should be applied to new models of larger size and higher complexity to be representative of realistic case-study.

Chapter 5

Applications to systems with poro-elasto-acoustic coupling

The aim of this chapter is to extend the investigations of chapter 4 to larger systems. Hence, cases where the PEM is coupled to different subsystems are investigated. Therefore, the models herein proposed consider multilayer systems containing PEM and other elastic materials to represent typical configurations for acoustic insulation packages.

A typical configuration sees PEM materials attached to impervious elastic layers that can be directly included on the surfaces where noise transmission has to be reduced, e.g., the walls of the passenger compartment of a vehicle. The two configurations chosen for this application are depicted in figure 5.3 and 5.9.

In section 5.1, the coupling procedure adopted for the modelling is reported. Section 5.3 shows the results for the numerical examples.

5.1 Modelling of poro-elasto-acoustic problems

The system represented in figure 5.3 is made up of two sub-systems. One is a PEM layer and the other is an impervious elastic layer. In the FE model they are described by two different meshes. The PEM is meshed with 8-noded hexahedron elements and the elastic layer with 4-noded quadrilateral elements.

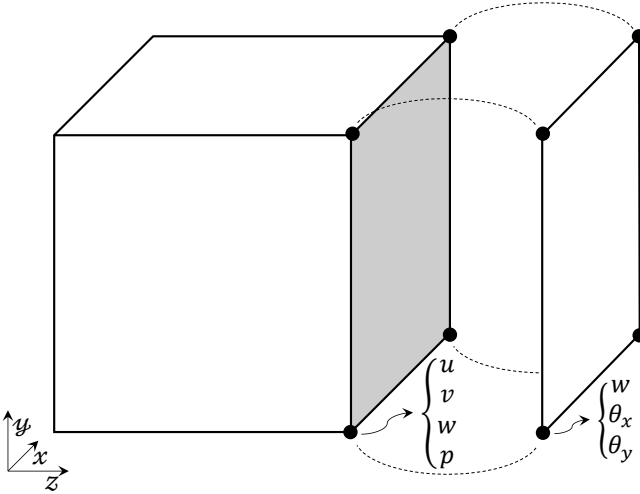


Figure 5.1: Elements at the interface between the elastic heavy layer and the PEM layer.

Each node of the hexahedron has 4 DOF, 3 displacements u, v, w that describe the motion of the solid phase of the PEM, and a scalar pressure p , that describes the state of the fluid phase. Each node of the quadrilateral elements has 3 DOF, 1 out-of-plane displacement w and 2 rotations θ_x, θ_y around the in-plane axes. In these examples, the dimensions of the quadrilateral elements are designed to fit exactly the area of the faces of the hexahedron elements (see figure 5.1). The continuity condition for the displacement (equation (2.6)) at the interface between the PEM layer and the elastic top layer can be written for each interface node as

$$\begin{Bmatrix} u_F \\ v_F \\ w_F \\ w_{HL} \\ \theta_{x,HL} \\ \theta_{y,HL} \end{Bmatrix} = \begin{bmatrix} 1 & 0 & 0 \\ 0 & 1 & 0 \\ 0 & 0 & 1 \\ 0 & 0 & 1 \\ 0 & -2/t & 0 \\ 2/t & 0 & 0 \end{bmatrix} \begin{Bmatrix} u_F \\ v_F \\ w_F \end{Bmatrix} \quad (5.1)$$

where the vector on the left hand side represents the list of the displacement DOF as they appear respectively in the hexahedron and in the plate element.

$$\begin{array}{c}
 \text{Top Layer} \\
 \\
 Z_P = G_0^T \left[\begin{array}{cc|cc}
 \overbrace{K_{HL} - \omega^2 M_{HL}} & & 0 & 0 \\
 \hline
 0 & & \underbrace{K - \omega^2 \tilde{M}} & -\tilde{C} \\
 0 & & -\omega^2 \tilde{C} & \tilde{H} - \omega^2 \tilde{Q}
 \end{array} \right] G_0 \\
 \text{PEM Layer}
 \end{array}$$

Figure 5.2: Continuity condition imposed using the partitioning method. The procedure results in a condensation of the linearly dependent DOF at the interface.

For the choice made of having the plate elements exactly corresponding to a face of the hexahedron elements, these DOF are among them linearly dependent and their relation is expressed by the matrix on the right hand side that can be indicated by the letter G_0 . A global G_0 can then transform a system containing all DOF of the 2 separated system into a smaller one that exploits the relations between the linearly dependent DOF located at the interface. This approach is also known as partitioning method [84] or Master-Slave method [85]. This same approach can be used to model the interactions in the model of figure 5.9 between foam and plate. The composition of the global model matrix for the system in figure 5.3 is reported in figure 5.2.

5.2 Reduction scheme

The approach adopted for the reduction of the multilayer systems of figure 5.3 and 5.9 follows that presented in sections 3.1.1 and in 3.2.1. This consists of the application of the POD for the ROB generation and of an appropriate affine representation of the model:

- a set of snapshots is chosen in the frequency range of interest and the basis generated using the SVD is applied to generate the required orthonormal basis;
- the models have to be represented using affine functions.

The procedure to obtain an affine representation with respect to frequency for the PEM is presented in section 4.1.2. For the linear elastic materials two layers should be included to the model: from equation (2.8) and neglecting damping, the stiffness terms are frequency independent while the inertia terms depend quadratically on frequency. The snapshots for the ROB of the 1-dimensional parametric problem (where the parameter is the frequency) are sampled using the *stratification sampling* [86] that can be seen as an equivalent version of the Latin hypercube for 1D cases: the frequency domain is divided into a number of *strata* and for each stratum a number of snapshots is computed at *quasi-random* frequency lines. This technique makes it easier to generate incremental improvements of the snapshot matrix: after the initial set of snapshots is chosen, additional points can be added using the same stratification approach if the trend of the *singular values* does not present the decrease in the decaying rate (sometimes indicated as *elbow* or *L-curve* [86]).

5.3 Results

5.3.1 Multilayer system containing PEM

The first example, a multilayer system containing PEM, represents a simplified version of the acoustic insulation liner used in the automotive industry [87]. Characterisation of the liner in terms of surface impedance matrix is pursued. The liner consists of a PEM layer of dimensions $825\text{mm} \times 425\text{mm} \times 14\text{mm}$ topped by a uniform homogeneous elastic heavy layer of thickness $t = 2\text{mm}$. Table 5.1 lists the material characteristics and the system is depicted in figure 5.3.

The top surface is divided into 8 parts that are farther on indicated as patches (as in [87, 88]) and shown in figure 5.3. For a thorough analysis of the performances of the presented ROM method, the model is tested with both pressure and velocity excitation reading both pressure and velocity output. The pressure excitation is applied on patch 1 on the heavy-layer side (figure 5.3), the velocity excitation on patch 1 on the PEM layer. The FE model contains 7123 DOF, required to obtain a good accuracy for the solution up to 1000 Hz, against a total of 44 DOF generated by the POD technique.

The two load cases are analysed in the following subsections.

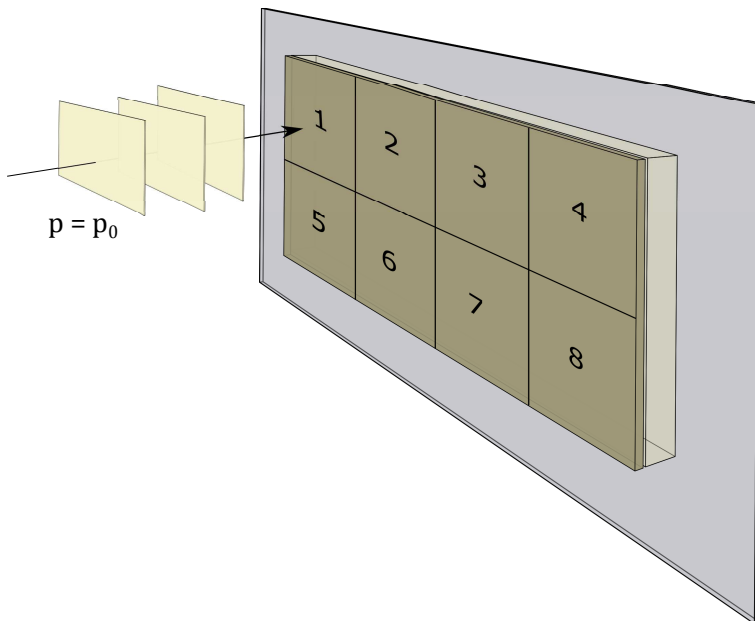


Figure 5.3: Multilayer system: a heavy layer and a foam layer clamped on a rigid wall

Pressure excitation

In this experiment, the PEM layer is completely clamped at the bottom side while the top side of the heavy layer has free conditions. On top of patch 1 a uniform pressure excitation is applied.

The results of the simulation are post-processed to retrieve the patch response functions in terms of pressure on the PEM side of the system and the patch transfer functions [88] in terms of velocity on the heavy layer side (Figure 5.4 and 5.5).

Velocity excitation

For this experiment, a uniform velocity is imposed on the bottom of the PEM layer at patch 1. At all the other patches, PEM layer is clamped. As in the previous experiment, the heavy-layer has stress release conditions on the top surface.

The output retrieved for this experiment are: patch velocity response on the heavy layer and patch pressure response on the PEM layer side (figure 5.6 and 5.7).

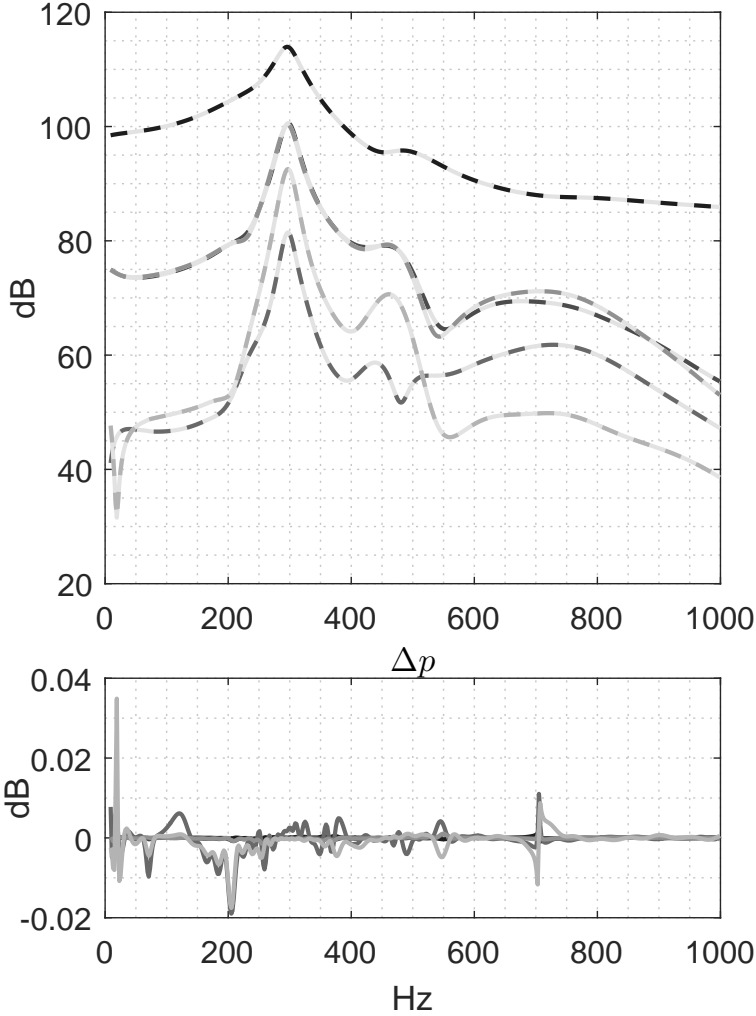


Figure 5.4: Patch pressure transfer functions for a pressure excitation of first patch. The graph on top shows the transfer functions, the graph at the bottom shows the difference in dB between the ROM and the FE used as reference. ■■ refers to patch 1; ■■ refers to patch 2; ■■ refers to patch 3; ■■ refers to patch 5; ■■ refers to patch 6. The light grey continuous lines in the graph on top are the transfer functions calculated with the FE model.

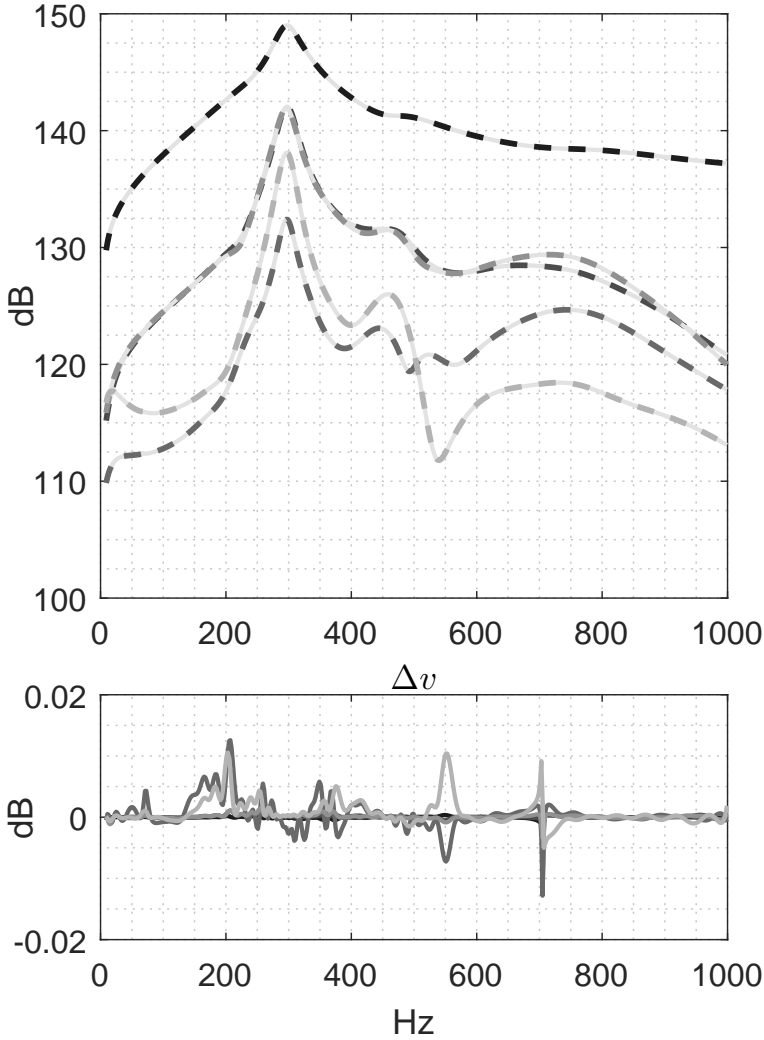


Figure 5.5: Patch velocity transfer functions for a pressure excitation of first patch. The graph on top shows the transfer functions, the graph at the bottom shows the difference in dB between the ROM and the FE used as reference. ■■ refers to patch 1; ■■ refers to patch 2; ■■ refers to patch 3; ■■ refers to patch 5; ■■ refers to patch 6. The light grey continuous lines in the graph on top are the transfer functions calculated with the FE model.

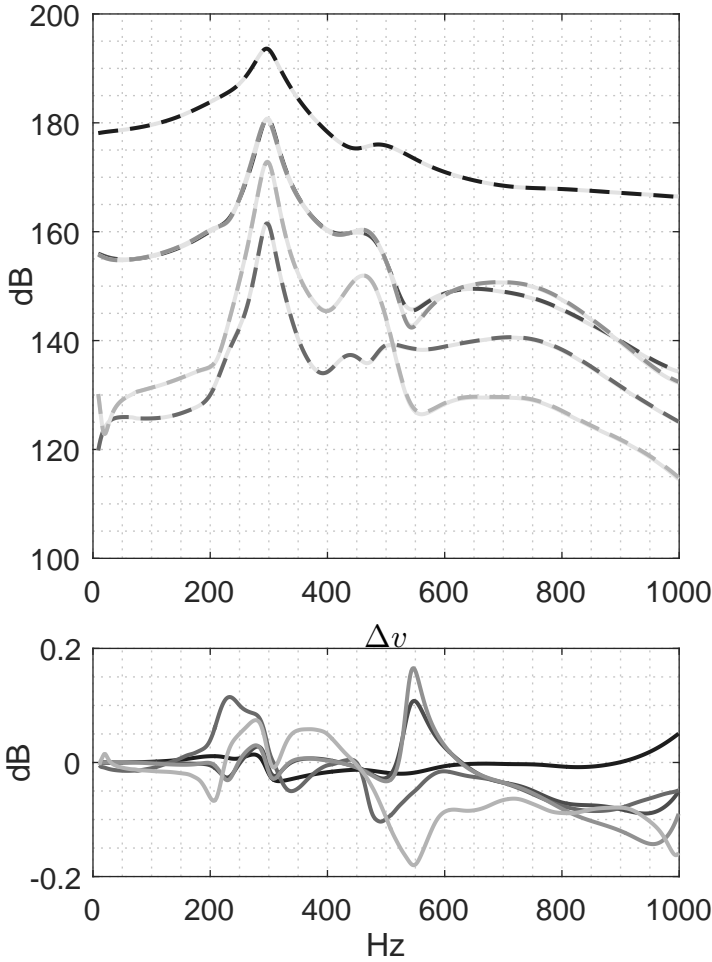


Figure 5.6: Patch velocity transfer functions for a velocity excitation of first patch at the bottom of the foam layer. The graph on top shows the transfer functions, the graph at the bottom shows the difference in dB between the ROM and the FE used as reference. ■■ refers to patch 1; ■■ refers to patch 2; ■■ refers to patch 3; ■■ refers to patch 5; ■■ refers to patch 6. The light grey continuous lines in the graph on top are the transfer functions calculated with the FE model.

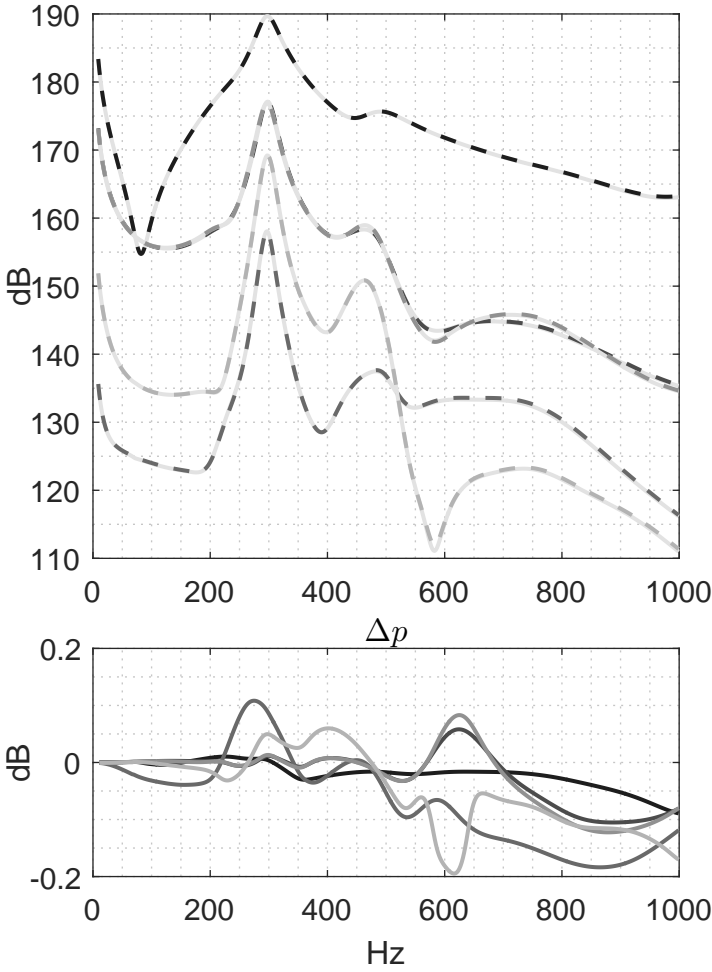


Figure 5.7: Patch pressure transfer functions for a velocity excitation of first patch at the bottom of the foam layer. The graph on top shows the transfer functions, the graph at the bottom shows the difference in dB between the ROM and the FE used as reference. ■■ refers to patch 1; ■■ refers to patch 2; ■■ refers to patch 3; ■■ refers to patch 5; ■■ refers to patch 6. The light grey continuous lines in the graph on top are the transfer functions calculated with the FE model.

From figures (5.4 - 5.7) it can be noted how the effects of the excitation diminish going far from the source (response of patch 3 and 6 is much lower than the response of patch 1). For this reason the results of the furthest patches (4, 7 and 8), where the signal to noise ratio is too low, are not considered in the assessment.

For both load cases, the level of accuracy for velocity and pressure quantities is high (see figures (5.4 - 5.7)); in fact, the frequency response functions are reconstructed within a ± 0.2 dB accuracy providing reliable solutions with respect to the original computational expensive models. It can be also noted how the error has spikes often corresponding to resonances or antiresonances and is really smooth and low far from these areas.

The computational gain of the ROM, obtained with this methodology, is shown in figure 5.8. For the specific case of these examples, where 1000 frequency lines per load case analysed were considered, the time required to retrieve the solution using the ROM was less than 11 % with respect to the FEM model of reference.

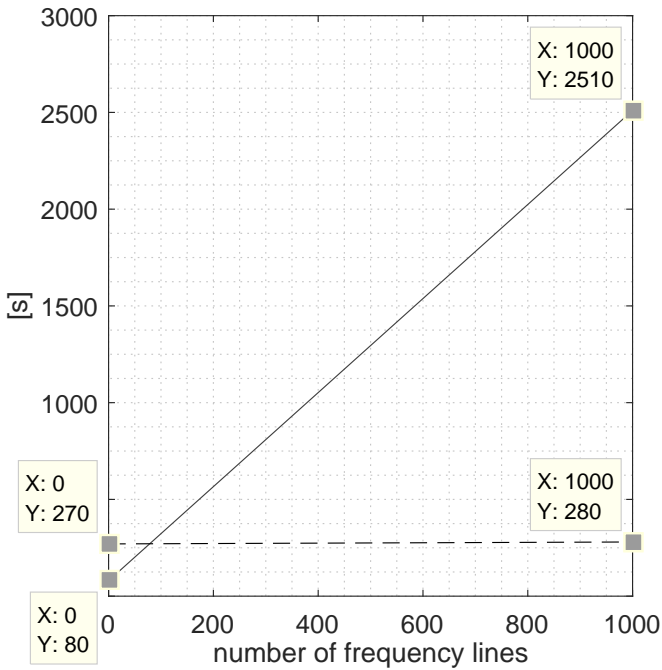


Figure 5.8: Computational gain obtain with the MOR approach (dashed line) presented against the FE simulation (solid line). The total computaional costs of the ROM for 1000 frequency lines of the reconstruction of the transfer functions are $12\times$ cheaper than the costs of the FOM.

Table 5.1: Parameters of the materials in the trim component; glasswool layer (GW-L), aluminium plate, poroelastic layer (PEM-L), heavy layer (H-L), rigid air cavity.

Quantity	Sym.	units	GW-L	Plate	PEM-L	H-L	Cavity
Structural density	ρ_s	$[kg/m^3]$	130	2700	68	1470	-
Young's modulus	E	$[MPa]$	4.4	7.0E4	2.5E-2	240	-
Poisson's ratio	ν	-	0.00	0.33	0.40	0.33	-
Structural loss factor	η	-	0.10	0.01	0.16	0.24	0.01
Open porosity	ϕ	-	0.94	-	0.91	-	-
Flow resistivity	σ	$[Ns/m^4]$	4.0E4	-	1.2E5	-	-
Tortuosity	α_∞	-	1.06	-	1.00	-	-
Char. visc. length	Λ	$[\mu m]$	56	-	10	-	-
Char. therm. length	Λ'	$[\mu m]$	110	-	74	-	-
Fluid density	ρ_0	$[kg/m^3]$	1.213	-	1.213	-	1.213
Kinematic viscosity	ν_0	$[m^2 s^{-1}]$	1.71E-5	-	1.71 E-5	-	-
Adiabatic index of fluid	γ	-	1.402	-	1.402	-	-
Compression modulus of fluid	\mathcal{K}	$[kPa]$	-	-	-	-	142

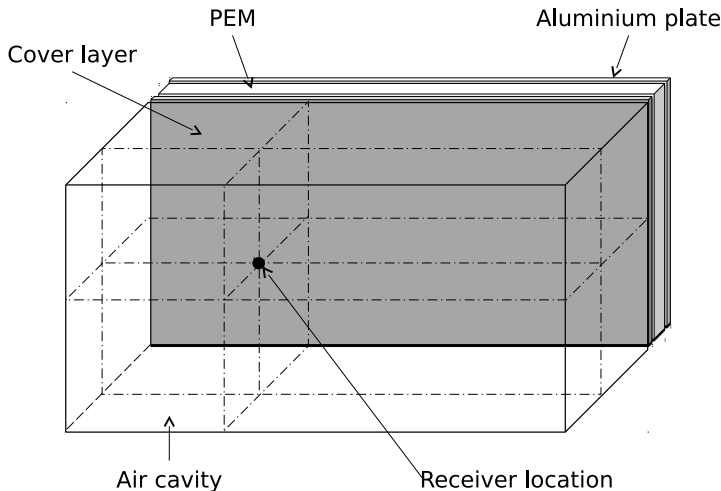


Figure 5.9: Multilayer system: a heavy layer and a foam layer clamped on a rigid wall.

5.3.2 Air cavity with surface absorption by means of an insulation liner ¹

In this example, the performances of a multilayer system containing PEM are analysed using the discussed MOR technique. A trim layer is coupled to an aluminium plate and to a rigid cavity filled with air to generate an acoustic-poroelastic problem representative of a simplified industrial case [87]. The trim layer consists of a PEM layer of dimensions $825\text{mm} \times 425\text{mm} \times 14\text{mm}$ topped by a uniform homogeneous heavy layer of thickness $t_2 = 2\text{mm}$; the supporting flexible aluminium plate has thickness $t_1 = 3\text{mm}$ and the air cavity has a height $h = 500\text{mm}$. All the sides of the absorbing layers are clamped to the rigid walls of the cavity and the system is excited with a force acting perpendicular to the liner directly on the aluminium plate. Table 5.1 lists the material characteristics of the different domains and the system is depicted in figure 5.9.

The FE model of this system contains 21444 DOF. 150 snapshots are required to generate a good POD basis in the range $]0 - 1000[\text{ Hz}$. This value is not estimated *a-priori* but through an iterative procedure based on the reducibility analysis of section 3.2.1 and starting from the initial guess of 80 (see Fig 5.10). In figure 5.10, it is shown the effect of increasing the number of snapshots. Adding 40 snapshots (i.e. at 120), the singular values do not show a clear elbow in the decay. At 140 snapshots, the required shape starts to appear.

¹Reproduced with permission from [81] © 2017, Acoustical Society of America.

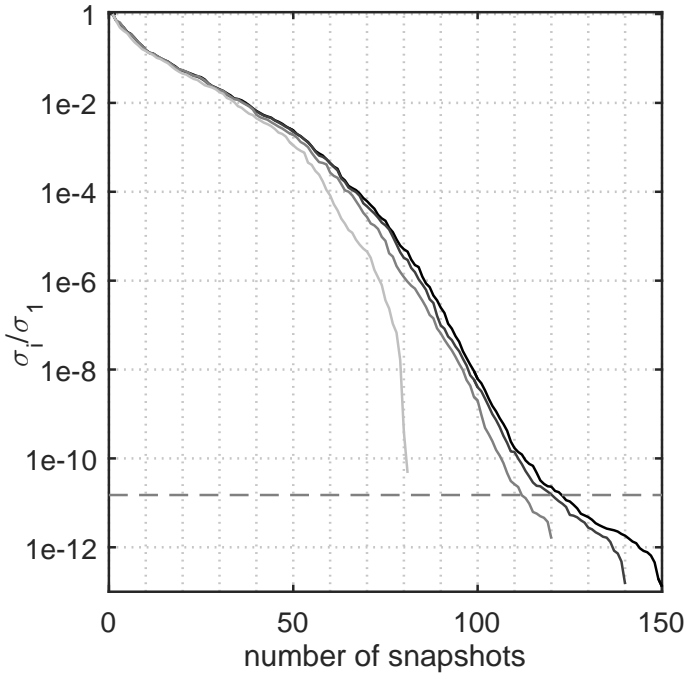


Figure 5.10: Reducibility assessment. Decay of the singular values for increasing number of snapshots. Increasing the number of snapshots brings to a change in the decaying rate of the singular values indicating a satisfactory amount of information. The horizontal dashed line shows the truncation threshold. ■ 80 snapshots; ■ 120 snapshots; ■ 140 snapshots; ■ 150 snapshots.

Additional precaution is taken in this case going to 150 confirming the trend. The truncation, done using $\varepsilon_{POD} = 10^{-11}$, leads to a POD basis of 114 vectors (i.e. DOF of the final reduced order model).

The results of figure 5.11 show the mean squared pressure in the cavity as well as the pressure in a single point identified as *receiver location* in figure 5.9. In figure 5.12, the mean squared velocities of the heavy layer and of the plate are shown. All the results show that the ROM and the original full FE generate solutions with differences contained within 0.01 dB.

The high level of accuracy of the methodology is also shown in figure 5.13a where the distribution of the normal velocity in a cut-through of the foam is displayed at a frequency of 200 Hz, a resonance of the system (figure 5.11).

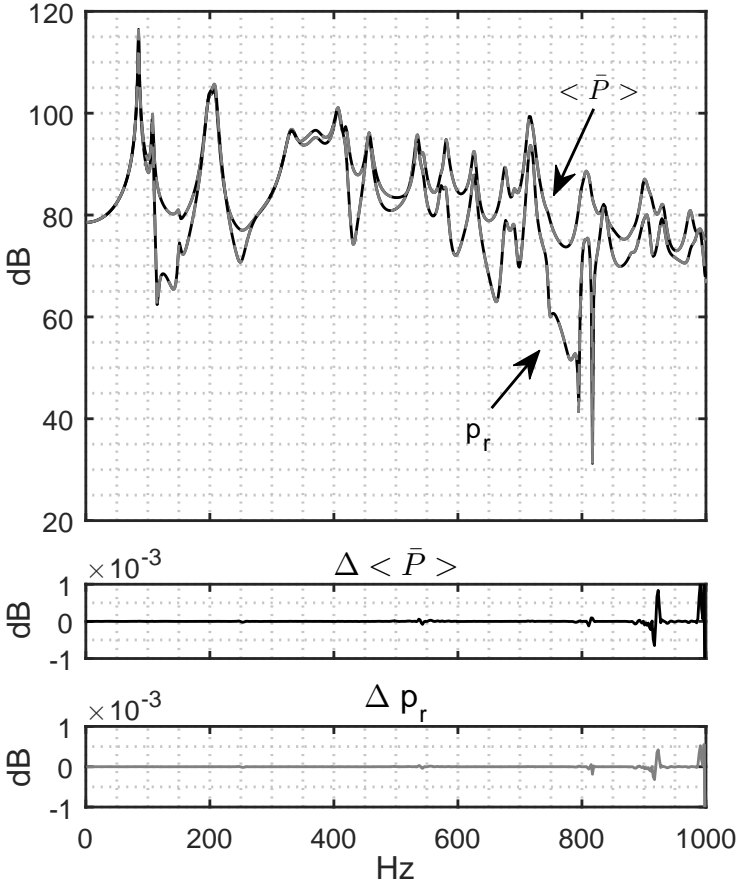


Figure 5.11: Simulation results of the system in figure 5.9. Mean squared pressure $\langle \bar{P} \rangle$ in the air cavity and pressure at receiver location p_r . The solid grey lines in the top graph refer to the direct simulation of the FE model. The dashed black lines refer to the ROM. The graph at the bottom represents the difference in decibel between direct FE results and ROM results.

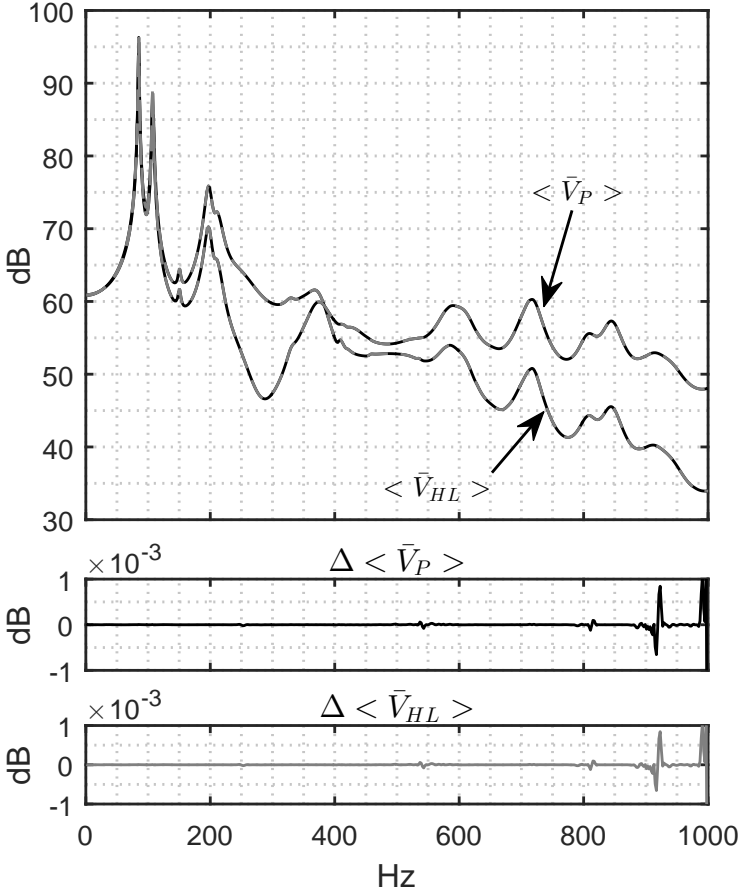
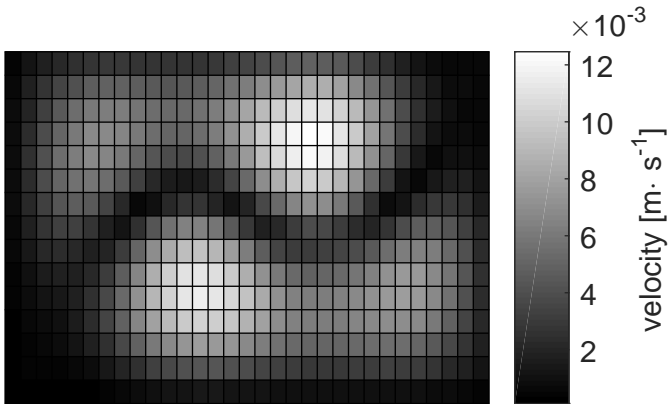
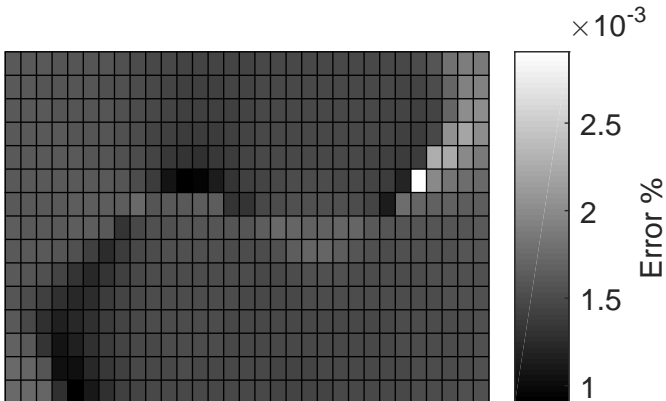


Figure 5.12: Simulation results of the system in figure 5.9. Mean squared velocities of the heavy layer $\langle \bar{V}_{HL} \rangle$ and of the aluminium plate $\langle \bar{V}_P \rangle$. The solid grey lines in the top graph refer to the direct simulation of the FE model. The dashed black lines refer to the ROM. The graph at the bottom represents the difference in decibel between the FE results and the ROM results.



(a) Normal velocities of the ROM.



(b) Percentage of error between the reference FE solution and that of the ROM.

Figure 5.13: Nodal normal velocities of a cut-through of PEM at 4.67mm from the interface with the plate. This motion pattern corresponds to the system resonance at 200 Hz (figure 5.11).

It can be observed how the percentage of relative error remains always below 0.003% (figure 5.13b).

Table 5.2: Calculation time for the HFM and for the ROM. The simulation ran on Python 3.5 and on an Intel(R) Core(TM) i5-4310U CPU 2.00GHz 2.60GHz

	offline T [s]	online T [s] 1 inversion	FRF T [s] 1000 freq lines
HFM	\emptyset	34	34e3
ROM	5.2e3	0.021	5.2e3

Concerning the computational performance, the full FE model requires 100 time units per calculation while the ROM needs only 0.05. The offline cost needs to be also considered; this is proportional to the computational cost of the FE model and to the number of snapshots needed to generate an accurate POD basis. For the above mentioned example, the computational cost for the calculation of 1000 frequency lines with the original FE model was 8 hours. With the reduced order model the total time to obtain a result in the same range is slightly over 1 hour, while the cost of the online simulation of the ROM is in the range of 20 seconds.

The reduction obtained in the numerical examples shows that the procedure suggested in this thesis could provide important benefits for investigating large frequency ranges while maintaining high level of accuracy with respect to its parental technique (i.e. FE solution). The relatively expensive cost for the creation of the ROB is compensated by the low number of DOF that makes the online simulation orders of magnitude faster than the reference simulation. Moreover, applications of this method to multidimensional problems and optimisation studies would generate even larger gains. In fact, the offline time would vanish if the ROM served an expensive optimisation procedure (e.g. Monte Carlo simulation).

5.4 Conclusions

In this chapter, the *model order reduction* (MOR) procedure of chapter 4 is adopted to improve the simulation efficiency of *Finite Element* (FE) models containing *poro-elastic materials* (PEM). The models analysed in the chapter are typical multilayer configurations for trim components used for acoustic insulation. In the second example, an absorption package is inserted in an air

cavity to reproduce a simplified passenger compartment. The results obtained with the method are satisfactory in terms of accuracy and speed-up. In the presented examples, satisfactory levels of accuracy are met in the full frequency range of interest enabling speed-ups between 7 and 9 times using 1000 frequency lines for the response reconstruction (including the preprocessing time). Great evidence is given in the case of the PEM layer coupled to a cavity and an aluminium plate. To generate the ROB, 150 snapshots were calculated. These led to a ROM containing 114 DOF against the parental FE model that contains 21440 DOF.

As discussed, the time for the reduced order model consist of an offline time (creation of the POD basis) and the actual simulation time. The latter weights on the total cost for less than 1% of the total. Moreover, following the same strategy, the RB method can be extended to consider multi-parameter variations (material characteristics, damping) providing even more important gains for design and optimisation methods such as Monte Carlo simulation.

For cases where the parameter range allows to have a *number of snapshots* that is much smaller than the *FE's DOF*, the proposed technique can offer a good level of reduction for any 3D structure containing PEM with, at least piece-wise, uniform properties.

Chapter 6

Multi-parameter study on vibroacoustic systems containing poroelastic materials

Optimization studies that require the exploration of large parameter spaces (e.g., Montecarlo simulations [4]), can be very expensive procedures especially if they involve optimisation of systems combined together (e.g. a mechanical system and its control unit [5, 6, 7]). In this context, PMOR is of great use as it enables repeated calculations at high rate.

In chapters 4 and 5, an RB method was implemented to calculate FRF of models containing PEM. In the conclusions to those chapters, it emerged that this method can be extended to include more parameters variations other than the frequency. Therefore, in this chapter, the method is applied to include variation of the flow resistivity which is the Biot parameter that most can affect the performances of the system analysed.

To summarise, the RB method requires an affine representation of the system in order to enable for a parametric ROM that employs a single global ROB. In this case, the same affine functions retrieved in section 4.1.2 can be used to include the other Biot parameters. On the other hand, the construction of the ROB is expected to be more challenging since it should be able to describe the

dynamic of the system in a larger parameter space. The possible difficulties and limitations could originate from many steps of the procedure: (i) sampling the parameter space with sufficient snapshots may result being an expensive operation; the number of snapshots can grow exponentially with the number of parameters if a tensorial sampling is employed; (ii) the application of the SVD could result being an impasse for the method if the number of snapshots sampled is too large; (iii) the dimensions of the ROB may be large and make the utilization of the ROM less attractive.

The performances of the method implemented in this chapter will be compared to those of chapters 4 and 5 and to the direct method. This will help as a guideline on when it can be considered to implement such a method or prefer another.

The models used for testing are made of a subsystem of PEM attached to a rigid surface as represented in figure 4.1 and to the multilayer system of figure 5.3.

6.1 Preliminary study on a single layer of PEM layer

A parametric study on model of figure 4.1 was used to establish which parameters can affect the performances of a PEM the most. From the analysis it emerged that only flow resistivity and the relative characteristic thermal and viscous lengths are relevant for this study. Moreover, the distribution of the flow resistivity can result to be non-constant through the material due to its production process [89].

As mentioned in the introduction, the affine representation derived in section 4.1.2 holds also for the Biot parameters and therefore for the *flow resistivity* (see section 2.2.1).

For the example of the single layer of PEM depicted in figure 4.1, the flow resistivity is perturbed in the range $[2e4 \ 5e4] \text{ Pa } m^{-1}s$ and the results are illustrated in figure 6.1. The ROB used for this parametric ROM contains 10 vectors. However, 45 snapshots were used to fully explore the new parameter space and generate the ROB.

Figure 6.1 shows how large variations of the parameters can be captured by the use of a PMOR approach with an advantage for the computation time. Nevertheless, the applicability of this approach should be studied on larger

models assuring that the resulting size of the parametric ROM will still provide computational advantages. In the following section, the method is applied to more complex models with large parameter space that will show its limits.

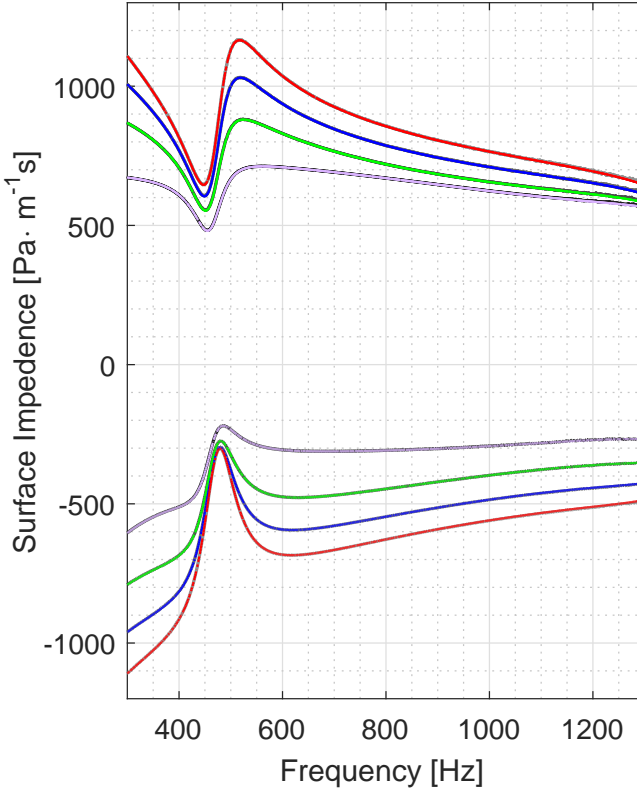


Figure 6.1: Surface impedance for variations of the flow resistivity in range $[2e4 \ 5e4] \text{ Pa m}^{-1}\text{s}$ and in the frequency range $[300 \ 1300] \text{ Hz}$. The red lines refer to $\sigma = 5e4 \text{ Pa m}^{-1}\text{s}$; the blue lines to $\sigma = 4e4 \text{ Pa m}^{-1}\text{s}$; the green lines to $\sigma = 3e4 \text{ Pa m}^{-1}\text{s}$; the violet lines to $\sigma = 5e4 \text{ Pa m}^{-1}\text{s}$; dashed lines refer to imaginary part, solid lines to real part. In grey scale are the solution obtained with the ROM that appear to lose some accuracy only in the higher frequency range.

6.2 Flow resistivity variations in the PEM layer of a trim component connected to an acoustic cavity

In this section, the influence on the results of the variation of the flow resistivity on the system of figure 5.9 is investigated.

The perturbations are considered between $[5e4 \ 12e4] \text{ Pam}^{-1}\text{s}$ and a global ROB is used to generate a RB model. These are typical values of flow resistivity and in this range is also expected to find the optimum in terms of noise reduction for the PEM components [15]. The reduced model is requested to generate data with comparable accuracy to the results obtained in section 5.3.2.

The RB method applied to this study is the same presented in section 4.1. The ROB is generated from the application of the POD method. The affine functions are retrieved in chapter 4 and used as in equations (4.16) or (4.17).

6.2.1 ROB generation for a 2-dimensional parametric space

In this problem, the parameter space varies again in 2 dimensions. The sampling criteria available for multidimensional spaces play an important role in the quality of the final result [40] and many are the options available for this task [40, 90]. As was shown in chapter 5, the graph of the singular value decay can give important indications about the quality of the ROB. In this section, the influence of sampling on the quality of the reduction is investigated.

Stratified sampling in frequency and random sampling in the flow resistivity

The first approach used to generate the snapshots for the POD is to continue using the stratified sampling for the frequency exploration in the range $]0 \ 1000 [\text{ Hz}$, as presented in chapter 5, and to opt for a random distribution of the values of the flow resistivity in the range $[5e4 \ 1.2e5] \text{ Pa m}^{-1}\text{s}$.

The basis is generated increasing the number of snapshots at each iteration as done in the one dimensional case of chapter 5.

The decay of the singular value for this sampling approach is shown in figure 6.2. The results show that with 800 snapshots the system does not appear to

have complete information and it would require even more samples. Using the same truncation as in chapter 5, this results in a ROB with 547 snapshots.

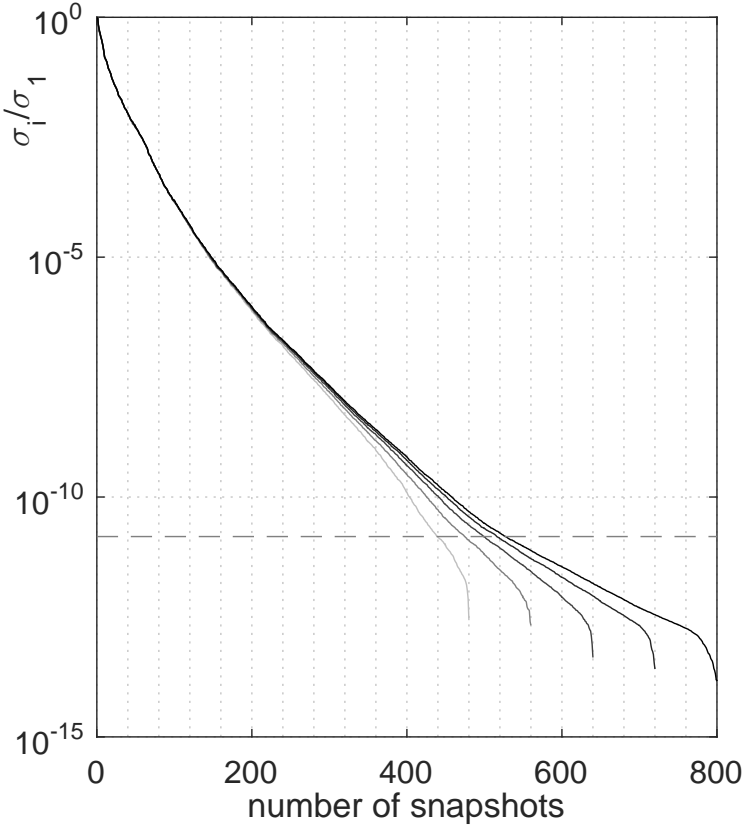


Figure 6.2: Decay of the singular values for different numbers of snapshots to generate a POD basis to include variations of the flow resistivity in the range $[5e4 \ 1.2e5] \text{ Pa m}^{-1}\text{s}$ with random sampling and in the low frequency range up to 1000 Hz with the stratified sampling.

■ 800 snapshots; ■ 720 snapshots; ■ 640 snapshots; ■ 560 snapshots; ■ 480 snapshots.

Comparing figure 6.2 to figure 5.10, the singular values reveal that the amount of information required to generate the ROB grows considerably when a second parameter variation is considered in the sampling. Another element to be

considered is that after 800 snapshots no clear plateau is present in the decay making it difficult to establish if the available information is sufficient to reconstruct solutions in all the parameter range. However, the analyses of the following sections, the case with 800 samples will be considered as sufficient and used to retrieve the ROB. The decision follows the observation that for values of $\sigma_i/\sigma_1 = 10^{-11}$ the difference between the 720 snapshots and the 800 snapshots appears to be small.

Tensorial sampling in frequency and random sampling in the flow resistivity

In this section the flow resistivity is sampled with 4 master values: $\{5e4, 7e4, 10e4, 12e4\} Pa m^{-1}s$. This will show how an unthoughtful sampling may lead to imprecise or wrong conclusions. Figure 6.3 shows the singular value decay with this choice of sampling. From a superficial look, it appears that the resulting ROB can cover well the parameter space as it shows the plateau as it would be expected for an SVD analysis of snapshots. However, as previously mentioned, the information is biased and linked to some master values of the flow resistivity and without including information from the in-between values. As a result, it can be expected a highly accurate result when the flow resistivity assumes one of these master values and a possibly poorer accuracy away from them.

The other observation is that the dimension of the ROB would result being rather small with 441 vectors (against the 547 necessary in the case of the random sampling) appearing to be more competitive than that obtained with the previous sampling.

In the result sections, the effect of the ROB obtained with the different pools of snapshots will be shown and further discussed.

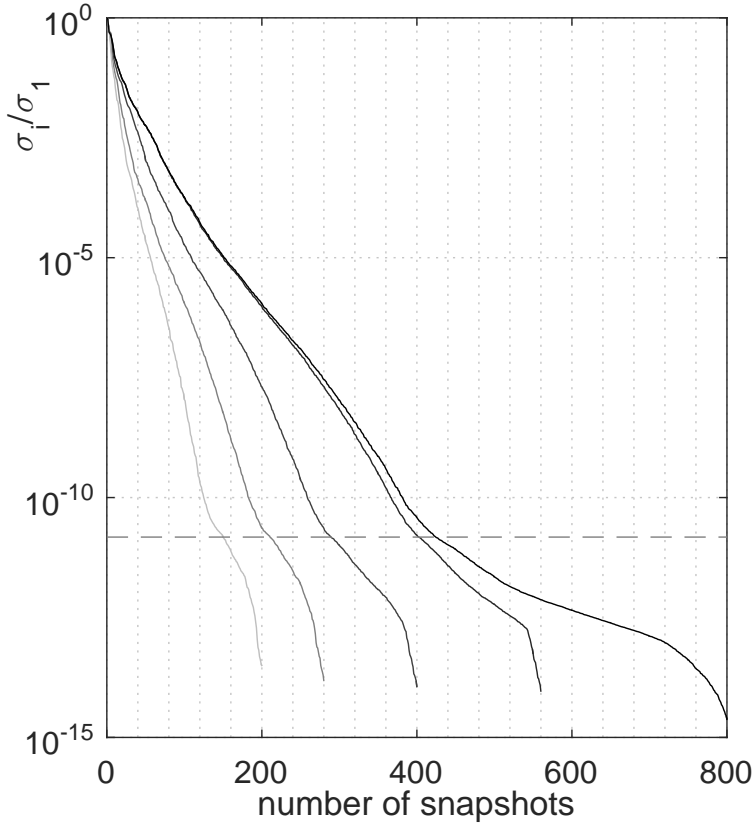


Figure 6.3: Decay of the singular values for different number of snapshots to generate a POD basis to include variations of the flow resistivity in range $[5e4 \ 1.2e5] \text{ Pa m}^{-1}\text{s}$ with 4 master values and in the low frequency range up to 1000 Hz with stratified sampling.

■ 720 snapshots; ■ 640 snapshots; ■ 560 snapshots; ■ 480 snapshots; ■ 320 snapshots.

6.3 Results

This section shows the results obtained with the ROB of sections 6.2.1 and 6.2.1. As in chapter 5, the accuracy is compared to that of the FE analysis of the models.

Using the ROB of section 6.2.1, the FRF appear to be accurate for all the values of the flow resistivity in the range. On the other hand, the dimensionality of the space, 547 vectors, is large and required 800 snapshots to be computed. The FRF obtained with this method are displayed in figures 6.4 6.5 and 6.6 respectively displaying the results for flow resistivity $5e4 Pa m^{-1}s$, $9e4 Pa m^{-1}s$ and $12e4 Pa m^{-1}s$. In all cases, the accuracy of the results is high and comparable to that of figure 5.11.

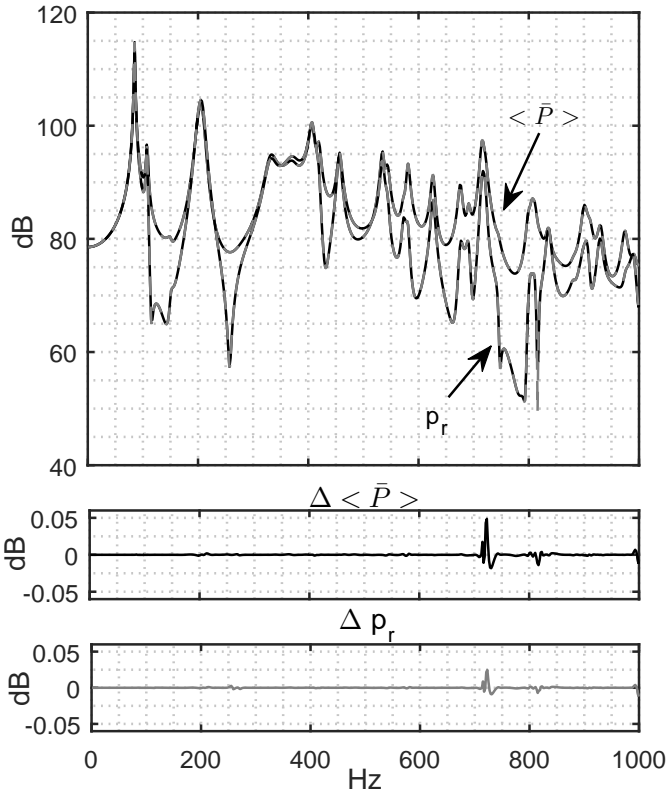


Figure 6.4: Simulation results of the system in figure 5.9 for flow resistivity of the PEM layer $\sigma = 5e4 Pa m^{-1}s$ using the ROB of section 6.2.1. Mean squared pressure $\langle \bar{P} \rangle$ in the air cavity and pressure at receiver location p_r . The solid grey lines in the top graph refer to the direct simulation of the FE model. The dashed black lines refer to the ROM. The graph at the bottom represents the difference in decibel between direct FE results and ROM results.

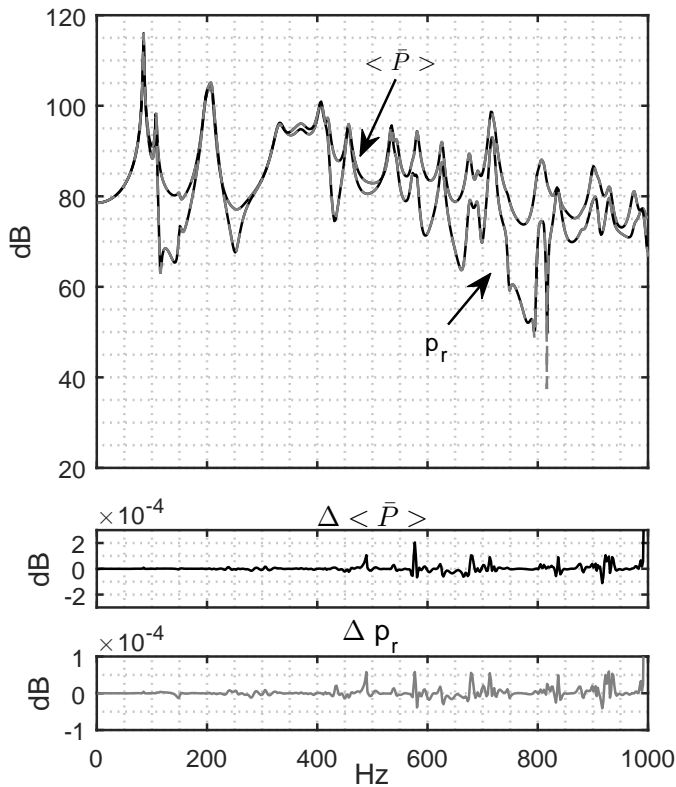


Figure 6.5: Simulation results of the system in figure 5.9 for flow resistivity of the PEM layer $\sigma = 9e4 \text{ Pa m}^{-1}\text{s}$ using the ROB of section 6.2.1. Mean squared pressure $\langle \bar{P} \rangle$ in the air cavity and pressure at receiver location p_r . The solid grey lines in the top graph refer to the direct simulation of the FE model. The dashed black lines refer to the ROM. The graph at the bottom represents the difference in decibel between direct FE results and ROM results.

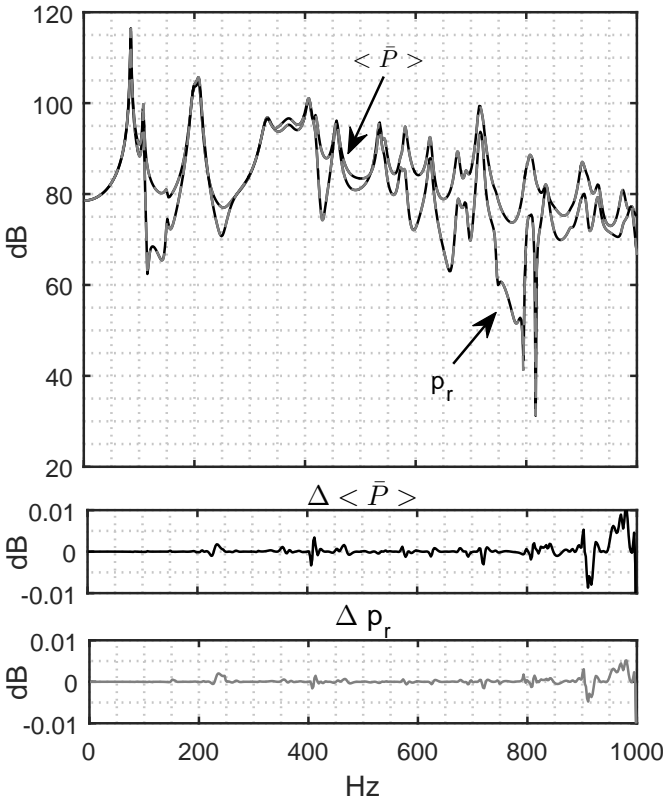


Figure 6.6: Simulation results of the system in figure 5.9 for flow resistivity of the PEM layer $\sigma = 12e4 \text{ Pa m}^{-1}\text{s}$ using the ROB of section 6.2.1. Mean squared pressure $\langle \bar{P} \rangle$ in the air cavity and pressure at receiver location p_r . The solid grey lines in the top graph refer to the direct simulation of the FE model. The dashed black lines refer to the ROM. The graph at the bottom represents the difference in decibel between direct FE results and ROM results.

Using the ROB obtained with the sampling of section 6.2.1, the results show what was expected in the discussion, the FRF appear to be very accurate in correspondence of the master values of the flow resistivity and a reduced accuracy far from these points.

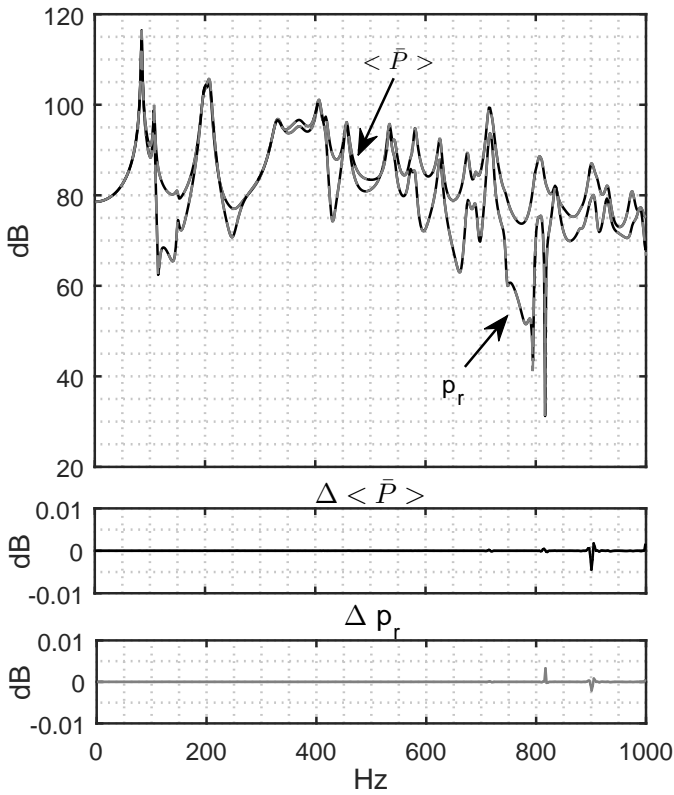


Figure 6.7: Simulation results of the system in figure 5.9 for flow resistivity of the PEM layer $\sigma = 12e4 \text{ Pa m}^{-1}\text{s}$ using the ROB of section 6.2.1. Mean squared pressure $\langle \bar{P} \rangle$ in the air cavity and pressure at receiver location p_r . The solid grey lines in the top graph refer to the direct simulation of the FE model. The dashed black lines refer to the ROM. The graph at the bottom represents the difference in decibel between direct FE results and ROM results.

In figures 6.8 and 6.9 the values assigned to the flow resistivity parameter are respectively $\sigma = 9e4 \text{ Pa m}^{-1}\text{s}$ and $\sigma = 11e4 \text{ Pa m}^{-1}\text{s}$ that are not used as input to generate the tensorial ROB. Despite the number of vectors in the ROB is 441, the FRF differs from the reference with discrepancies up to 3 dB.

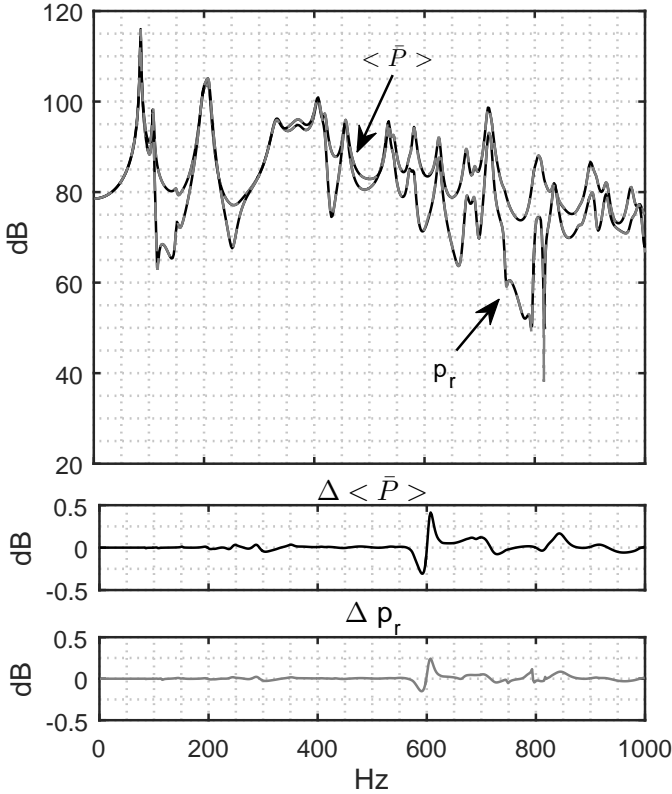


Figure 6.8: Simulation results of the system in figure 5.9 for flow resistivity of the PEM layer $\sigma = 9e4 \text{ Pa m}^{-1}\text{s}$ using the ROB of section 6.2.1. Mean squared pressure $\langle \bar{P} \rangle$ in the air cavity and pressure at receiver location p_r . The solid grey lines in the top graph refer to the direct simulation of the FE model. The dashed black lines refer to the ROM. The graph at the bottom represents the difference in decibel between direct FE results and ROM results.

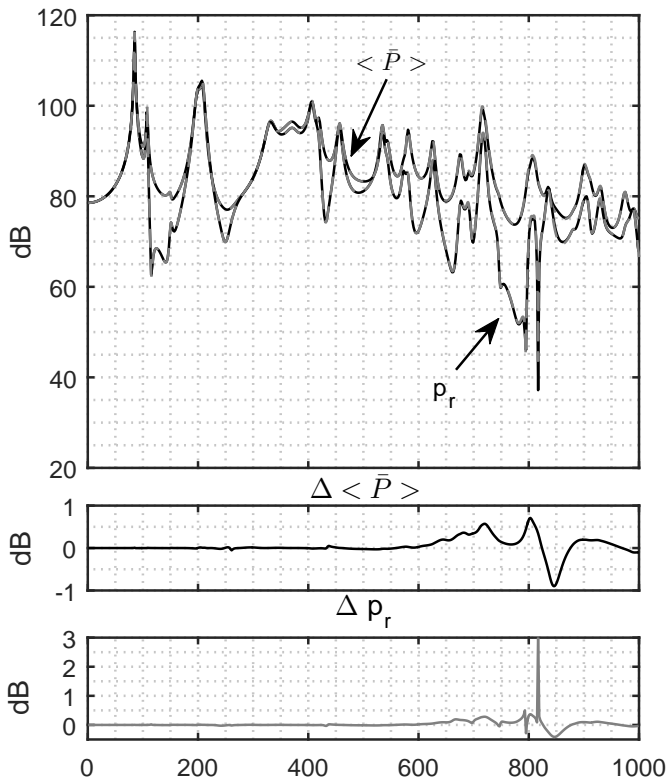


Figure 6.9: Simulation results of the system in figure 5.9 for flow resistivity of the PEM layer $\sigma = 11e4 \text{ Pa m}^{-1}\text{s}$ using the ROB of section 6.2.1. Mean squared pressure $\langle \bar{P} \rangle$ in the air cavity and pressure at receiver location p_r . The solid grey lines in the top graph refer to the direct simulation of the FE model. The dashed black lines refer to the ROM. The graph at the bottom represents the difference in decibel between direct FE results and ROM results.

The computational costs indicated, even for this case where only one of the possible parameters of interest for an optimisation problem is accounted, show the need for refinements of the technique for this kind of parametric studies. Moreover, the accuracy offered by the ROM start to slightly decrease. In fact, even though the difference with reference solution is acceptable for industrial application, may become critical if it would grow further (e.g. in case of larger parameter spaces).

The number of snapshots went up to 800 from the 150 used in the application of MOR of section 5.3.2 where all the parameters were constant. This increase of computation time of more than 5 times suggests that, in case of larger parameter spaces, it may be more convenient to opt for partitioning of the parameter space into smaller ones rather than using a single global ROB. In case the optimisation technique would require a small number of iterations to converge to a satisfying solution, computing a new ROM as in section 5.3.2 for each configuration of the flow resistivity may be preferable to having a single ROB.

Further expansions of the parameter space cannot be undertaken by the presented method without some adaptations: first of all, the results suggest that the snapshot method would require a high number of samples; this may be compensated by the implementation of greedy algorithms for the construction of the ROB. However, the number of vectors included in the ROB was large and suggests that, even using a wiser approach for the parameter space exploration, it may be necessary to make partitions of the parameter space applying methods like PEBL-ROM [25].

6.4 conclusions

In this chapter, an application of the RB method for parametric studies of system containing PEM was presented. The method adopted was exhaustively described in chapters 4 and 5 and here extended to include multi-parameter investigations.

The parameters considered are those of the PEM, i.e., the Biot parameters. Of these, the parameter that can affect the acoustic performances of the material the most is the flow-resistivity that was therefore chosen for the numerical analysis.

The construction of the ROB proved to be challenging and requiring thoughtful sampling when the method of snapshots is employed. In fact, the results

showed that, a correct choice for the sampling of the parameter space can determine the success or failure to generate an accurate parametric ROM. The reasonable choice to explore the flow resistivity domain in a small number of values revealed to be not as accurate as assigning random values to it.

More was revealed by the singular value decay. In case of the tensorial sampling, the decay of the singular values (figure 6.2.1) shows a graph where it seems that some of the information contained in the snapshots are redundant and the singular values plateau towards low values. However, the graph cannot tell if the sampling of the parameter space is done correctly. In fact, from the comparison with the singular values of the random sampling (figure 6.2.1), it appears that the ROB requires more information that is not available in the snapshots of the tensorial sampling.

In the analysis, reducibility limitations emerged. With 800 snapshots, the trend of the singular values continue decaying linearly and without a clear plateau as in figure chapter 5. This leads to large ROB that could compromise the applicability of the method or even, in worse scenarios, inapplicability of the method, e.g., the SVD operation becomes too expensive.

The results suggest that, for larger parameter spaces than the one herein tackled, should be addressed refining the methodology through adaptive ROB construction and/or partitioning the parameter space.

Chapter 7

Model Order Reduction of Lattice Girder

The research discussed in this chapter investigates the possibility of applying PMOR to structural finite-element models consisting of beam elements as FOM. It is shown that for these models, the system matrices (mass and stiffness) can often be represented as an affine function of a small set of scalar parameter functions. The constituent matrices of this affine relation can be reduced offline, such that the online computational cost is independent of the FOM size. The cross-sectional and material parameters for the beams are considered in this work.

It is shown how a very efficient reduction can be performed by using a constant projection space when the manifold associated with the parameter space of interest has a small Kolmogorov n -width.

The work-flow to generate the PROM is as follow: parameter sample generation of the FOM; selection of the appropriate scalar parameter functions; use the FOM to construct the local ROB (modal space) for a single parameter; generate the global ROB through an *ad-hoc* developed greedy algorithm. This procedure is validated numerically on a FE model of a gantry bridge. This example demonstrates the speed-up for evaluating different parameter responses from the PROM in comparison to the FOM while still maintaining the required accuracy.

7.1 Introduction

One of the goals of this work is to develop a PMOR technique that minimises the simulation time for FE models of lattice girder by bringing all the expensive computation offline. This PMOR scheme is based on an affine representation made *ad-hoc* for models of beam networks and a global projection space is used considering problems of small Kolmogorov n -width. The two together allow to generate a ROM completely independent from the computational load of the original FOM.

In literature, affine functions to describe the stiffness matrix variation of a plate with the thickness are already used for PMOR. In [28], the authors use Taylor expansions to retrieve affine functions of stiffness matrices. More generally, low order polynomial curve fitting could be used. In either case, this approach suffer an exponential growth of the affine functions with the number of parameters considered in the ROM.

The lattice girder is modelled as a network of beams. This allows to generate the affine functions of the model based on Timoschenko beam theory. This approach decreases considerably the amount of functions needed for an accurate description and enables an accurate analysis of multi-parameter perturbations.

The results of this research are exploited in the work of Moten et al. [5, 6, 7] in the field of optimisation of controllers simultaneously with the mechanical system of application.

This chapter refers to the research presented in [82, 91] and is organised as follows. In section 1.3.2 (from [82]), the PMOR scheme is described. In section 7.2 (from [82]), the affine functions of the parameters are derived based on physical considerations of the beam and are used to describe the system matrices. The developed greedy algorithm to generate the global projection space is presented in section 3.2.3 taken from [82]. In section 7.3, an application to a gantry-bridge for laser cutting is presented. The bridge presents a network of simple beams all characterised by a hollow rectangular cross-section. Comparisons with the results of the FE model are shown.

7.2 Affine representation for beams

Projection based MOR applies to a vast range of detailed numerical models. Structural FE models will be used in this work to study the dynamics of a

network of beams.

The starting hypothesis is the existence of a finite-dimensional set of functions of the parameters of interest that can describe the matrix variation. In Hong et al. [28], the variation of the stiffness of a plate with respect to one geometrical parameter is described without the need of interpolation using a Taylor polynomial. A general polynomial expansion of d variables of order η would lead to η^d monomials and in a multivariate problem, as the one herein presented, this approach results unfeasible and a different approach has to be found.

The proposed approach is to look into the mechanism of deformation of the beam element and to find the affine function of the parameters needed to describe the system matrices. The 3D beam element refers to a straight bar with uniform cross-section that can undergo axial, bending, and torsional deformation. The shape functions of a 3D beam element have to describe a few different phenomena: longitudinal displacement, axial torque, transversal deflections and rotations. The beam element has two nodes located at its extremities, each having six DOF. Herein, linear elastic behaviour of the material is considered.

Considering the reference frame to be the three principal axes, it is convenient finding the stiffness quantities through force and moment equilibrium equations at the nodes. In fact, using this shrewdness, the stiffness matrix of a single 3D beam element is strongly decoupled and can be divided in sub-matrices [92]. The global stiffness matrix of the beam element contains all the necessary information to generate the affine functions used in the presented method. Below, formulas describing load-displacement relations of the DOF in the 3D beam element are discussed in order to find a minimal set of basic functions that can describe the relation between the design parameters and the system matrices used to simulate the system behaviour.

Axial translation and rotation

The submatrix corresponding to axial load is a 2 by 2 matrix. The entries are all proportional to

$$k_1 = \frac{EA}{L}, \quad (7.1)$$

where E is the young modulus, A is the cross section, L the length of the beam. The submatrix relative to the axial torsional DOF is also 2 by 2 with

entries proportional to

$$k_4 = \frac{GJ}{L} \quad (7.2)$$

In this equation J is a shape factor [93] that is introduced in place of the polar moment of inertia to account for the warping of the surfaces during axial rotation of non-circular cross-sections. The dimension of this factor is $[m^4]$. This can be generally expressed as a function of the geometrical parameters that define the cross section. In [94], the expressions of J are listed for many different geometries.

Transverse deflection and rotation

The mechanism of deformation due to transverse load is a complex phenomenon that is governed by partial differential equations that not always have a known exact solution. However, in the hypothesis of small deformation, accepted approximations are available and used. These are Euler-Bernoulli beam theory, Rayleigh beam theory and Timoshenko beam theory, from least to most accurate. The first is only valid for slender beams as it does not include any effect due to shear, and rotational inertia are neglected. Rayleigh theory includes rotational inertia but this brings very little improvements as it still considers an undistorted cross-section during bending. The deflection calculated according to Timoshenko beam theory includes the effect of shear [95]. Effect of shear has to be taken into account for non-slender beams and this is of crucial importance in a FE model where, if a dense mesh is used, the characteristic length of the beam elements would result in short beams where the shear effect is dominant and cannot be neglected.

The methodology herein presented uses Timoshenko beam theory. The two mechanisms of deformation, bending and shear, can be thought to work in series. In fact, one of the fundamental hypothesis to derive this theory is that the total deflection equals the sum of the deflection due to bending and the deflection due to shear

$$d(x) = d_b(x) + d_s(x) \quad (7.3)$$

where, d_b and d_s refer to bending and shear deformations respectively. To find the total deflection, the two contributions are retrieved solving the following

differential equations separately

$$\frac{\partial^2 d_b}{\partial x^2} = \frac{P_z x}{EI_y} \quad (7.4)$$

$$\frac{\partial d_s}{\partial x} = -\frac{P_z}{kAG}. \quad (7.5)$$

Equation (7.4) relates the bending moment (given by the vertical loading force times its distance in the horizontal direction $M_y = P_z x$) and the displacement of the beam. I_y is the moment of inertia about y -axis.

Equation (7.5) describes the relations between the shear force and the transverse displacement; k is the form factor for shear defined as

$$k = \frac{A}{I_y^2} \int_A \frac{Q^2}{b^2} dA \quad (7.6)$$

where Q is the first moment, b is the distance of the infinitesimal area dA from the neutral plane for bending. Simplifications of equation (7.6) are available for most common cross-sections. The application presented in section 7.3 uses hollow rectangular cross-section of which in [96] is given an approximation for the form factor

$$k = \frac{A}{A_{web}} \quad (7.7)$$

with A_{web} being the portion of surface as indicated in figure 7.1.

Once the general solutions of the differential equations (7.4) and (7.5) are calculated, boundary conditions typically used in FE can be applied to generate the expressions of the stiffness. The sub-matrix for the transverse deflection and rotation can be written as

$$k_d = \begin{bmatrix} R & L/2 \cdot R & -R & -L/2 \cdot R \\ L/2 \cdot R & L^2/4 \cdot R + EI/L & L/2 \cdot R & L^2/4 \cdot R - EI/L \\ -R & L/2 \cdot R & R & -L/2 \cdot R \\ -L/2 \cdot R & L^2/4 \cdot R - EI/L & -L/2 \cdot R & L^2/4 \cdot R + EI/L \end{bmatrix} \quad (7.8)$$

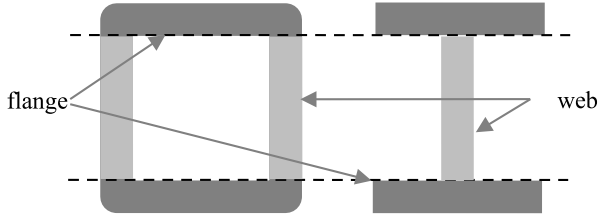


Figure 7.1: Cross-sectional surface partitioning [91]. The portions indicated as flange are those where most bending energy is absorbed. The shear is dominant in the web. The notation comes from the I -shaped cross-section and it is used analogously for the hollowed rectangular cross-section [96].

where

$$R = \frac{12EI}{L^3} [1 + 12EI/(kAGL^2)]^{-1}. \quad (7.9)$$

The affine function

From equations (7.1) - (7.9), affine functions that can describe all the entries of the stiffness matrix (approximately) can be generated. If the parameters of interest are those of the cross-section, it is possible to take all the independent expressions that contain the parameters and an affine representation of the stiffness matrix can be made

$$K(\mu) = \sum_{i=1}^{n_f} \mathcal{A}_i f_i(\mu). \quad (7.10)$$

\mathcal{A}_i represents the i -th matrix of coefficients of the corresponding basic function f_i . The parameters that can be taken into account are those that define the cross-section and the material properties. In section 7.3, where an example is given, elements characterised by hollow rectangular cross-sections are adopted and the parameters taken into account are h, w, t being height, width and wall thickness. Therefore, equations (7.1) - (7.9) are simplified and rewritten to generate an independent set of base functions. The chosen basic functions are

summarised in table 7.1.

From affine function (7.1) and (7.9) of table 7.1, one can notice how the length of the beam is not an invariant of the problem in this case: if the system contains 2 beams of same cross-section but different length, equations (7.1) and (7.9) have to be evaluated for both lengths. However, as most beam meshes show relatively high regularity, a sufficient number of beams with the same parameters are typically present, such that a useful reduction can be obtained.

The Least Square (LS) problem to solve is used to find the coefficient matrices \mathcal{A}_i of equation (7.10), for each element of matrix K and M as described in equations (3.4) and (3.5).

In section 7.2, affine functions are identified for the stiffness matrix. For the mass matrix, suitable affine functions can also be provided following a similar approach. For the element with hollowed cross-section of the example in section 7.3 a lumped mass matrix is used; therefore, the resulting affine functions are

$$m_x = m_y = m_z = \rho \frac{L}{2} A \quad (7.11)$$

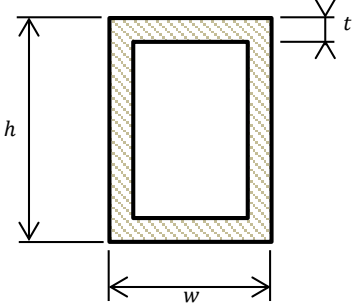
where ρ is the volumetric density, m_x, m_y and m_z are the 3 mass components. For the rotational inertia

$$J_x = \rho \frac{L}{2} J \quad (7.12)$$

where J is the polar moment of inertia. The mass matrix used in this work is a lumped mass matrix and this justifies the selection of base functions (7.11) and (7.12).

The scheme of equation (7.10) adds an important constraint: the full order matrices used to feed the LS method should be all of same dimensions. Therefore, parameter variations should not affect the topology of the discretisation in this case. In the following section, the parametric matrices are projected while maintaining the affine dependency.

Table 7.1: Example of affine functions derived for a beam with hollow rectangular cross-section [91].

Cross-section	Affine functions	Description	#
	$A = 2(h + w)t - 4t^2$	From equation (7.1)	1
	$J = \frac{2t^2(h-t)^2(w-t)}{(h+w)t-2t^2}$	From equation (7.2)	2
	$I_y = \frac{hw^3}{12} - \frac{(h-t)^3(w-t)}{12}$	From equation (7.8)	3
	$I_z = \frac{hw^3}{12} - \frac{(h-t)(w-t)^3}{12}$	From equation (7.8)	4
	$I_y \left[1 + \frac{12EI_y}{\kappa_1 AGL^2} \right]^{-1}$	From equation (7.8)	5
	$I_z \left[1 + \frac{12EI_z}{\kappa_2 AGL^2} \right]^{-1}$	From equation (7.8)	6

7.3 Case study

This section shows an application of the developed PMOR scheme to a gantry crane for laser cutting. The gantry refers to a lattice girder structure that is used to move objects over an area to perform planar machining operation. Therefore, a gantry should be designed according to the excitations, the velocity of operations and the weight to be carried during the operations. The initial design of the gantry is shown in figure 7.2. A combination of high-speed manoeuvres and heavy loading may cause the entire structure to malfunction or resonate.

The main components of this gantry are the bridge, two motors, and a laser head (figure 7.2). The bridge is attached to a railway allowing translation orthogonally to its main axis; on the bridge, a second railway guides the translation of the laser head. In this configuration, the bridge itself is expected to be the most sensitive to the large accelerations of the manufacturing process. Therefore, the system is described as a network of beams (see figure 7.3) to which lumped mass and stiffness are attached where motors and laser head are located.

If materials and topology of the structure are already selected, optimisation

and analysis of dynamic characteristics concern the cross-sections of the beams only. In this model, 3 cross-sections are used to model the different trusses (figure 7.4) and they are assembled in a way to ensure good compatibility for welding. There is a rectangular cross section described by h , w and 2 other squared cross-sections one of edge h and one of edge w . All beams are hollow and the wall thickness is t . The material is assumed steel and the structure is

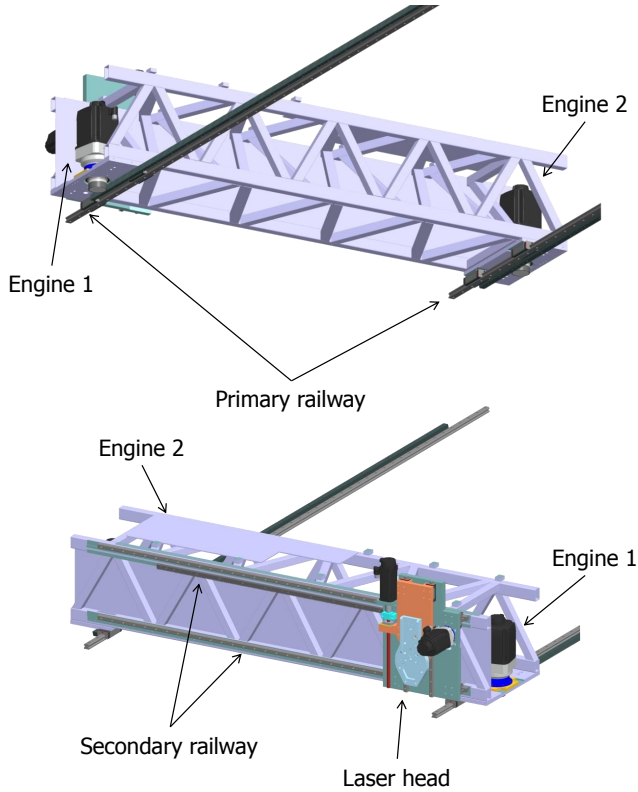


Figure 7.2: Gantry bridge of the laser-cutting machine [91].

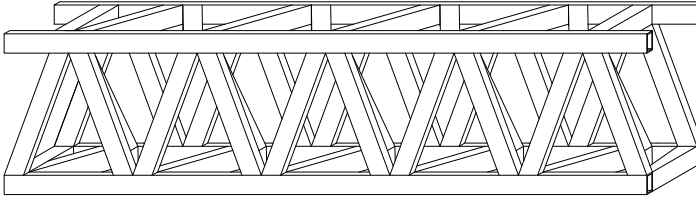


Figure 7.3: Gantry bridge of the laser-cutting machine [91].

constrained in four nodes allowing only translation along the rails (y -axis).

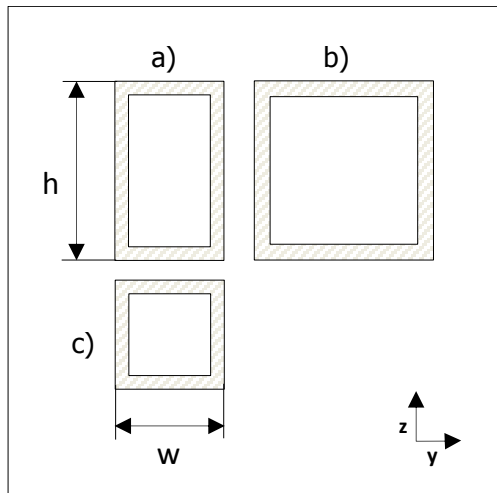


Figure 7.4: Cross-sections used in the model. Cross-section a) is rectangular of dimensions h and w , b) and c) are squared of edge h and w respectively. The wall-thickness t is the same for all the three cross-sections.

7.3.1 Preprocessing and detailed parametric model generation

The gantry is modelled using 1836 DOF and the matrices are generated using NX Nastran. As discussed in section 7.2, the parameter variation should not affect the mesh topology; the number of elements and their connectivity should not change between one configuration and the other.

The equations listed in table 7.1 are rearranged and simplified according to the parameters of interest to generate the set of independent affine functions. It was mentioned in 3.1.2 that if the gathered functions contain redundant information, numerical issues might occur resulting in poor quality of the results. An example of this issue is given here considering the cross-sectional areas adopted in the truss: being A_R, A_H, A_W cross-sectional areas of rectangle, square of edge h and square of edge w respectively.

Table 7.2: List of functions retrieved according to table 7.1 and derived unique monomials [91].

Original functions	Independent functions
$A_R = 2(ht + wt - 2t^2)$ $A_H = 4(th - t^2)$ $A_W = 4(tw - t^2)$	th tw t^2

One may notice that for small wall-thickness with respect to the other dimensions, they are numerically linearly dependent and they reduce to

$$A_R \approx 1/2A_H + 1/2A_W.$$

The issue is solved by making the monomial decomposition of the three functions (table 7.2) as discussed in section 7.2.

When the set of basic functions is complete, the sampling has to be done in order to apply the LS method. The result of the LS method provides the matrices of coefficients for the affine representation of the model as in equation (7.10). The affine model is generated using a high number of sampling points and gives good results in terms of accuracy as shown in figure 7.5, where a collocated frequency response function (FRF) at the left motor is shown.

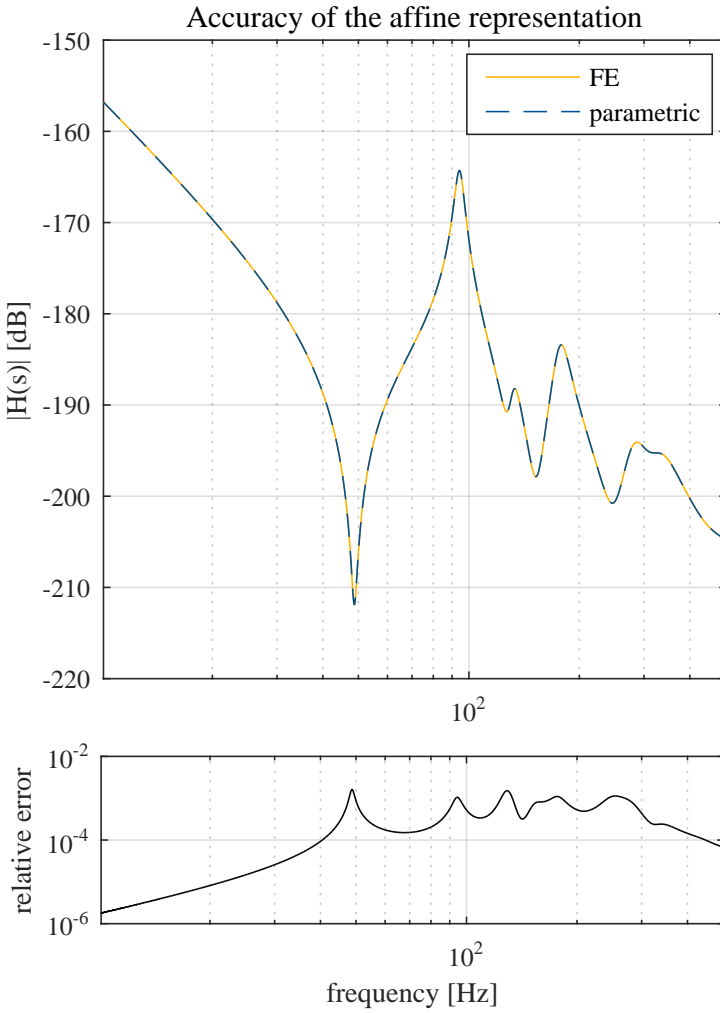


Figure 7.5: Configuration of the motor. Collocated FRF. The representation is split in two. Above the Transfer Function (TF) obtained with the matrices of Nastran is plotted with the TF obtained with the unreduced parametric mode [91].

7.3.2 PMOR using the Modal-SVD approach

To retrieve the global ROB, the portion of the parameter space that is of interest is sampled using a small number of discrete combinations of the parameters. In a first phase, the sampling points may be chosen according to the factorial design [90] where an upper and lower level is chosen for each of the parameters and all the possible combinations are evaluated.

The range of the parameters evaluated in this example are given in table 7.3.

Table 7.3: List of functions retrieved according to table 7.1 and derived unique monomials [91].

Parameter	min [m]	max [m]
height h	5e-2	7e-2
width w	3e-2	5e-2
thickness t	1.5e-3	3e-3

The global projection space V is obtained with an incremental refinement of the initial $2k$ factorial sampling leading to a ROM of 184 DOF. Assessments are made for many combinations of the parameters in the region of interest that give exhaustive results. These assessments are resumed in figure 7.6 and figure 7.7. Figure 7.6 shows a comparison of FRF of the end-effector (the laser head) positioned in this case in the centre. The figure shows the result of the unreduced model (exact solution), computed for the combination $h = 0.06m, w = 0.04m, t = 0.002m$. With the parametric ROM, the same solution is reconstructed and the result shows to be very accurate. An aspect to underline is that for the specific parameter configuration, the local ROB was not used to construct the global ROB. For this reason, the figure shows two other FRF at the same location but for different parameter configurations whose local ROB are used in the matrix of equation (3.11) to generate the global ROB. The accuracy of the model is also assessed looking at deformation patterns at the lower natural frequencies (figure 7.7). Therefore, figure 7.7 contains a table of graphs that represents the evolution of the error for different parameter configurations. All configurations show the relative error to be well below 1 %.

The ROM discussed in this section reduced the size of the problem of 90%. The simulation time is reduced by 98% however, an offline cost for preparation of the ROM should be accounted for. In the table 7.4, these performances are compared.

Table 7.4: Calculation time for the HFM and from the ROM based on the Modal-SVD ROB. The simulation run using Matlab R2015b on an Intel(R) Core(TM) i5-4310U CPU 2.00GHz 2.60GHz

	offline T [s]	online T [s] 1 inversion	FRF simulation T [s] 1000 freq. lines
HFM	∅	7.1	7100
ROM	2.3	0.1	102

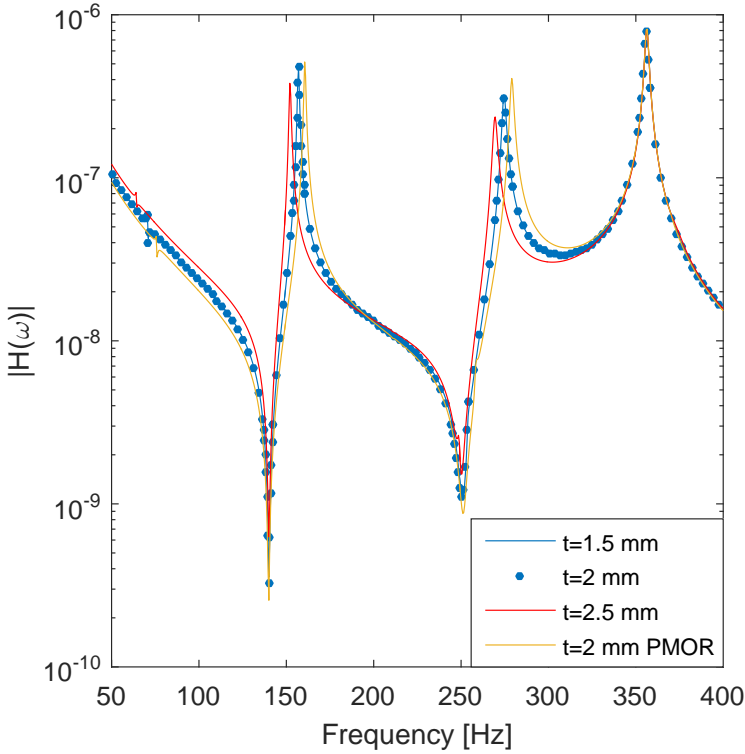


Figure 7.6: Comparison on the frequency response function located at the laser head. The parametric FE model is used as reference. The FRF are calculated on two configuration points where ROB used for the PMOR are retrieved and the comparison is given at an intermediate point where the local ROB is not available. [91].

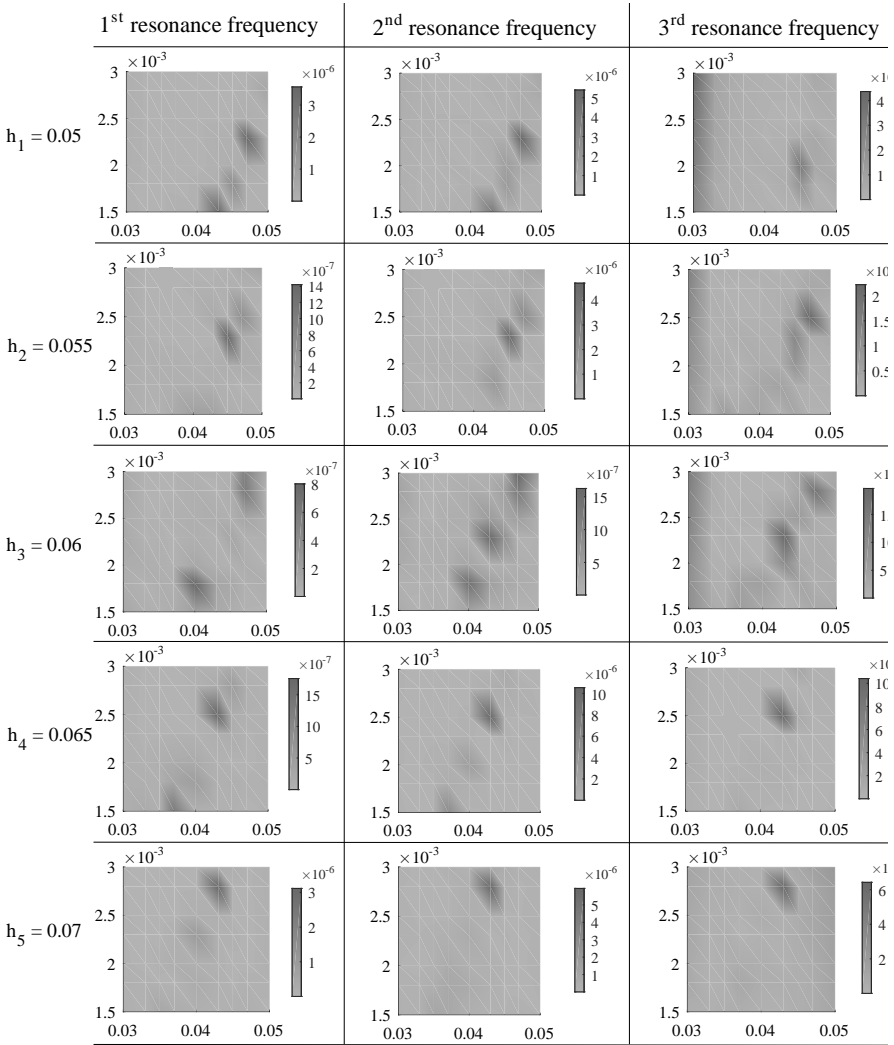


Figure 7.7: Relative error plots for different parameter combinations in the region of interest. The lowest 3 frequencies are evaluated as they are dominated by the bending behaviour who is the most important for the application of this example. In each row of the table, the parameter h is held constant. The parameters t and w are used as variable in each graph. The surface shows the evolution of the relative error. [91].

A posteriori improvements of the ROB can be made changing the samples used to build the global ROB and/or changing the number of mode-shapes used to represent each local configuration. These can be also obtained by means of the above-mentioned greedy algorithm that with incremental improvements of the global ROB, gives a better threshold between accuracy and dimension of the parametric ROM.

7.3.3 PMOR using the greedy algorithm

The greedy algorithm presented in section 3.2.3 yields the required accuracy in 8 iterations. The resulting ROB counts 195 generalised coordinates. In figure 7.8, the representation of the sample points selected through the greedy algorithm is given.

To assess the reduction accuracy, a number of parameter configurations is taken and compared with the result of the full order model. In figure 7.9 the decay of the residual and of the actual error are plotted in logarithmic scale.

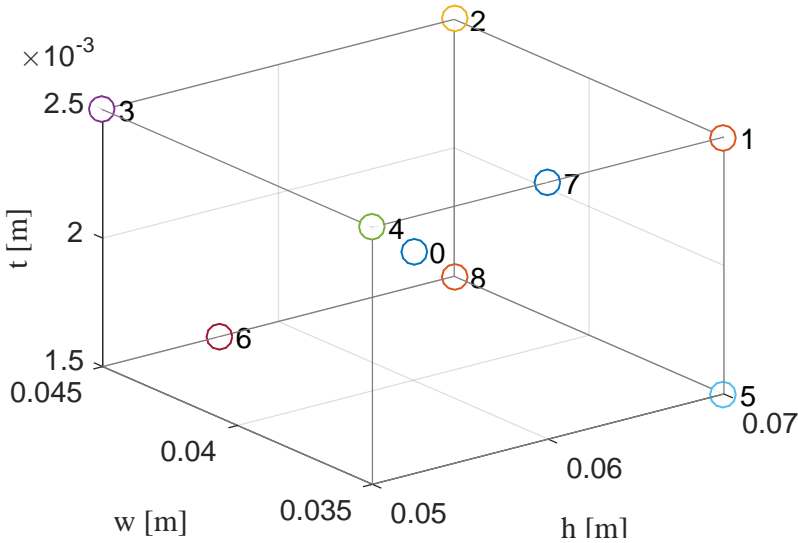


Figure 7.8: The prism represents the parameter domain that is gridded and used to construct the global ROB through the greedy algorithm presented in section 3.2.3. The enumerated points represent the parameter configuration selected by the greedy algorithm at each iteration [82].

Although the results seem very promising, it should be underlined that the error in figure 7.9 only accounts for the error committed on the eigenvalue and not the error on the eigenvectors. Figure 7.10 shows the collocated frequency response functions for the load case described and for all the parameters of the model. Finally in Figure 7.11, the error between the FRF computed with the ROM and the FOM are plotted.

The good results for eigenvalues of figure 7.9 could be expected as they are aligned with the theoretical discussion of section 3.2.3. Nevertheless, the error representation of Figure 7.11 shows that also the FRF can be represented very accurately in the chosen parameter range.

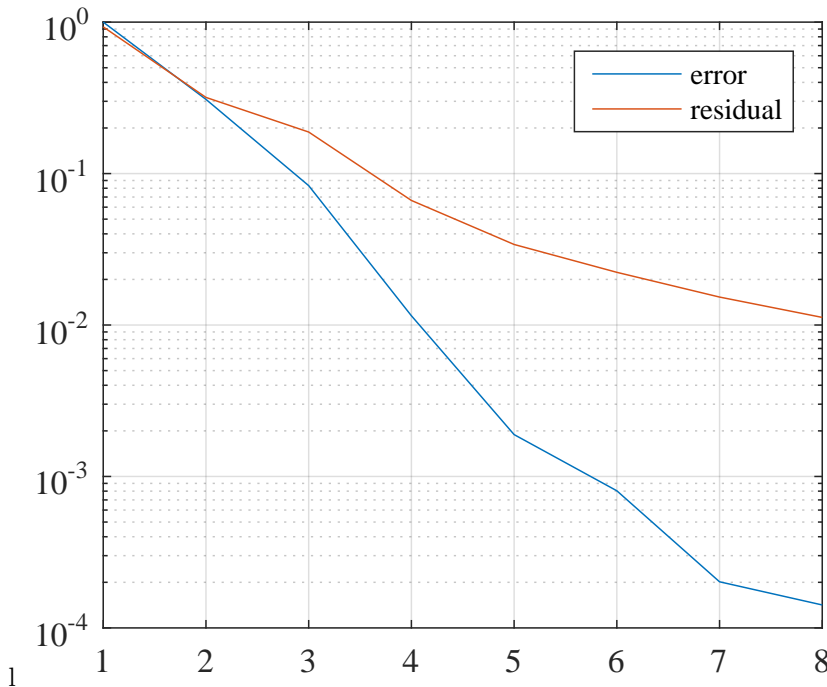


Figure 7.9: Normalised value of the actual error and of the residual at each iteration [82].

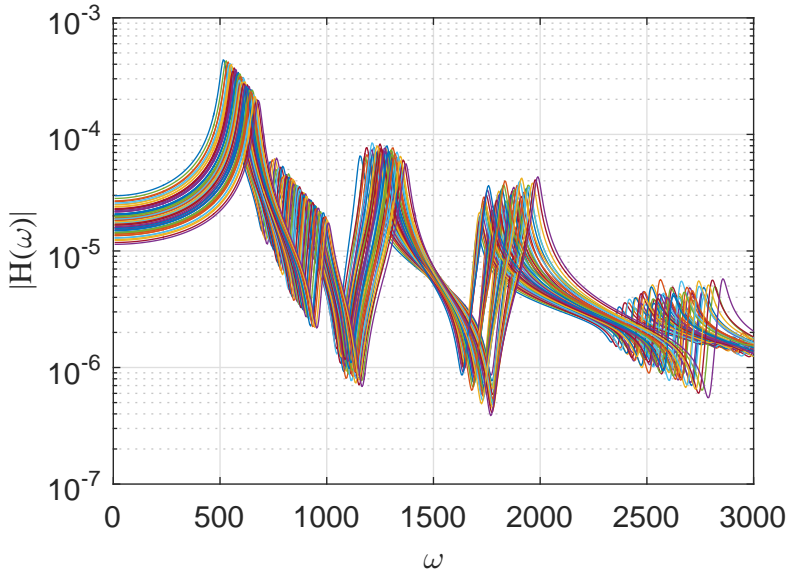


Figure 7.10: Collocated frequency response functions of the gantry bridge at the centre point where the load is imposed. Each response function line is generated using the ROM and corresponds to a different parameter configuration in the range of interest [82].

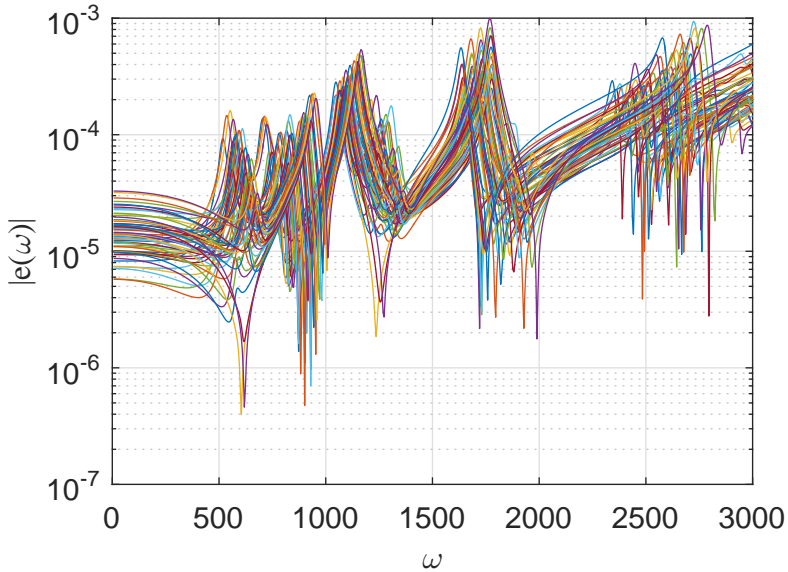


Figure 7.11: Error distribution for the FRF plotted in figure 7.10. $e(\omega) = \left| \frac{y_{ROM}(\omega) - y_{FOM}(\omega)}{y_{FOM}(\omega)} \right|$ [82].

7.4 Conclusions

In this chapter, a methodology for parametric model order reduction (PMOR) of a FE model consisting of beam elements is presented. The method consists of two parts; in the first, an affine representation of the FE model, based on mechanics of material and beam theory, is retrieved; in the second part, a global ROB is generated for the parameter range to be investigated. The size of the resulting parametric ROM is completely independent from the size of the original model and, if the problem to be investigated presents a small Kolmogorov n -width, good trade-off between accuracy and reduction is obtainable.

An important benefit of the presented methodology is the capability of accounting for multi-parameter variations during simulation. This is obtained without recurring to expensive interpolations of the FE model or generic polynomials of high order. because both interpolations of the FE and generic polynomials scale badly with the number of parameters. Moreover, a general set of polynomial functions might bring numerical issues in the implementation of the LS method employed in this work.

The method to generate the reduced basis is refined when the greedy algorithm is used instead of the method based on SVD to construct the global ROB. This reduces the size of the ROB for a given accuracy as these are better controlled through the error estimation improving the computational capabilities of the ROM.

The greedy algorithm developed relies on an original estimation of the error based on the residual of the approximated eigenvalue problem. In fact, the aim of the method is to generate a global ROB from the eigenvectors of the system for different configuration of the parameters. Moreover, this allows to have some information on the expected accuracy of the ROM otherwise unavailable for purely modal basis. Therefore, the proposed methodology sums up the advantages of incremental improvements offered by the greedy algorithm to modal synthesis techniques.

Nevertheless, the correlation between the proposed residual and the actual error has to be still understood. In fact, even though the decay of the actual error appears to be faster than that of the proposed residual, it is not clear if this is generally true and what should be set as threshold to trigger the break in the greedy algorithm. Therefore, further analysis are needed to thoroughly understand the potential of the proposed scheme.

Further improvements could also regard the implementation of the iterative process. In the current scheme, at each iteration the temporary ROB is enriched by a full local ROB corresponding to the worst parameter configuration. Including some parameter correlated to the eigenfrequency in optimisation scheme could allow to filter only the strictly necessary vectors. This could also minimise the number of generalised coordinates with improvements in memory management and performances of the simulation.

Chapter 8

Conclusion

8.1 Discussion

This thesis proposes some developments of *Model Order Reduction* (MOR) in the field of elastodynamics and poroelasticity modelling.

Through the thesis, it was often discussed how simulations have become a pillar of technological development supporting theory and experiments. However, it was recognised how, in digital industry, the calculation time for virtual models is required to be low. This brought to the overall goal of the work of improving the computational performances of 3D simulations based on the Finite Element Method (FEM).

The models of physical phenomena result in systems of partial differential equations (PDE) that in many cases cannot be solved in closed form and require discretisation techniques that provide numerical approximations of their solutions. In particular, the FEM is the most popular discretisation method of the time and it is used in this thesis to generate *high fidelity models* (HFM). Though FE models show to give accurate results, they can often result to be large with high computational requirements. For example, the vibro-acoustic simulations of systems containing *poroelastic materials* (see chapter 4, 5 and 6) require heavy refinements of the meshes resulting and large models to solve. In this regard, MOR is presented as a measure to compensate the effects of these large simulations.

Throughout the text, a distinction between Model Order Reduction (MOR) and

Parametric Model Order Reduction (PMOR) is made: while MOR techniques are expected to generate a reduction of the DOF for a given configuration of the model, the PMOR techniques should provide reduction for a range of parameter configurations. This makes their use particularly appealing in optimisation schemes and co-simulation.

Maintaining the parameter dependency after the reduction is the objective of PMOR techniques. In the thesis this is obtained employing RB methods and using closed form affine representations of the models and *global* reduced order basis (ROB).

The affine representation, when implementable, allows the separation of the quantities that depend on the parameters and therefore enables the projection step to be offline as it affects only a set of parameter independent matrices. This makes the online step (the simulation) completely independent on the size of the original model with great advantage for the computational costs. In the text, closed form affine representations are developed for poroelastic materials (PEM) based on the Biot theory and for Timoshenko beams. In the former class of problem, the PEM, the affine functions involved all of the Biot parameters and the frequency; in the latter, the affine functions involved the geometrical parameters of the cross section and the material characteristics.

Two methods are presented to retrieve affine representations (see section 3.1): an intrusive one that can be applied when the user has full access to the discretised PDE of the HFM; and a non-intrusive that is based on a least square approximation that is applicable even when the HFM is a *black box* (e.g., when the HFM originates from a commercial software). Both methods show satisfactory results: the intrusive approach having as advantage a validity range equal to the HFM and as disadvantage the fact that cannot be applied when the source code is not available; the non intrusive approach cannot be considered having same validity range of the HFM but the fitting can be done to include the whole parameter range of interest with a high level of accuracy.

The global ROB is a subspace of the domain of the HFM. Its fundamental characteristic is that, within this space, a *reduced order model* (ROM) can describe accurately the solution for all the parameter configurations of interest for the simulation. Moreover, for optimal reduction, the size of the ROM should be kept as small as the accuracy requirements allow.

Few approaches on how to generate adaptive ROB are developed and investigated. The work on elastodynamic problems (chapter 7 suggests a method on how to generate PMOR using the greedy algorithm in combination to modal synthesis. The greedy algorithm is based on the evaluation of

the residuals of the associated eigenvalue problem for different parameter configurations. The results show a strong correlation between the decay of the real error and the residual of the eigenvalue that is cheaper to compute. This makes the proposed greedy algorithm a possible alternative for the creation of adaptive global ROB. However, even though it appears to be a good upper bound for the error, its validity conditions should still be investigated and the relation between the error estimator and the real error has to be better understood.

The work done on PMOR applied to space frames is exploited in the work of Moten [5] where the parametric ROM is used to perform simulation of interconnected systems (i.e., system level optimisation of structure and controller together).

The method proposed for PEM models gives an alternative to get over the challenge of the nonlinear frequency dependency of its matrices. This is obtained considering the frequency itself as a parameter and generating the basis via Proper Orthogonal Decomposition (POD).

The POD is a popular method in the field of fluid-dynamics and in general when there are strongly nonlinear phenomena involved. Applying it to the problem of PEM appeared to be an appropriate choice. In fact, it accounts for the frequency nonlinearities of PEM and appears to be efficient and straightforward to implement. Moreover, unlike most of the previous MOR methodologies proposed for PEM, it is able to cope with the mixed u - p FE formulation that gives extra computational advantage.

The POD implementation is based on a *singular value decomposition* (SVD) that is a computationally expensive matrix factorization. In chapter 6, it is shown how the dimensionality of the problem could easily lead to require large amounts of *snapshots* (i.e., the pool of solution vectors used to generate the ROB) and exposes to the limitations of the SVD. However, in the applications where only the frequency is considered in the parametric problem (chapter 5) the SVD does not represent an issue. In fact, as the frequency range of interest for vibro-acoustic simulations is rather low, the matrix of snapshots is usually rectangular with number of rows (corresponding to the number of DOF of the HFM) much larger than the number of columns (corresponding to the number of snapshots). Therefore, the theoretical computational complexity of the SVD applied to such matrix depends quadratically on the number of snapshots and only linearly on the number of DOF making it comparable to the computational costs of other matrix operations used in the POD (for example the inversion of the system matrix performed to compute the snapshots). Therefore, in

multi-parameter studies, as shown in chapter 6 where the required number of snapshots could grow to the point that the method fails, it is recommended that the ROB is built using adaptive techniques like the greedy algorithm proposed in the study of chapter 7 and/or a partition of the parametric domain is done.

To conclude, the approach of generating a reduction using an RB method based exploiting POD in the frequency domain appears to have numerous advantages especially in those applications where the models have nonlinear frequency dependencies that may jeopardise the applicability of conventional frequency-domain MOR approaches.

8.2 Future research

The results of the thesis highlighted few points that still need some attention for future research:

- the relations between actual error and error estimators. In particular, in chapter 3, the residual of the eigenvalue problem associated with the HFM fed with the approximated eigenpairs coming from the ROM;
- extension of the PMOR applications to PEM using partition to cover a larger set of configurations of the system;
- combination of the PMOR for PEM to other methods successfully employed in the literature, in particular the Padé approximation.
- in the applications to PEM, study of non constant and piece-wise constant material parameters distribution within the component.

The greedy algorithm presented in chapter 3 and applied in chapter 7 has some aspects that could be further investigated. It was recognised a correlation between the decay of the residual of the eigenvalue problem associated with the HFM fed with the approximated eigenpairs coming from the ROM decay of the actual error ROM/HFM. However, it was not specified any quantitative relations between the two quantities nor on their decay rate. New simulations on different systems and with different parameter ranges should be conducted to understand if any quantitative relation can be determined between the two.

Chapter 6 shows a multi-parameter application of the method developed in chapters 4 and 5 for PEM. The parametrisation is done on the frequency

and on the flow resistivity. The study shows that, for larger systems, the applicability of the method as it's used in chapter 5 is on its limit and further extensions of the parameter space (e.g., a third parameter) would require finer approaches for the generation of the ROM. Suggested techniques are adaptive approaches (e.g., greedy algorithm used in chapter 7) and/or partitioning of the parametric space to use multiple ROM. As discussed in chapter 6, the offline time for the presented method is already high for the 2 parameters case and the benefits of its usage would be evident only in optimisation techniques that require a high number of iterations or if the resulting ROM could be simulated in real-time for multilevel optimisations. Hence, these two problems could lead future research: reducing the offline calculations and find better trade-off in the online phase that could enable real-time computations.

With respect to PEM modelling, PEM components may often have non-uniform parameter distributions over the volume (due to their production technology). It could be of interest showing how to use the PMOR method to systems with piece-wise constant characteristics. This could be combined with multi-parameter variations studies to define optimisations of acoustic (or thermal) sound packages.

Finally, it could be interesting to combine the results obtained in chapters 4 and 5 with the work on the Padé approximation applied to PEM presented in references [59, 60] in substitution to the modal approach previously proposed.

Bibliography

- [1] W. Schilders, “Introduction to model order reduction,” in *Model Order Reduction: Theory, Research Aspects and Applications* (W. H. A. Schilders, H. A. van der Vorst, J. Rommes, H.-G. Bock, F. de Hoog, A. Friedman, A. Gupta, H. Neunzert, W. R. Pulleyblank, T. Rusten, F. Santosa, A.-K. Tornberg, L. L. Bonilla, R. Mattheij, and O. Scherzer, eds.), pp. 3–32, Berlin, Heidelberg: Springer Berlin Heidelberg, 2008.
- [2] F. E. Cellier, *Continuous System Modeling*. New York, NY: Springer New York, 1991. DOI: 10.1007/978-1-4757-3922-0.
- [3] P.-L. Caylar, K. Naik, and O. Noterdaeme, “Digital in industry: From buzzword to value creation | McKinsey & Company.” url: <https://www.mckinsey.com/business-functions/digital-mckinsey/our-insights/digital-in-industry-from-buzzword-to-value-creation>, 2018-01-19.
- [4] R. Y. Rubinstein and D. P. Kroese, *Simulation and the Monte Carlo Method*. John Wiley & Sons, Sept. 2011.
- [5] S. Moten, *Enhancing Model Based System Engineering for Mechatronic Systems. Combining Advanced Modeling and Control Techniques*. PhD thesis, Oct. 2016.
- [6] S. Moten, “A combined use of the adaptive inverse plant modeling and iterative learning control strategy for service load simulations,” 2015.
- [7] S. Moten, “An integrated simulation approach for the design and analysis of complex mechatronic systems,” 2014.
- [8] F. Naets, *Developement of system-level model reduction techniques for flexible multibody simulation*. PhD thesis, KU Leuven, 2013.

- [9] F. Chinesta, R. Keunings, and A. Leygue, *The Proper Generalized Decomposition for Advanced Numerical Simulations*. SpringerBriefs in Applied Sciences and Technology, Cham: Springer International Publishing, 2014. DOI: 10.1007/978-3-319-02865-1.
- [10] A. Quarteroni and G. Rozza, eds., *Reduced Order Methods for Modeling and Computational Reduction*. Cham: Springer International Publishing, 2014. DOI: 10.1007/978-3-319-02090-7.
- [11] W. H. A. Schilders and A. Lutowska, “A novel approach to model order reduction for coupled multiphysics problems,” in *Reduced Order Methods for Modeling and Computational Reduction* (A. Quarteroni and G. Rozza, eds.), pp. 1–49, Cham: Springer International Publishing, 2014.
- [12] A. Quarteroni, A. Manzoni, and F. Negri, “Extension to Nonaffine Problems,” in *Reduced Basis Methods for Partial Differential Equations*, vol. 92, pp. 193–214, Cham: Springer International Publishing, 2016.
- [13] A. Quarteroni, A. Manzoni, and F. Negri, *Reduced Basis Methods for Partial Differential Equations*. Springer, 2016.
- [14] Y. Maday and E. M. Ronquist, “The reduced basis element method: Application to a thermal fin problem,” *SIAM Journal on Scientific Computing*, vol. 26, no. 1, pp. 240–258, 2004.
- [15] J. F. Allard, *Propagation of Sound in Porous Media*. Dordrecht: Springer Netherlands, 1993. DOI: 10.1007/978-94-011-1866-8.
- [16] Y. Saad, *Iterative methods for sparse linear systems*. the Society for Industrial and Applied Mathematics, 2003.
- [17] B. Besselink, U. Tabak, A. Lutowska, N. van de Wouw, H. Nijmeijer, D. J. Rixen, M. E. Hochstenbach, and W. H. A. Schilders, “A comparison of model reduction techniques from structural dynamics, numerical mathematics and systems and control,” *Journal of Sound and Vibration*, 2013.
- [18] N. Atalla and F. Sgard, *Finite Element and Boundary Methods in Structural Acoustics and Vibration*. CRC Press, Apr. 2015.
- [19] K. D. C., D. L. Margolis, and R. C. Rosenberg, *System Dynamics - Modeling, Simulation, and Control of Mechatronic Systems*. Wiley-Blackwell, 2012.

- [20] Y. Yue and K. Meerbergen, “Parametric model order reduction of damped mechanical systems via the block arnoldi process,” *Applied Mathematics Letters*, vol. 26, no. 6, pp. 643 – 648, 2013.
- [21] K. Meerbergen and Z. Bai, “The lanczos method for parameterized symmetric linear systems with multiple right-hand sides,” *SIAM Journal on Matrix Analysis and Applications*, vol. 31, no. 4, pp. 1642–1662, 2010.
- [22] O. Dazel, F. Sgard, and C.-H. Lamarque, “Application of generalized complex modes to the calculation of the forced response of three-dimensional poroelastic materials,” *Journal of Sound and Vibration*, vol. 268, no. 3, pp. 555 – 580, 2003.
- [23] C. Batifol, M. N. Ichchou, and M.-A. Galland, “Hybrid modal reduction for poroelastic materials,” *Comptes Rendus Mécanique*, vol. 336, no. 10, pp. 757 – 765, 2008.
- [24] H. Panzer, J. Mohring, R. Eid, and B. Lohmann, “Parametric Model Order Reduction by Matrix Interpolation,” *at - Automatisierungstechnik Methoden und Anwendungen der Steuerungs-, Regelungs- und Informationstechnik*, vol. 58, no. 8, pp. 475–484, 2010.
- [25] D. Amsallem and B. Haasdonk, “Pebl-rom: Projection-error based local reduced-order models,” *Advanced Modeling and Simulation in Engineering Sciences*, vol. 3, p. 6, Mar 2016.
- [26] D. Amsallem and C. Farhat, “An online method for interpolating linear parametric reduced-order models,” *SIAM Journal on Scientific Computing*, vol. 33, no. 5, pp. 2169–2198, 2011.
- [27] A. Quarteroni, A. Manzoni, and F. Negri, “Construction of RB Spaces by the Greedy Algorithm,” in *Reduced Basis Methods for Partial Differential Equations*, vol. 92, pp. 141–154, Cham: Springer International Publishing, 2016.
- [28] S. K. Hong, B. I. Epureanu, and M. P. Castanier, “Next-generation parametric reduced-order models,” *Mechanical Systems and Signal Processing*, vol. 37, pp. 403–421, 2013.
- [29] G. Heirman, *Model reduction techniques to improve the efficiency of flexible multibody simulations*. PhD thesis, KU Leuven, 2011.
- [30] J. F. Villena and M. E. Silveira, “Order reduction techniques for coupled multi-domain electromagnetic based models,” Eindhoven : Technische Universiteit Eindhoven, 2008.

- [31] R. W. Freund, “Sprim: Structure-preserving reduced-order interconnect macromodeling,” in *Proceedings of the 2004 IEEE/ACM International Conference on Computer-aided Design, ICCAD '04*, (Washington, DC, USA), pp. 80–87, IEEE Computer Society, 2004.
- [32] A. Vandendorpe and P. Van Dooren, “Model reduction of interconnected systems,” in *Model Order Reduction: Theory, Research Aspects and Applications* (W. H. A. Schilders, H. A. van der Vorst, and J. Rommes, eds.), pp. 305–321, Berlin, Heidelberg: Springer Berlin Heidelberg, 2008.
- [33] A. Van de Walle, *The power of model order reduction in vibroacoustics and its applications in model-based sensing*. PhD thesis, Jan. 2018.
- [34] A. C. Antoulas, *Approximation of Large-Scale Dynamical Systems (Advances in Design and Control) (Advances in Design and Control)*. Philadelphia, PA, USA: Society for Industrial and Applied Mathematics, 2005.
- [35] V. Simoncini, “A New Iterative Method for Solving Large-Scale Lyapunov Matrix Equations,” *SIAM Journal on Scientific Computing*, vol. 29, pp. 1268–1288, Jan. 2007.
- [36] T. Wolf, H. K. F. Panzer, and B. Lohmann, “Model Order Reduction by Approximate Balanced Truncation: A Unifying Framework / Modellreduktion durch approximatives Balanciertes Abschneiden: eine vereinigende Formulierung,” *at - Automatisierungstechnik*, vol. 61, no. 8, pp. 545–556, 2013.
- [37] J. Fehr, M. Fischer, B. Haasdonk, and P. Eberhard, “Greedy-based approximation of frequency-weighted gramian matrices for model reduction in multibody dynamics,” *ZAMM - Journal of Applied Mathematics and Mechanics / Zeitschrift für Angewandte Mathematik und Mechanik*, vol. 93, no. 8, pp. 501–519, 2013.
- [38] W. H. A. Schilders, H. A. van der Vorst, J. Rommes, H.-G. Bock, F. de Hoog, A. Friedman, A. Gupta, H. Neunzert, W. R. Pulleyblank, T. Rusten, F. Santosa, A.-K. Tornberg, L. L. Bonilla, R. Mattheij, and O. Scherzer, eds., *Model Order Reduction: Theory, Research Aspects and Applications*, vol. 13 of *Mathematics in Industry*. Berlin, Heidelberg: Springer Berlin Heidelberg, 2008.
- [39] Z. Bai and Y. Su, “Dimension reduction of large-scale second-order dynamical systems via a second-order arnoldi method,” *SIAM Journal on Scientific Computing*, vol. 26, no. 5, pp. 1692–1709, 2005.

- [40] A. Quarteroni, A. Manzoni, and F. Negri, “Construction of RB spaces by SVD-POD,” in *Reduced Basis Methods for Partial Differential Equations*, vol. 92, pp. 115–140, Cham: Springer International Publishing, 2016.
- [41] J. Edmonds, “Matroids and the greedy algorithm,” *Mathematical Programming*, 1971.
- [42] T. Grätsch and K.-J. Bathe, “A posteriori error estimation techniques in practical finite element analysis,” *Computers & Structures*, vol. 83, no. 4, pp. 235 – 265, 2005.
- [43] M. A. Biot, “Theory of propagation of elastic waves in a fluid saturated porous solid. i. low frequency range,” *The Journal of the Acoustical Society of America*, vol. 28, no. 2, pp. 168–178, 1956.
- [44] M. A. Biot, “Theory of propagation of elastic waves in a fluid saturated porous solid. ii. high frequency range,” *The Journal of the Acoustical Society of America*, vol. 28, no. 2, pp. 179–191, 1956.
- [45] D. L. Johnson, J. Koplik, and R. Dashen, “Theory of dynamic permeability and tortuosity in fluid-saturated porous media,” *Journal of Fluid Mechanics*, vol. 176, p. 379–402, 1987.
- [46] Y. Champoux and J. Allard, “Dynamic tortuosity and bulk modulus in air-saturated porous media,” *Journal of Applied Physics*, vol. 70, no. 4, pp. 1975–1979, 1991.
- [47] M. A. Biot, “The elastic coefficients of the theory of consolidation,” *Journal of Applied Mechanics*, vol. 24, pp. 594–601, 1957.
- [48] O. Dazel, B. Brouard, N. Dauchez, and A. Geslain, “Enhanced biot’s finite element displacement formulation for porous materials and original resolution methods based on normal modes,” vol. 95, no. 3, pp. 527–538, 2009.
- [49] N. Atalla, R. Panneton, and P. Debergue, “A mixed displacement-pressure formulation for poroelastic materials,” vol. 104, no. 3, pp. 1444–1452, 1998.
- [50] N. Atalla, M. A. Hamdi, and R. Panneton, “Enhanced weak integral formulation for the mixed (u_,p_) poroelastic equations,” *The Journal of the Acoustical Society of America*, vol. 109, no. 6, pp. 3065–3068, 2001.
- [51] W. Desmet, *A Wave Based prediction technique for coupled vibro-acoustic analysis*. PhD thesis, KU Leuven, 1998.

- [52] E. Deckers, *A Wave Based approach for steady-state Biot models of poroelastic materials*. PhD thesis, KU Leuven, 2011.
- [53] E. Trefftz, “Ein gegenstück zum ritzschen verfahren,” in *2nd International Congress on Applied Mechanics, Zurich, Switzerland, 1926*.
- [54] B. Campolina, N. Atalla, and N. Dauchez, “Assessment of the validity of statistical energy analysis and transfer matrix method for the prediction of sound transmission loss through aircraft double-walls,” in *Acoustics 2012* (S. F. d’Acoustique, ed.), (Nantes, France), 2012.
- [55] R. H. Lyon and R. G. DeJong, “Chapter 4 - the estimation of response statistics in statistical energy analysis,” in *Theory and Application of Statistical Energy Analysis (Second Edition)*, pp. 81–107, Boston: Newnes, 1995. DOI: 10.1016/B978-0-7506-9111-6.50008-7.
- [56] F. C. Sgard, N. Atalla, and R. Panneton, “A modal reduction technique for the finite element formulation of biot’s poroelasticity equations in acoustics applied to multilayered structures,” vol. 103, no. 5, p. 2882, 1998.
- [57] R. Rumpler, J.-F. Deü, and P. Göransson, “A modal-based reduction method for sound absorbing porous materials in poro-acoustic finite element models,” vol. 132, no. 5, pp. 3162–3179, 2012.
- [58] O. Dazel, B. Brouard, J.-P. Groby, and P. Göransson, “A normal modes technique to reduce the order of poroelastic models: application to 2D and coupled 3D models,” vol. 96, no. 2, pp. 110–128, 2013.
- [59] R. Rumpler, P. Göransson, and J.-F. Deü, “A finite element approach combining a reduced-order system, padé approximants, and an adaptive frequency windowing for fast multi-frequency solution of poro-acoustic problems,” *International Journal for Numerical Methods in Engineering*, vol. 97, no. 10, pp. 759–784, 2014.
- [60] J.-D. Chazot, B. Nennig, and E. Perrey-Debain, “Harmonic response computation of poroelastic multilayered structures using zpst shell elements,” *Computers & Structures*, vol. 121, no. Supplement C, pp. 99 – 107, 2013.
- [61] W. Heylen, S. Lammens, and P. Sas, *Modal Analysis Theory and Testing*. Katholieke Universiteit Leuven, Departement Werktuigkunde, 1999.
- [62] H. Bouhioi and M. Hodgson, “Finite-element modelling of the vibro-acoustical behaviour of poro-elastic materials,” in *135th Meeting of the Acoustical Society of America, Seattle, U.S.A., 1998*.

- [63] O. Dazel, F. Sgard, C.-H. Lamarque, and N. Atalla, “An extension of complex modes for the resolution of finite-element poroelastic problems,” *Journal of Sound and Vibration*, vol. 253, no. 2, pp. 421 – 445, 2002.
- [64] R. A. Frazer, W. J. Duncan, and A. R. Collar, *Elementary matrices and some applications to dynamics and differential equations*. The University Press, 1938.
- [65] R. Van Beeumen, K. Meerbergen, and W. Michiels, “Compact rational krylov methods for nonlinear eigenvalue problems,” *SIAM Journal on Matrix Analysis and Applications*, vol. 36, no. 2, pp. 820–838, 2015.
- [66] R. Rumppler, *Efficient finite element approach for structural-acoustic applications including 3D modelling of sound absorbing porous materials*. PhD thesis, Conservatoire national des arts et metiers - CNAM, 2012.
- [67] O. Zienkiewicz, R. Taylor, and J. Zhu, “2 - a direct physical approach to problems in elasticity: Plane stress,” in *The Finite Element Method Set (Sixth Edition)* (O. Zienkiewicz, R. Taylor, and J. Zhu, eds.), pp. 19 – 53, Oxford: Butterworth-Heinemann, sixth edition ed., 2005.
- [68] K. Kunisch and S. Volkwein, “Galerkin proper orthogonal decomposition methods for parabolic problems,” *Numerische Mathematik*, vol. 90, pp. 117–148, Nov 2001.
- [69] P. C. Hansen, *Rank-deficient and Discrete Ill-posed Problems: Numerical Aspects of Linear Inversion*. SIAM, 2005.
- [70] D. S. Watkins, *Fundamentals of Matrix Computations*. Wiley and Sons, 2002.
- [71] L. N. Trefethen and D. Bau, *Numerical Linear Algebra*. SIAM, Jan. 1997.
- [72] L. N. Trefethen and D. B. III, *Numerical Linear Algebra*. SIAM, June 1997.
- [73] A. Duval, J. Baratier, C. Morgenstern, L. Dejaeger, N. Kobayashi, and H. Yamaoka, “Trim fem simulation of a dash and floor insulator cut out modules with structureborne and airborne excitations,” *The Journal of the Acoustical Society of America*, vol. 123, no. 5, pp. 3532–3532, 2008.
- [74] A. Duval, L. Dejaeger, C. Morgenstern, and J.-F. Rondeau, “Novel technique for the introduction of curved trims in SEA / Virtual SEA models using poroelastic finite elements in the middle (and high) frequency range,” Oct. 2010.

- [75] J.-F. Rondeau, A. Duval, J. Monet-Descombey, and L. Dejaeger, “Equivalent curvatures broadband Insertion Loss simulation technique coupling Virtual SEA and BEM/FEM approaches,” Sept. 2013.
- [76] N. Dauchez, S. Sahraoui, and N. Atalla, “Convergence of poroelastic finite elements based on biot displacement formulation,” *The Journal of the Acoustical Society of America*, vol. 109, no. 1, pp. 33–40, 2001.
- [77] O. Dazel and G. Gabard, “Discontinuous galerkin methods for poroelastic materials,” *The Journal of the Acoustical Society of America*, vol. 133, no. 5, pp. 3242–3242, 2013.
- [78] J.-D. Chazot, E. Perrey-Debain, and B. Nennig, “The partition of unity finite element method for the simulation of waves in air and poroelastic media,” *The Journal of the Acoustical Society of America*, vol. 135, no. 2, pp. 724–733, 2014.
- [79] O. Dazel, B. Brouard, C. Depollier, and S. Griffiths, “An alternative biot’s displacement formulation for porous materials,” *The Journal of the Acoustical Society of America*, vol. 121, no. 6, pp. 3509–3516, 2007.
- [80] O. Dazel, B. Brouard, N. Dauchez, A. Geslain, and C.-H. Lamarque, “A free interface CMS technique to the resolution of coupled problem involving porous materials, application to a monodimensional problem,” vol. 96, no. 2, pp. 247–257, 2010.
- [81] E. Lappano, M. Polanz, W. Desmet, and D. Mundo, “A parametric model order reduction technique for poroelastic finite element models,” *The Journal of the Acoustical Society of America*, vol. 142, no. 4, pp. 2376–2385, 2017.
- [82] E. Lappano, F. Naets, W. Desmet, D. Mundo, and E. Nijman, “A greedy sampling approach for the reduced order basis construction for structural dynamics models,” in *ISMA - International conference on Noise and Vibration Engineering*, 2016.
- [83] R. Rumpler, P. Göransson, and J.-F. Deü, “A residue-based mode selection and sorting procedure for efficient poroelastic modeling in acoustic finite element applications,” *The Journal of the Acoustical Society of America*, vol. 134, no. 6, pp. 4730–4741, 2013.
- [84] N. Atalla and F. Sgard, “Solving uncoupled structural acoustics and vibration problems using the finite-element method,” in *Finite Element and Boundary Methods in Structural Acoustics and Vibration*, CRC Press, 2015.

- [85] “Introduction To Finite Element Methods (ASEN 5007) Course Material.” url: <https://www.colorado.edu/engineering/CAS/courses.d/IFEM.d/>.
- [86] M. H. Hansen, W. N. Hurwitz, and W. G. Madow, *Sample survey methods and theory: Methods and applications*. Wiley & Sons, Jan. 1953.
- [87] C. G. Albert, G. Veronesi, E. Nijman, and J. Rejlek, “Prediction of the vibro-acoustic response of a structure-liner-fluid system based on a patch transfer function approach and direct experimental subsystem characterisation,” *Applied Acoustics*, vol. 112, no. Supplement C, pp. 14 – 24, 2016.
- [88] M. Polanz, E. Nijman, and M. Schanz, “ThePatch-Transfer-Function (PTF) method applied to numerical models of trim materials including poro-elastic layers.,” 2018.
- [89] F. Pompoli, P. Bonfiglio, K. V. Horoshenkov, A. Khan, L. Jaouen, F.-X. Bécot, F. Sgard, F. Asdrubali, F. D’Alessandro, J. Hübel, N. Atalla, C. K. Amédin, W. Lauriks, and L. Boeckx, “How reproducible is the acoustical characterization of porous media?,” *The Journal of the Acoustical Society of America*, vol. 141, no. 2, pp. 945–955, 2017.
- [90] D. C. Montgomery, *Design and Analysis of Experiments*. John Wiley & Sons, July 2008.
- [91] E. Lappano, F. Naets, M. Vermaut, W. Desmet, and D. Mundo, “Development of a parametric model order reduction approach for beam-based structures,” in *9th International Styrian Noise, Vibration & Harshness Congress: The European Automotive Noise Conference*, SAE International, jun 2016.
- [92] J. S. Przemieniecki, “Chapter 5 – Stiffness properties of structural elements,” in *Theory of Matrix Structural Analysis*, pp. 61–128, New York, U.S.A.: McGraw-hill, 1968.
- [93] S. Timoshenko and J. N. Goodier, *Theory of Elastic Stability*. McGraw-hill, 1963.
- [94] W. C. Young and R. G. Budynas, *Roarks’s Formulas for Stress and Strain*. McGraw-hill, 2002.
- [95] A. Labuschagne, N. F. J. van Rensburg, and A. J. van der Merwe, “Comparison of linear beam theories,” *Mathematical and Computer Modelling*, 2009.

- [96] J. M. Gere and S. Timoshenko, *Mechanics of Materials*. PWS Publishing company, 1997.

Curriculum Vitae

Personal data

Ettore Lappano
03 February 1989
Cosenza, Italia
ettore.lappano@gmail.com

Professional Experience

(Aug 2015 - today) Junior Researcher - Marie Curie fellow

Virtual Vehicle research centre - NVH and friction department (Austria)

- Vibro-acoustic simulations and analyses of trim components
- Model Order Reduction applied to poroelastic material models

(Jun 2014 - Jul 2015) PhD Researcher - Marie Curie fellow

KU Leuven - Noise & Vibration Research group (Belgium)

- Dynamics simulations and analyses of crane for laser cutting
- Model Order Reduction applied to lattice girders

(Jan 2014 - Jun 2014) PhD Researcher

University of Calabria – Department of Mechanical Engineering (Italy)

- 1D modelling of meshing gears

Education

(2014 - 2018) Ph.D in Engineering

KU Leuven (Belgium) and University of Calabria (Italy),
in collaboration with Virtual Vehicle (Austria)

Thesis: Model Order Reduction techniques for lattices girder
and poroelastic material models

Note: My Ph.D was hosted by University of Calabria whit a
scholarship of 7 months, by the KU Leuven university
with a Marie Curie fellowship, by Virtual Vehicle with
a Marie Curie fellowship and later employed as a
Junior Researcher to work on topics of mutual interest.

(2011 - 2013) M.Sc. in Mechanical Engineering

University of Calabria (Italy) - grade: 110/110 cum Laude

Thesis: Analysis of the adhesive properties of micro-structured
surfaces

Note: During my M.Sc. at University of Calabria, I was awarder
two scholarships as exchange student: I spent 1 semester at
the Queen Mary University of London (United Kingdom)
and 1 semester at the Queensland University of Technology,
Brisbane (Australia)

(2009 -2011) B.Sc. in Mechanical Engineering

University of Calabria (Italy) - grade: 110/110 cum Laude

Thesis: Analysis of stress concentration in a perforated plate
under uniaxial tension

(2001 - 2013) Conservatoire Diploma in classical guitar

Conservatorio di Cosenza (Italy)

Note: Equivalent to Master of Arts

(2003 - 2008) Scientific High school

Liceo Scientifico Pitagora, Cosenza (Italy) – grade: 100/100

List of publications

Articles in international journals

E. Lappano, M. Polanz, W. Desmet, D. Mundo. *A parametric Model Order Reduction technique for poroelastic Finite Element models*. Journal of Acoustic Society of America, (2017).

Article in academic book

E. Lappano, E. Nijman, F. Naets, W. Desmet and D. Mundo. *A Parametric Model Order Reduction for simulations of beam-based structures*. In “eLiQuiD” Best Engineering Training in Electric, Lightweight and Quiet Driving, KU Leuven, 2016.

Articles in international conference proceedings

Lappano E., Naets F., Vermaut M., Desmet W., Mundo D., *Development of a parametric model order reduction technique for beam-based structures*, SAE Techniocal Paper No. 2016-01-1857, New York, 2016.

Lappano E., Naets F., Desmet W., Mundo D., Nijman E., *A greedy sampling approach for the projection basis construction in parametric model order reduction for structural dynamics models*, Proceedings of ISMA2016, 2016.

Abstracts in international conference proceedings

Lappano E., Naets F., Vermaut M., Mundo D., Desmet W. (2015). *A Parametric Model Order Reduction approach for beam-based structures*. Congress on Reduced Basis, POD and PGD Model Reduction Techniques. Cachan, France, 4-6 November 2015.

Abstracts in national conference proceedings

Palermo A., Lappano E., Mundo D., Toso A., Desmet W. (2014). *Una tecnica per includere gli effetti della coppia istantanea sulla dinamica non lineare delle ruote dentate*. Congresso Nazionale del Coordinamento della Meccanica Italiana. Napoli, 30 June - 1 July.

FACULTY OF ENGINEERING SCIENCE
DEPARTMENT OF MECHANICAL ENGINEERING
NOISE & VIBRATION RESEARCH GROUP

Celestijnenlaan 300

B-3001 Leuven

secretariaat.pma@mech.kuleuven.be

<https://www.mech.kuleuven.be/en/research/mod/>



FACOLTÀ DI INGEGNERIA
DIPARTIMENTO DI INGEGNERIA MECCANICA ENERGETICA E GESTIONALE
GRUPPO DI MECCANICA APPLICATA ALLE MACCHINE

Ponte P. Bucci 45C

87036 Rende (CS) Italy

direttore.dimeg@unical.it

http://www.unical.it/portale/strutture/dipartimenti_240/dimeg/

